SIAM J. IMAGING SCIENCES
Vol. 10, No. 4, pp. 2165–2216
© 2017 Society for Industrial and Applied Mathematics

Matched-Filter and Correlation-Based Imaging for Fast Moving Objects Using a Sparse Network of Receivers*

J. Fournier†, J. Garnier‡, G. Papanicolaou§, and C. Tsogka¶

Abstract. In this paper we consider the problem of imaging a fast moving small object. The imaging system consists of a powerful emitter and several passive receivers located on the ground. Our aim is to compare the well-known matched-filter imaging method with correlation-based imaging. Imaging with correlations has the advantage of not requiring any knowledge about the probing pulse and the emitter position, both assumed known with high accuracy in the case of matched-filter imaging. But correlation-based imaging requires recording fully resolved signals without down-ramping while matched-filer imaging does not. To account for the fast moving target's velocity, Doppler compensation is necessary for both imaging methods. Our resolution analysis, from first principles, shows that with the two methods we have similar resolution in the cross-range direction, for both the location and the velocity of the moving target. In the range direction, matched-filter imaging has better resolution mainly because it benefits from the signal bandwidth, which is not true for correlation-based imaging that relies on travel time differences. We also analyze the role of the number of receivers and show that a small number of them sparsely distributed provides an image with resolution close to the one obtained with a dense array of comparable overall size.

Key words. passive imaging, matched filter, cross correlation, sparse network

AMS subject classifications. 78A45, 78A46, 35R30, 49N30, 78M35, 78M99

DOI. 10.1137/17M112364X

1. Introduction.

The study of imaging fast moving objects is motivated by the need to detect, track, and image small energetic debris (1–10 cm) revolving around the earth at a low orbit (200 km–2000 km) [18]. This is of interest because of the large amount of debris which substantially increases the risk of satellite damage from collisions [16, 12]. There are roughly 700,000 pieces of debris of size larger than 1 cm in low earth orbit (LEO) and there is concern that future collisions may have a chain reaction effect that would lead to an unacceptably risky environment [22].

In this paper, we model the small fast moving debris as a pointlike reflector moving with constant velocity, $\boldsymbol{V}_T$. Debris are not necessarily in stable orbit but their motion follows

*Received by the editors March 31, 2017; accepted for publication (in revised form) August 15, 2017; published electronically November 21, 2017.
http://www.siam.org/journals/siims/10-4/M112364.html
Funding: The work of the third author was partially supported by AFOSR grant FA9550-14-1-0275. The work of the fourth author was partially supported by AFOSR grants FA9550-14-1-0275 and FA9550-17-1-0238.
†Département de Mathématiques et Applications, École Normale Supérieure, 75005 Paris, France (jacques.fournier@ens.fr).
‡Centre de Mathématiques Appliquées, École Polytechnique, 91128 Palaiseau Cedex, France (josselin.garnier@polytechnique.edu).
§Department of Mathematics, Stanford University, Stanford CA 94305 (papanicolaou@stanford.edu).
¶Applied Math Unit, University of California, Merced, Merced, CA 95343 (ctsogka@ucmerced.edu).

Copyright © by SIAM. Unauthorized reproduction of this article is prohibited.

Downloaded 11/28/17 to 171.67.216.21. Redistribution subject to SIAM license or copyright; see http://www.siam.org/journals/ojsa.php

Downloaded 11/28/17 to 171.67.216.21. Redistribution subject to SIAM license or copyright; see http://www.siam.org/journals/ojsa.php

Newton's law and therefore we seek to reconstruct the six unknowns that characterize their trajectories: the three components of the position and of the velocity. The imaging data are the scattered signals from a train of incident pulses emitted by a powerful transmitter located on the ground. The receivers are also assumed to be located on the ground and span an area of diameter a, which defines the physical aperture of the imaging system. In synthetic aperture radar (SAR), a single airborne transmit/receive element is moving and its trajectory defines the synthetically created aperture of the imaging system [7, 8]. Analogously, the trajectory of the moving target defines an inverse synthetic aperture (ISAR) of length $T_{\rm tot}|\boldsymbol{V}_T|$ with $T_{\rm tot}$ the total recording time during the data gathering process. Other important parameters of the imaging system are the central frequency, f_o, and the bandwidth, B, which are determined by the emitter. We consider here a system operating at high frequency with a relatively large bandwidth, such as the X-Band (8–12 GHz) or the S-Band (2–4 GHz) regimes.

In this context, we study the well-established matched-filter imaging method [5, 19] and compare its performance with a correlation-based imaging method. Correlation-based imaging for fast moving objects has been considered in [2] where it was shown that two well-separated airborne pairs of receivers are sufficient for determining the target's location and velocity. We adopt here a simpler configuration with the receivers located on the ground. Since the speed of the airborne platforms is always small compared to the one of the object to be imaged, our analysis can be easily extended to moving airborne receivers. Recent developments on passive radar systems can be found in the special issue [1].

In matched-filter imaging the recorded signals are Doppler compensated as in [5, 17, 19] and synchronized with travel time delays so as to maximize the correlation with the emitted pulse, which is assumed known. The synchronization requires knowledge of the emitter location with high accuracy. Correlation-based imaging relies on cross correlations of signals between pairs of receivers. The signals are also Doppler compensated and synchronized, and must be recorded without down-ramping [1]. However, in this case the synchronization does not require knowledge of the emitter location since only time differences matter. For correlation-based imaging we do not need to know the pulse profile or the emission times but we need to record the whole train of scattered pulses. In this paper we assume a sufficiently high sampling rate so that the real-valued scattered signal can be recorded as in [2, 1].

Correlation-based imaging has been shown to be more robust to medium fluctuations such as atmospheric lensing [13] and aberrations [15]. This would be true for receivers that are not located on the ground but are flying above the turbulent atmosphere. Indeed, considering airborne receivers transforms the passive correlation-based problem to a virtual source array imaging problem that has been studied for stationary receiver arrays in [9, 10, 11]. The key idea is that passive correlation-based imaging becomes equivalent to having a virtual active array at the location of the passive receivers. By moving the receivers above the turbulent atmosphere, the atmospheric fluctuation effects on imaging are minimized and imaging resolution is as if we were in a homogeneous, fluctuation-free medium.

Correlation-based imaging is passive because it can be carried out using opportunistic, unknown emitters. In the imaging setting considered in this paper, opportunistic sources could be global navigation satellite systems (GNSS). This has been considered in [14] and it is shown that the main challenge in this case is the low signal-to-noise ratio because the scattered signal received at a terrestrial receiver is very weak. The approach proposed in [14]

Copyright © by SIAM. Unauthorized reproduction of this article is prohibited.

Downloaded 11/28/17 to 171.67.216.21. Redistribution subject to SIAM license or copyright; see http://www.siam.org/journals/ojsa.php

relies on matched filtering and careful signal processing that exploits the Doppler shift of the reflected signal by the fast moving object.

We present in this paper a rigorous resolution analysis for both the matched-filter and the correlation-based imaging methods. We study the corresponding point spread functions and show that the two methods have similar resolution in cross range. Cross range is the coordinate that is orthogonal to the direction of the receivers/scatterer that defines the range. Note that it is the final resolution estimates that are comparable, while the computations for image formation in each case are quite different. The cross-range resolution estimate is $\lambda_o H_T/a$ with H_T being the altitude of the moving target and λ_o being the central wavelength. This is the well-known Rayleigh resolution formula. In the direction of the target's velocity, the ISAR aperture plays a role when it is big enough and the resolution estimate becomes $\lambda_o(\frac{H_T}{a} \wedge \frac{H_T}{2|\boldsymbol{V}_T|T_{\rm tot}})$ for the matched filter, the wedge symbol, $\wedge$, means the minimum between the two quantities. In the range direction we see the biggest difference between the two methods: matched-filter resolution is $\frac{c_o}{2B}$ and relies on the bandwidth, while for the correlation-based imaging we obtain $\lambda_o \frac{H_T^2}{a^2}$. In correlation-based imaging range resolution does not depend on the bandwidth because the corresponding imaging function relies only on arrival-time differences. The resolution estimates for the velocity are given by the corresponding ones for the location divided by the recording time $T_{\rm tot}$. This is not true for the velocity estimate along the range direction provided by the matched filter for which we obtain the extremely precise estimate $\frac{\lambda_o}{2T_{\rm tot}}$.

Our resolution estimates suggest that the moving object can be localized with very high accuracy, of the order of the wavelength of the imaging system. The estimated resolutions for the X-band and the S-band surveillance systems are given in Tables 4 and 5, respectively. Our analytical resolution estimates are validated with detailed numerical simulations. Moreover, our numerical results suggest that around 10 receivers are enough so as to achieve the theoretical resolution estimates with an aperture diameter of about 400 kilometers. This empirical rule of the order of 10 receivers is furthermore proven to be correct theoretically when considering a regular grid of receivers, both for the matched-filter and the correlation-based imaging method.

The resolution analysis carried out in this paper concerns the case of a point reflector and, consequently, it characterizes the behavior of the point spread function of the two imaging methods analyzed. This is a basic step towards imaging extended objects but does not account for many effects that could play an important role for general scatterers. Indeed, under the assumption of the single scattering (Born) approximation, it is possible to predict the image of an extended object by convolution of the object's reflectivity with the point spread function derived in this paper. However, the reflectivity function of an extended object may be complicated in the sense that it may depend strongly on the illumination and observation angles, as well as on the frequency. Therefore, it would be interesting to adapt the imaging methodology and study the resolution that can be obtained for directional and frequency dependent reflectivities of extended objects.

This paper is organized as follows. We begin with the data model and the problem setup in section 2. The two imaging methods are presented in section 3 and the resolution analysis is carried out in section 4. In section 5 we present numerical simulations that verify our

Copyright © by SIAM. Unauthorized reproduction of this article is prohibited.

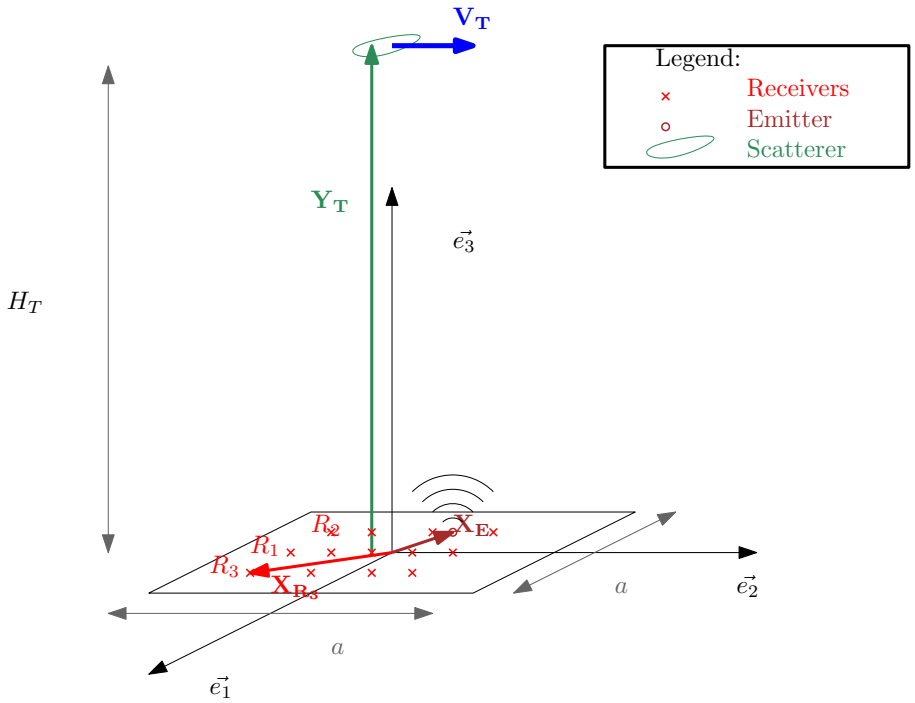

Figure 1. *Schematic of the imaging system's geometry. The receivers $R_1, R_2, \ldots, R_N$ are located on the ground covering a domain of diameter a. The object to be imaged is moving with speed $\mathbf{V}_T$ at height H_T.*

theoretical resolution estimates. We also investigate the role that the number of receivers play in image resolution. Our results suggest that a small number of receivers of the order of 10 are sufficient so as to observe the theoretical resolution estimates. The theoretical analysis of this surprising result is considered in section 6. We end with our conclusions in section 7.

2. Data model.

We introduce in this section the configuration of our imaging system and the model we use for the recorded data set.

2.1. Problem setup.

We assume that a transmitter antenna is located on the ground at location $\boldsymbol{X}_E$. The probing pulse emitted by the transmitter is

$$f(t) = F(Bt)e^{-i\omega_o t} + F(Bt)e^{i\omega_o t} = 2F(Bt)\cos(\omega_o t), \tag{2.1}$$

where the bandwidth B is smaller than the central frequency ω_o, and the baseband pulse F is real valued and compactly supported.

There is a network of distributed receivers on the ground, at positions $\boldsymbol{X}_R$, $R = 1, \ldots, N$. The network covers a region with diameter a. We consider the following two situations: a regular grid of receiver locations or a random grid. In the first case, the receiver locations are the abscissas of a quadrature integral approximation of the surface density function $p(\boldsymbol{x}/a)$. In the second case, the receiver locations are random, independently and identically distributed with the surface density function $p(\boldsymbol{x}/a)/a^2$ (with p such that $\int p(\boldsymbol{x})d\boldsymbol{x} = 1$). A schematic of the system's geometry is shown in Figure 1.

Copyright © by SIAM. Unauthorized reproduction of this article is prohibited.

Downloaded 11/28/17 to 171.67.216.21. Redistribution subject to SIAM license or copyright; see http://www.siam.org/journals/ojsa.php

Downloaded 11/28/17 to 171.67.216.21. Redistribution subject to SIAM license or copyright; see http://www.siam.org/journals/ojsa.php

The target to be imaged is taken to be pointlike and moving with constant velocity $\boldsymbol{V}_T$ along the trajectory $\boldsymbol{X}_T(t) = \boldsymbol{Y}_T + \boldsymbol{V}_T t$, $t \in (-T_{\text{tot}}/2, T_{\text{tot}}/2)$. The extension of the resolution analysis that we present to a trajectory $(\boldsymbol{X}_T(t), \boldsymbol{V}_T(t))$, $t \in (-T_{\text{tot}}/2, T_{\text{tot}}/2)$, that can be determined by a flow given the initial position and velocity, is straightforward.

With no loss of generality, we consider a reference frame such that (1) the origin is on the ground and given by the orthogonal projection of the target position $\boldsymbol{Y}_T$ onto the ground and (2) the target position $\boldsymbol{Y}_T$ is along the third axis of the reference frame. In other words, the ground is horizontal and the position $\boldsymbol{Y}_T$ of the target at time 0 is vertical and of the form $\boldsymbol{Y}_T = (0, 0, H_T)$, where H_T is the altitude of the target (see Figure 1). By denoting $\boldsymbol{m}_{\boldsymbol{X}} = \frac{\boldsymbol{X}}{|\boldsymbol{X}|}$ and $\mathbf{P}_X^{\perp} = \mathbf{I}_d - \boldsymbol{m}_{\boldsymbol{X}}\, {}^t\boldsymbol{m}_{\boldsymbol{X}}$, we have, for any space vector, $\boldsymbol{X} = (X_1, X_2, X_3)$: $X_3 = \boldsymbol{m}_{\boldsymbol{Y}_T} \cdot \boldsymbol{X}$, and $\boldsymbol{X}_\perp = (X_1, X_2, 0) = \mathbf{P}^{\perp}_{\boldsymbol{Y}_T} \boldsymbol{X}$. Let us also denote $\langle ., . \rangle_\perp$ as the bilinear form associated with $\mathbf{P}^{\perp}_{\boldsymbol{Y}_T}$.

2.2. The direct and scattered waves. Let us assume that the transmitter at $\boldsymbol{X}_E$ emits a short pulse $f(t)$ whose compact support is in $(0, \infty)$. The total field $u(t, \boldsymbol{x})$ is the solution of the wave equation

$$\frac{1}{c^2(t, \boldsymbol{x})} \frac{\partial^2 u}{\partial t^2} - \Delta u = f(t)\delta(\boldsymbol{x} - \boldsymbol{X}_E), \tag{2.2}$$

where the velocity model consists of a uniform background and a localized perturbation ϱ_T centered at $\boldsymbol{X}_T(t)$,

$$\frac{1}{c^2(t, \boldsymbol{x})} = \frac{1}{c_o^2}\Big(1 + \varrho_T\big(\boldsymbol{x} - \boldsymbol{X}_T(t)\big)\Big).$$

The scalar wave equation that we consider here is used quite often instead of the full Maxwell's equations as a model for radar applications since it captures the main features of the scattering problem [6]. The scattered field, $u^{(1)}(t, \boldsymbol{x})$, is defined as the difference between the total field $u(t, \boldsymbol{x})$, solution of (2.2), and the incident field $u^{(0)}(t, \boldsymbol{x})$ which is the solution of the wave equation (2.2) in the absence of the target ($\varrho_T = 0$),

$$\frac{1}{c_o^2} \frac{\partial^2 u^{(0)}}{\partial t^2} - \Delta u^{(0)} = f(t)\delta(\boldsymbol{x} - \boldsymbol{X}_E). \tag{2.3}$$

The incident field has the form

$$u^{(0)}(t, \boldsymbol{x}) = \int_0^t d\tau f(\tau) G(t - \tau, \boldsymbol{x}, \boldsymbol{X}_E), \tag{2.4}$$

where $G(t, \boldsymbol{X}, \boldsymbol{Y})$ denotes the Green's function, that is the response recorded at point $\boldsymbol{X}$ when a Dirac pulse is sent from point $\boldsymbol{Y}$ at time zero. In a homogeneous medium, the Green's function is given by

$$G(t, \boldsymbol{X}, \boldsymbol{Y}) = \frac{1}{4\pi\, |\boldsymbol{X} - \boldsymbol{Y}|} \delta\left(t - \frac{|\boldsymbol{X} - \boldsymbol{Y}|}{c_o}\right). \tag{2.5}$$

Copyright © by SIAM. Unauthorized reproduction of this article is prohibited.

Downloaded 11/28/17 to 171.67.216.21. Redistribution subject to SIAM license or copyright; see http://www.siam.org/journals/ojsa.php

Using this expression in (2.4) we obtain

$$u^{(0)}(t,\boldsymbol{x}) = \frac{1}{4\pi\,|\boldsymbol{x}-\boldsymbol{X}_E|} f\left(t - \frac{|\boldsymbol{x}-\boldsymbol{X}_E|}{c_o}\right). \tag{2.6}$$

From (2.2) and (2.3) we deduce that the scattered field $u^{(1)}(t,\boldsymbol{x}) = u(t,\boldsymbol{x}) - u^{(0)}(t,\boldsymbol{x})$ is a solution of

$$\frac{1}{c_o^2}\frac{\partial^2 u^{(1)}}{\partial t^2} - \Delta u^{(1)} = -\frac{1}{c_o^2}\varrho_T(\boldsymbol{x}-\boldsymbol{X}_T(t))\frac{\partial^2(u^{(0)}+u^{(1)})}{\partial t^2}(t,\boldsymbol{x}),$$

so that

$$u^{(1)}(t,\boldsymbol{x}) = -\frac{1}{c_o^2}\int_0^t d\tau \int d\boldsymbol{y} G(t-\tau,\boldsymbol{x},\boldsymbol{y})\varrho_T(\boldsymbol{y}-\boldsymbol{X}_T(\tau))\frac{\partial^2}{\partial\tau^2}(u^{(0)}+u^{(1)})(\tau,\boldsymbol{y}).$$

In the Born approximation, we can neglect $u^{(1)}$ on the right-hand side, so that

$$u^{(1)}(t,\boldsymbol{x}) = -\frac{1}{c_o^2}\int_0^t d\tau \int d\boldsymbol{y} G(t-\tau,\boldsymbol{x},\boldsymbol{y})\varrho_T(\boldsymbol{y}-\boldsymbol{X}_T(\tau))\frac{\partial^2}{\partial\tau^2}u^{(0)}(\tau,\boldsymbol{y}).$$

In the pointlike approximation for the scatterer, we find that $u^{(1)}$ is given by

$$u^{(1)}(t,\boldsymbol{x}) = -\frac{\rho}{c_o^2}\int_0^t d\tau G(t-\tau,\boldsymbol{x},\boldsymbol{X}_T(\tau))\frac{\partial^2}{\partial\tau^2}u^{(0)}(\tau,\boldsymbol{y})\mid_{\boldsymbol{y}=\boldsymbol{X}_T(\tau)},$$

where $\rho = \int \varrho_T(\boldsymbol{x})d\boldsymbol{x}$ is the reflectivity of the target. Substituting the expression for $u^{(0)}$ and integrating by parts twice, we obtain

$$u^{(1)}(t,\boldsymbol{x}) = -\frac{\rho}{c_o^2}\int_0^t d\tau \int_0^\tau d\tau' f''(\tau')G(\tau-\tau',\boldsymbol{X}_T(\tau),\boldsymbol{X}_E)G(t-\tau,\boldsymbol{x},\boldsymbol{X}_T(\tau)).$$

Therefore the scattered field recorded by the receiver at $\boldsymbol{x} = \boldsymbol{X}_R$ has the form

$$\begin{aligned} u_{\mathrm{s},R}(t) = -\frac{\rho}{c_o^2}\int_0^t d\tau \frac{1}{4\pi|\boldsymbol{X}_T(\tau)-\boldsymbol{X}_E|} f''\left(\tau - \frac{|\boldsymbol{X}_T(\tau)-\boldsymbol{X}_E|}{c_o}\right) \\ \times \frac{1}{4\pi|\boldsymbol{X}_R-\boldsymbol{X}_T(\tau)|}\delta\left(t-\tau-\frac{|\boldsymbol{X}_R-\boldsymbol{X}_T(\tau)|}{c_o}\right). \end{aligned}$$

If we introduce

$$\Phi(\tau;t) = t - \tau - \frac{|\boldsymbol{Y}_T - \boldsymbol{X}_R + \tau\boldsymbol{V}_T|}{c_o},$$

then we have

$$\delta\left[\Phi(\tau;t)\right] = \frac{\delta[\tau-\tau(t)]}{|\partial_\tau\Phi(\tau(t);t)|},$$

with $\tau(t)$ the unique zero of $\tau \to \Phi(\tau;t)$ in $(0,t)$. Denoting

$$\boldsymbol{D}(t) = \boldsymbol{Y}_T - \boldsymbol{X}_R + t\boldsymbol{V}_T, \tag{2.7}$$

Copyright © by SIAM. Unauthorized reproduction of this article is prohibited.

Downloaded 11/28/17 to 171.67.216.21. Redistribution subject to SIAM license or copyright; see http://www.siam.org/journals/ojsa.php

we write

$$\begin{aligned}\Phi(\tau;t) &= t-\tau-\frac{|\boldsymbol{Y}_T-\boldsymbol{X}_R+\tau\boldsymbol{V}_T|}{c_o}\\ &= t-\tau-\frac{|\boldsymbol{Y}_T-\boldsymbol{X}_R+t\boldsymbol{V}_T-(t-\tau)\boldsymbol{V}_T|}{c_o}\\ &= t-\tau-\frac{|\boldsymbol{D}(t)-(t-\tau)\boldsymbol{V}_T|}{c_o}.\end{aligned}$$

The unique zero of $\tau\to\Phi(\tau;t)$ in $(0,t)$, can be found as the root of the quadratic equation

$$(t-\tau)^2\left(1-\frac{|\boldsymbol{V}_T|^2}{c_o^2}\right)+2(t-\tau)\frac{\boldsymbol{V}_T}{c_o}\cdot\frac{\boldsymbol{D}(t)}{c_o}-\frac{|\boldsymbol{D}(t)|^2}{c_o^2}=0.$$

We find that $\tau(t)$ is given by

$$\tau(t)=t-\frac{|\boldsymbol{D}(t)|}{c_o\big(1-\big|\frac{\boldsymbol{V}_T}{c_o}\big|^2\big)}\left[\sqrt{1-\left|\frac{\boldsymbol{V}_T}{c_o}\right|^2+\left(\frac{\boldsymbol{V}_T}{c_o}\cdot\frac{\boldsymbol{D}(t)}{|\boldsymbol{D}(t)|}\right)^2}-\frac{\boldsymbol{V}_T}{c_o}\cdot\frac{\boldsymbol{D}(t)}{|\boldsymbol{D}(t)|}\right]. \tag{2.8}$$

We also have

$$|\partial_\tau\Phi(\tau(t);t)|=\left|1+\frac{\boldsymbol{V}_T}{c_o}\cdot\frac{\boldsymbol{D}(\tau(t))}{|\boldsymbol{D}(\tau(t))|}\right|.$$

Substituting into the expression for $u_{\mathrm{s},R}(t)$ we obtain

$$u_{\mathrm{s},R}(t)=-\frac{\rho f''\Big(\tau(t)-\frac{|\boldsymbol{X}_T(\tau(t))-\boldsymbol{X}_E|}{c_o}\Big)}{(4\pi)^2c_o^2|\boldsymbol{X}_T(\tau(t))-\boldsymbol{X}_E||\boldsymbol{X}_R-\boldsymbol{X}_T(\tau(t))|\left|1+\frac{\boldsymbol{V}_T}{c_o}\cdot\frac{\boldsymbol{D}(\tau(t))}{|\boldsymbol{D}(\tau(t))|}\right|}. \tag{2.9}$$

This is the Born approximation for the scattered field. The forward model that we use to compute the data is based on $u_{\mathrm{s},R}(t)$ given by (2.9) since it is only the scattered field that is used in imaging.

2.3. Doppler factors. To construct an imaging function it is important to identify the Doppler factors that affect the measurements. Here we assume that the transmitter at $\boldsymbol{X}_E$ emits the pulse $f(\cdot-s)$ around time s. We want to consider the structure of the received signal at time $t+s$ for t in a small time window with width ΔT. We denote by H_T the typical altitude of the target.

Assuming $|\boldsymbol{V}_T|\ll c_o$, $|\boldsymbol{V}_T|\Delta T\ll H_T$, and $|\boldsymbol{V}_T|^2\Delta T^2\ll\lambda_o H_T$, we can expand the distances and neglect the quadratic terms in $|\boldsymbol{V}_T|/c_o$ to obtain

$$\begin{aligned}|\boldsymbol{X}_T(s+t)-\boldsymbol{X}_E| &\approx |\boldsymbol{X}_T(s)-\boldsymbol{X}_E|+t\boldsymbol{V}_T\cdot\frac{\boldsymbol{X}_T(s)-\boldsymbol{X}_E}{|\boldsymbol{X}_T(s)-\boldsymbol{X}_E|},\\ |\boldsymbol{X}_T(s+t)-\boldsymbol{X}_R| &\approx |\boldsymbol{X}_T(s)-\boldsymbol{X}_R|+t\boldsymbol{V}_T\cdot\frac{\boldsymbol{X}_T(s)-\boldsymbol{X}_R}{|\boldsymbol{X}_T(s)-\boldsymbol{X}_R|}.\end{aligned}$$

Copyright © by SIAM. Unauthorized reproduction of this article is prohibited.

As the target position is $\boldsymbol{X}_T(s) = \boldsymbol{Y}_T + s\boldsymbol{V}_T$, and as $\|f'''\|_\infty \sim \omega_o^3 \|F\|_{W^{\infty,3}} \sim \omega_o \|f''\|_\infty$, we can approximate (2.9) as follows:

$$u_{\mathrm{s},R}(s+t) = -\frac{\rho f''\Big(s + \gamma_{\mathrm{s}}(\boldsymbol{X}_T(s), \boldsymbol{V}_T, \boldsymbol{X}_R)t - t_{\mathrm{s}}(\boldsymbol{X}_T(s), \boldsymbol{V}_T, \boldsymbol{X}_R)\Big)}{(4\pi c_o |\boldsymbol{X}_T(s)|)^2} + o\left(\frac{\rho \|f''\|}{4\pi H_T^2}\right) \tag{2.10}$$

with

$$\gamma_{\mathrm{s}}(\boldsymbol{X}, \boldsymbol{V}, \boldsymbol{X}_R) = 1 - \frac{\boldsymbol{V}}{c_o} \cdot \left(\frac{\boldsymbol{X} - \boldsymbol{X}_E}{|\boldsymbol{X} - \boldsymbol{X}_E|} + \frac{\boldsymbol{X} - \boldsymbol{X}_R}{|\boldsymbol{X} - \boldsymbol{X}_R|}\right) \tag{2.11}$$

and

$$t_{\mathrm{s}}(\boldsymbol{X}, \boldsymbol{V}, \boldsymbol{X}_R) = \frac{|\boldsymbol{X} - \boldsymbol{X}_E|}{c_o} + \frac{|\boldsymbol{X} - \boldsymbol{X}_R|}{c_o} \gamma_{\mathrm{s}}(\boldsymbol{X}, \boldsymbol{V}, \boldsymbol{X}_R). \tag{2.12}$$

From (2.10), we see that the scattered signal recorded at $\boldsymbol{X}_R$ is essentially a pulse received at the sum of travel times from the transmitter to the target and from the target to the receiver, up to some modification due to the Doppler effect which is characterized by the Doppler factor γ_{s}. We note that γ_{s} is very close to one because the target velocity, while large, is still much smaller than the velocity of light c_o.

As we will see next, the expression (2.10) of the scattered signal is the key element used to design our imaging function.

3. Imaging methods.

In this section we describe two imaging methods, the matched-filter one, which is the standard imaging method for this problem and a correlation-based imaging approach. Let us first describe the data gathering process to gain some insight on how an imaging function should process the available data.

During the observation time window $(-T_{\mathrm{tot}}/2, T_{\mathrm{tot}}/2)$ the transmitter emits a large number $N_E = [T_{\mathrm{tot}}/\Delta T_E]$ of pulses $f(t - S_j)$ around times $S_j = j\Delta T_E$, $j = -N_E/2, \ldots, N_E/2 - 1$. The N receivers record the scattered signals $u_{\mathrm{s},R}(S_j + t)$, $R = 1, \ldots, N$, during a time interval that is long enough to capture the scattered signals, but smaller than ΔT_E. This is the input data set that we use to image the moving target. Note that we consider here a transmitter that emits a large number of short pulses $f(t - S_j)$ whose support is of the order of $1/B$ with B being the bandwidth. This is different than the chirped pulses which are usually used in radar for achieving a good signal-to-noise ratio. In terms of resolution, however, the results are the same whether a train of chirped pulses or a train of short pulses is used.

Specifically, we consider the regime in which

$$1/B \ll 2H_T/c_o \ll \Delta T_E \ll T_{\mathrm{tot}}$$

with $1/B$ the pulse duration, $2H_T/c_o$ the round trip time from the ground to the target, ΔT_E the time spacing between two pulses, and T_{tot} the total duration.

We also assume that

$$\lambda_o \ll |\boldsymbol{V}_T| T_{\mathrm{tot}} \sim a \sim |\boldsymbol{X}_E| \ll H_T,$$

where H_T is the typical altitude of the target.

The specific assumptions under which our resolution analysis is carried out are summarized in Hypothesis 1 (section 4.1) for the matched-filter and in Hypothesis 2 (section 4.2) for the correlation-based imaging function.

Copyright © by SIAM. Unauthorized reproduction of this article is prohibited.

Downloaded 11/28/17 to 171.67.216.21. Redistribution subject to SIAM license or copyright; see http://www.siam.org/journals/ojsa.php

Downloaded 11/28/17 to 171.67.216.21. Redistribution subject to SIAM license or copyright; see http://www.siam.org/journals/ojsa.php

We can see from (2.10) that the received signals have the form of pulses, time delayed and scaled by specific Doppler factors. A matched filter or a correlation-based imaging function must compensate for these Doppler factors, as in [17, 19] or [20, 21]. Since the Doppler factors depend on the receiver and target positions, they can be estimated locally and that is why we will first introduce a small-aperture imaging function and then form an imaging function from a sum of such terms.

3.1. The matched-filter imaging function. The idea behind the matched-filter imaging function is that we want to match the received signal with the emitted pulse. The matching process involves the assumed initial position and speed of the object $(\boldsymbol{Y}, \boldsymbol{V})$, and this matching can be shown to be maximal at the true position $(\boldsymbol{Y}_T, \boldsymbol{V}_T)$. The matching process takes into account the Doppler compensation factor $\gamma_{\mathrm{s}}(\boldsymbol{X}, \boldsymbol{V}, \boldsymbol{X}_R)$,

(3.1)
$$\mathcal{I}^{\mathrm{MF}}(\boldsymbol{Y}, \boldsymbol{V}) = \frac{1}{N_E} \sum_{j=1}^{N_E} \mathcal{I}_j^{\mathrm{MF}}(\boldsymbol{Y} + \boldsymbol{V} S_j, \boldsymbol{V}),$$

(3.2)
$$\mathcal{I}_j^{\mathrm{MF}}(\boldsymbol{X}, \boldsymbol{V}) = \frac{1}{N} \sum_{R=1}^{N} \int f\left(\gamma_{\mathrm{s}}(\boldsymbol{X}, \boldsymbol{V}, \boldsymbol{X}_R)\left(t - \frac{|\boldsymbol{X} - \boldsymbol{X}_R|}{c_o}\right) - \frac{|\boldsymbol{X} - \boldsymbol{X}_E|}{c_o}\right) u_{\mathrm{s},R}(S_j + t) dt.$$

This imaging function requires knowledge of the transmitter and receiver positions $\boldsymbol{X}_E$ and $\boldsymbol{X}_R$. We also need to know the pulse profile f. In practice, if one wants to image a region around some point $\boldsymbol{Y}_T$, then the jth scattered signal needs only to be recorded during a short time around $2|\boldsymbol{Y}_T - \boldsymbol{X}_E|/c_o$. The pulse profile could be different from one pulse emission to another one, meaning that f may depend on j, but in that case, it is necessary to know all the emitted pulses. An equivalent version of matched filter can be obtained with the following change of variable $t \to |\boldsymbol{X} - \boldsymbol{X}_R|/c_o + (t + |\boldsymbol{X} - \boldsymbol{X}_E|/c_o)/\gamma_{\mathrm{s}}(\boldsymbol{X}, \boldsymbol{V}, \boldsymbol{X}_R)$,

(3.3)
$$\mathcal{I}_j^{\mathrm{MF}}(\boldsymbol{X}, \boldsymbol{V}) = \frac{1}{N} \sum_{R=1}^{N} \int f(t) u_{\mathrm{s},R}\left(S_j + \frac{|\boldsymbol{X} - \boldsymbol{X}_R|}{c_o} + \frac{t + \frac{|\boldsymbol{X} - \boldsymbol{X}_E|}{c_o}}{\gamma_{\mathrm{s}}(\boldsymbol{X}, \boldsymbol{V}, \boldsymbol{X}_R)}\right) dt.$$

3.2. The correlation-based imaging function. The correlation-based imaging function cross correlates the scattered signals recorded by pairs of receivers and migrates them with the appropriate Doppler compensation factors,

(3.4)
$$\mathcal{I}^{\mathrm{CC}}(\boldsymbol{Y}, \boldsymbol{V}) = \frac{1}{N_E} \sum_{j=1}^{N_E} \mathcal{I}_j^{\mathrm{CC}}(\boldsymbol{Y} + \boldsymbol{V} S_j, \boldsymbol{V}),$$

$$\mathcal{I}_j^{\mathrm{CC}}(\boldsymbol{X}, \boldsymbol{V}) = \frac{1}{N^2} \sum_{R,R'=1}^{N} \int u_{\mathrm{s},R}\left(S_j + \frac{|\boldsymbol{X} - \boldsymbol{X}_R|}{c_o} + \frac{t + \frac{|\boldsymbol{X} - \boldsymbol{X}_E|}{c_o}}{\gamma_{\mathrm{s}}(\boldsymbol{X}, \boldsymbol{V}, \boldsymbol{X}_R)}\right)$$

(3.5)
$$\times\, u_{\mathrm{s},R'}\left(S_j + \frac{|\boldsymbol{X} - \boldsymbol{X}_{R'}|}{c_o} + \frac{t + \frac{|\boldsymbol{X} - \boldsymbol{X}_E|}{c_o}}{\gamma_{\mathrm{s}}(\boldsymbol{X}, \boldsymbol{V}, \boldsymbol{X}_{R'})}\right) dt.$$

Copyright © by SIAM. Unauthorized reproduction of this article is prohibited.

Downloaded 11/28/17 to 171.67.216.21. Redistribution subject to SIAM license or copyright; see http://www.siam.org/journals/ojsa.php

For the correlation-based imaging function, it is not necessary to know the pulse profile f which could be different from one emission to another one. It is not necessary either to know the emission times with accuracy but we need to record the whole train of scattered signals. This is because the correlation-based imaging function is formed by migrating the cross correlations of the scattered signals over all receiver pairs $R-R'$ as can be seen in (3.4)–(3.5). Therefore the whole train of the scattered signals is needed to form the $\mathcal{I}^{\rm CC}$ image. Moreover correlation-based imaging has been shown to be robust to medium fluctuations when in a suitable imaging configuration [9, 11, 10].

The correlation-based imaging function does not depend on the transmitter position $\boldsymbol{X}_E$, as can be seen by the change of variable $t \to t - |\boldsymbol{X} - \boldsymbol{X}_E|/c_o$:

$$\mathcal{I}_j^{\rm CC}(\boldsymbol{X},\boldsymbol{V}) = \frac{1}{N^2}\sum_{R,R'=1}^{N}\int u_{{\rm s},R}\left(S_j + \frac{|\boldsymbol{X}-\boldsymbol{X}_R|}{c_o} + \frac{t}{\gamma_{\rm s}(\boldsymbol{X},\boldsymbol{V},\boldsymbol{X}_R)}\right) \times u_{{\rm s},R'}\left(S_j + \frac{|\boldsymbol{X}-\boldsymbol{X}_{R'}|}{c_o} + \frac{t}{\gamma_{\rm s}(\boldsymbol{X},\boldsymbol{V},\boldsymbol{X}_{R'})}\right) dt. \tag{3.6}$$

Depending on our knowledge regarding the pulse train and the receiving system's memory/computation capacity we may consider other correlation-based imaging functions. We refer to Appendix A for some different choices of correlation-based imaging functions.

Remark 1. We do not use in this paper the analytic signal convention which is typically used in radar. We consider instead a real compactly supported signal in time as in (2.1) and keep both positive and negative frequencies. We find that following this convention, used in geophysics and elsewhere, simplifies the presentation. If instead one uses the analytic signal, the time domain signal is complex and therefore the cross-correlation should be defined with one of the two signals being complex conjugated. The resolution estimates, however, are the same independently of the convention used.

4. Resolution analysis.

In this section we derive the resolution properties of both the matched-filter and the correlation-based imaging functions. To determine the important scales for our imaging problem we first recall the typical values for the different parameters appearing in the imaging setup.

Parameter regime for the resolution analysis. We want to image the location and velocity of a fast moving object, such as a satellite or a piece of debris, that moves at a low orbit around the earth. A typical value for the height of the orbit is $H_T = 5\cdot 10^5$ m and the speed for such objects is $V_T = 7\cdot 10^3$ m/s. The source that we use for imaging is located on the ground and is emitting a train of pulses f with relatively large bandwidth $B = 0.6\cdot 10^9$ Hz at a high central frequency $f_o = 10\cdot 10^9$ Hz (X-band). We assume that the scattered field can be recorded at a large number of receivers over an area on the ground of diameter $a = 1.7\cdot 10^5$ m. The time duration of the recordings is of order $T_{\rm tot} = 11$ s. Let us also recall the speed of light $c_o = 3\ 10^8$ m/s. These values are given here as a specific case and it is easy to check that the hypotheses we made so far are satisfied with this set of values. In the following, the theoretical assumptions are always made explicit and are not tied to this particular set of parameters. The orders of magnitude are only mentioned here to motivate our ordering hypotheses, and

Copyright © by SIAM. Unauthorized reproduction of this article is prohibited.

Table 1
Typical values of the parameters for our imaging configuration.

V_T	$7 \cdot 10^3$ m/s
H_T	$5 \cdot 10^5$ m
a	$1.7 \cdot 10^5$ m
B	$0.6 \cdot 10^9$ Hz
f_o	$10 \cdot 10^9$ Hz
c_o	$3 \cdot 10^8$ m/s
T_{tot}	11 s

to show that such hypotheses are indeed reasonable. The values of the parameters are also summarized in Table 1.

4.1. The matched-filter imaging function. We use the expression (2.10) of the scattered field and the following elementary formula,

$$f(\alpha t+\beta)=\frac{1}{2\pi\alpha}\int_{\mathbb{R}}\widehat{f}\left(\frac{\omega}{\alpha}\right)\exp\left(-i\left(t+\frac{\beta}{\alpha}\right)\omega\right)d\omega \quad \text{for } \alpha>0 \text{ and } \beta\in\mathbb{R}$$

with $\widehat{f}$ denoting the Fourier transform defined as

$$\widehat{f}(\omega)=\int_{\mathbb{R}} f(t)\exp(i\omega t)dt,$$

to write the partial imaging function (3.2) in the Fourier domain as

$$\mathcal{I}_j^{\mathrm{MF}}(\boldsymbol{X},\boldsymbol{V})=\frac{k_o^2\rho}{(4\pi|\boldsymbol{X}_T|)^2}\frac{1}{2\pi N}\sum_{R=1}^{N}\int_{\mathbb{R}}d\omega\,\overline{\widehat{f}\Big(\frac{\omega}{\gamma_{\mathrm{s}}(\boldsymbol{X},\boldsymbol{V},\boldsymbol{X}_R)}\Big)}\,\widehat{f}\left(\frac{\omega}{\gamma_{\mathrm{s}}(\boldsymbol{X}_T,\boldsymbol{V}_T,\boldsymbol{X}_R)}\right)$$
$$\times\exp\left(i\frac{\omega}{c_o}\left(\frac{|\boldsymbol{X}_T-\boldsymbol{X}_E|}{\gamma_{\mathrm{s}}(\boldsymbol{X}_T,\boldsymbol{V}_T,\boldsymbol{X}_R)}-\frac{|\boldsymbol{X}-\boldsymbol{X}_E|}{\gamma_{\mathrm{s}}(\boldsymbol{X},\boldsymbol{V},\boldsymbol{X}_R)}+|\boldsymbol{X}_T-\boldsymbol{X}_R|-|\boldsymbol{X}-\boldsymbol{X}_R|\right)\right).$$

Using that $\frac{\omega_o}{B}\frac{|\boldsymbol{V}_T|}{c_o}=o(1)$, we can approximate $\widehat{f}(\frac{\omega}{\gamma_{\mathrm{s}}(\boldsymbol{X},\boldsymbol{V},\boldsymbol{X}_R)})$ by $\widehat{f}(\omega)$ in the expression above. Moreover, assuming that $\frac{\omega_o H_T}{c_o}\frac{|\boldsymbol{V}_T|^2}{c_o^1}\ll 1$, then $\frac{1}{\gamma_{\mathrm{s}}}$ needs only to be expanded up to first order inside the exponential and this leads to

$$\mathcal{I}_j^{\mathrm{MF}}(\boldsymbol{X},\boldsymbol{V})\approx\frac{k_o^2\rho}{(4\pi|\boldsymbol{X}_T|)^2}\frac{1}{2\pi N}\sum_{R=1}^{N}\int_{\mathbb{R}}d\omega|\widehat{f}(\omega)|^2$$
$$\times\exp\left(i\frac{\omega}{c_o}\big(|\boldsymbol{X}_T-\boldsymbol{X}_E|+|\boldsymbol{X}_T-\boldsymbol{X}_R|-|\boldsymbol{X}-\boldsymbol{X}_E|-|\boldsymbol{X}-\boldsymbol{X}_R|\right)$$
$$\times\exp\left(i\frac{\omega}{c_o}|\boldsymbol{X}_T-\boldsymbol{X}_E|\frac{\boldsymbol{V}_T}{c_o}\cdot\left(\frac{\boldsymbol{X}_T-\boldsymbol{X}_R}{|\boldsymbol{X}_T-\boldsymbol{X}_R|}+\frac{\boldsymbol{X}_T-\boldsymbol{X}_E}{|\boldsymbol{X}_T-\boldsymbol{X}_E|}\right)\right)$$
$$\times\exp\left(-i\frac{\omega}{c_o}|\boldsymbol{X}-\boldsymbol{X}_E|\frac{\boldsymbol{V}}{c_o}\cdot\left(\frac{\boldsymbol{X}-\boldsymbol{X}_R}{|\boldsymbol{X}-\boldsymbol{X}_R|}+\frac{\boldsymbol{X}-\boldsymbol{X}_E}{|\boldsymbol{X}-\boldsymbol{X}_E|}\right)\right).$$

Copyright © by SIAM. Unauthorized reproduction of this article is prohibited.

Downloaded 11/28/17 to 171.67.216.21. Redistribution subject to SIAM license or copyright; see http://www.siam.org/journals/ojsa.php

Downloaded 11/28/17 to 171.67.216.21. Redistribution subject to SIAM license or copyright; see http://www.siam.org/journals/ojsa.php

If the number of receivers is large enough, we can replace $\frac{1}{N}\sum_{R=1}^{N}$ by $\frac{1}{a^2}\int_{\mathbb{R}^2} d\boldsymbol{x}_R p(\boldsymbol{x}_R/a)$ in the expression for $\mathcal{I}_j^{\rm MF}(\boldsymbol{X},\boldsymbol{V})$. This effectively means that the data depend on 4 variables: the slow time S_j, the fast time t, and the surface of receivers $\boldsymbol{x}_R$. We assume further that $2\pi B < \omega_o$ and that the baseband pulse is symmetric and essentially supported in $[-2\pi, 2\pi]$ so that we can write

$$|\widehat{f}(\omega)|^2 = \frac{1}{B^2}\left|\widehat{F}\left(\frac{\omega-\omega_o}{B}\right)\right|^2 + \frac{1}{B^2}\left|\widehat{F}\left(\frac{\omega+\omega_o}{B}\right)\right|^2,$$

and using a change of variables by recentering and rescaling ω such that $\omega = \omega_o + B\tilde{\omega}$, $\tilde{\omega}$ being dimensionless, we get

$$|\widehat{f}(\omega_o + B\tilde{\omega})|^2 = \frac{1}{B^2}|\widehat{F}(\tilde{\omega})|^2.$$

Consequently, the expression for $\mathcal{I}_j^{\rm MF}(\boldsymbol{X},\boldsymbol{V})$ becomes

$$\begin{aligned}\mathcal{I}_j^{\rm MF}(\boldsymbol{X},\boldsymbol{V}) = \frac{k_o^2\rho}{32\pi^3|\boldsymbol{X}_T|^2 B a^2}\int_{\mathbb{R}^2} d\boldsymbol{x}_R p\left(\frac{\boldsymbol{x}_R}{a}\right)\int_{\mathbb{R}} d\tilde{\omega}|\widehat{F}(\tilde{\omega})|^2 \\ \times \exp\left(i\frac{\omega_o+B\tilde{\omega}}{c_o}\big(|\boldsymbol{X}_T-\boldsymbol{X}_E|+|\boldsymbol{X}_T-\boldsymbol{X}_R|-|\boldsymbol{X}-\boldsymbol{X}_E|-|\boldsymbol{X}-\boldsymbol{X}_R|\big)\right. \\ \times \exp\left(i\frac{\omega_o+B\tilde{\omega}}{c_o}|\boldsymbol{X}_T-\boldsymbol{X}_E|\frac{\boldsymbol{V}_T}{c_o}\cdot\left(\frac{\boldsymbol{X}_T-\boldsymbol{X}_R}{|\boldsymbol{X}_T-\boldsymbol{X}_R|}+\frac{\boldsymbol{X}_T-\boldsymbol{X}_E}{|\boldsymbol{X}_T-\boldsymbol{X}_E|}\right)\right) \\ \left.\times \exp\left(-i\frac{\omega_o+B\tilde{\omega}}{c_o}|\boldsymbol{X}-\boldsymbol{X}_E|\frac{\boldsymbol{V}}{c_o}\cdot\left(\frac{\boldsymbol{X}-\boldsymbol{X}_R}{|\boldsymbol{X}-\boldsymbol{X}_R|}+\frac{\boldsymbol{X}-\boldsymbol{X}_E}{|\boldsymbol{X}-\boldsymbol{X}_E|}\right)\right)\right)\end{aligned}$$

with $\boldsymbol{X}_R = (\boldsymbol{x}_R, 0)$ and $\boldsymbol{X}_T = \boldsymbol{X}_T(S_j) = \boldsymbol{Y}_T + \boldsymbol{V}_T S_j$.

In the expression of $\mathcal{I}_j^{\rm MF}(\boldsymbol{X},\boldsymbol{V})$ above we write only the first term corresponding to $\widehat{F}(\frac{\omega-\omega_o}{B})$. The second term is the complex conjugate of the first one and it does not bring any new information so it is omitted. We will follow this convention throughout the rest of the paper and omit systematically the second complex conjugate term from the imaging functions' expressions. Remark that the term which is at twice the carrier frequency ($2\omega_o$) vanishes when the bandwidth of $\widehat{F}$ is smaller than ω_o as is the case here.

We note that the partial imaging function, $\mathcal{I}_j^{\rm MF}(\boldsymbol{X},\boldsymbol{V})$, tries to match the measured sum of travel times $|\boldsymbol{X}_T-\boldsymbol{X}_E|+|\boldsymbol{X}_T-\boldsymbol{X}_R|$ by the candidate one $|\boldsymbol{X}-\boldsymbol{X}_E|+|\boldsymbol{X}-\boldsymbol{X}_R|$ corresponding to the target starting from point $\boldsymbol{X}$ in the search domain at time 0 and traveling with speed $\boldsymbol{V}$.

Our first main result is the following expression that determines the resolution of the matched-filter imaging function:

$$\begin{aligned}\left|\mathcal{I}^{\rm MF}(\boldsymbol{X},\boldsymbol{V})\right| = \frac{k_o^2\rho}{32\pi^3 H_T^2 B T_{\rm tot}}\left|\int_{-T_{\rm tot}/2}^{T_{\rm tot}/2} ds\int_{\mathbb{R}} d\tilde{\omega}|\widehat{F}(\tilde{\omega})|^2\frac{1}{a^2}\int_{\mathbb{R}^2} d\boldsymbol{x}_R p\left(\frac{\boldsymbol{x}_R}{a}\right)\right. \\ \left.\times\exp\Big(i(\Phi_{\mathcal{I}^{\rm MF}}+\epsilon_{\mathcal{I}^{\rm MF}})(\boldsymbol{Y}-\boldsymbol{Y}_T,\boldsymbol{V}-\boldsymbol{V}_T,\boldsymbol{X}_R,\boldsymbol{X}_E,s)\Big)\right|,\end{aligned} \tag{4.1}$$

Copyright © by SIAM. Unauthorized reproduction of this article is prohibited.

Downloaded 11/28/17 to 171.67.216.21. Redistribution subject to SIAM license or copyright; see http://www.siam.org/journals/ojsa.php

where the phase $\Phi_{\mathcal{I}^{\mathrm{MF}}}$ is given by

(4.2)
$$\begin{aligned}
&\Phi_{\mathcal{I}^{\mathrm{MF}}}(\boldsymbol{Y}-\boldsymbol{Y}_T,\boldsymbol{V}-\boldsymbol{V}_T,\boldsymbol{X}_R,s)\\
&\quad=\frac{\omega_o+\tilde{\omega}B}{c_o}\left(\frac{s}{H_T}\underbrace{\langle \boldsymbol{V}-\boldsymbol{V}_T,\boldsymbol{X}_R+\boldsymbol{X}_E\rangle_\perp}_{(\boldsymbol{V}_T)_\perp\text{resolution}}\right.\\
&\qquad\qquad-\frac{2}{H_T^2}\langle s\boldsymbol{V}_T,\boldsymbol{X}_R+\boldsymbol{X}_E\rangle_\perp\left(\underbrace{(\boldsymbol{Y}-\boldsymbol{Y}_T)_3}_{Y_3\text{ mixed aperture effect}}+s\underbrace{(\boldsymbol{V}-\boldsymbol{V}_T)_3}_{V_3\text{ mixed aperture effect}}\right)\\
&\qquad\qquad+\frac{1}{H_T}\underbrace{\langle \boldsymbol{Y}-\boldsymbol{Y}_T,\boldsymbol{X}_R+\boldsymbol{X}_E\rangle_\perp}_{\boldsymbol{Y}_\perp\text{ physical aperture effect}}\\
&\qquad\qquad-2s\underbrace{(\boldsymbol{V}-\boldsymbol{V}_T)_3}_{V_3\text{ ISAR effect}}-\frac{2s}{H_T}\underbrace{\langle \boldsymbol{Y}-\boldsymbol{Y}_T,\boldsymbol{V}_T\rangle_\perp}_{Y_2\text{ ISAR effect}}-\frac{2s^2}{H_T}\underbrace{\langle \boldsymbol{V}-\boldsymbol{V}_T,\boldsymbol{V}_T\rangle_\perp}_{V_2\text{ ISAR effect}}\\
&\qquad\qquad\left.-2\frac{\tilde{\omega}B}{c_o}\underbrace{(\boldsymbol{Y}-\boldsymbol{Y}_T)_3}_{Y_3\text{ bandwidth effect}}\right).
\end{aligned}$$

The derivation is presented in detail in Appendix B.2 and holds under the following hypotheses, which are actually verified for the typical values of the parameters shown in Table 1, as discussed below.

Hypothesis 1 (matched filter). *Our resolution analysis for the matched filter imaging function is valid under the following assumptions:*

- $\frac{a+T_{\mathrm{tot}}|\boldsymbol{V}_T|}{H_T}=o(1)$*; for the values of Table 1 we have* $\frac{a+T_{\mathrm{tot}}|\boldsymbol{V}_T|}{H_T}\approx 0.5$.
- $\frac{|\boldsymbol{V}_T|}{c_o}\ll(\frac{a+T_{\mathrm{tot}}|\boldsymbol{V}_T|}{H_T})^2$*, which is true since* $2.3\cdot 10^{-5}\ll 2.4\cdot 10^{-1}$.
- $\frac{H_T^2}{c_o(a+T_{\mathrm{tot}}|\boldsymbol{V}_T|)T_{\mathrm{tot}}}\ll 1$*, indeed we have* $3.1\cdot 10^{-4}\ll 1$.
- $\frac{\lambda_o}{H_T}\ll 16(\frac{a+T_{\mathrm{tot}}|\boldsymbol{V}_T|}{H_T})^4$*, which is verified as* $6.2\cdot 10^{-8}\ll 9.1\cdot 10^{-1}$.
- *Finally we assume that* $\frac{c_o}{2B}<\frac{4\lambda_o H_T^2}{(a+T_{\mathrm{tot}}|\boldsymbol{V}_T|)^2}$*, which is verified since* 25 *cm* $<$ 50 *cm.*

Under the above hypothesis we have $\epsilon_{\mathcal{I}^{\mathrm{MF}}}=o(\Phi_{\mathcal{I}^{\mathrm{MF}}})$. Our analysis is valid in the vicinity of the true target location and velocity, that is, for $|\boldsymbol{X}_T-\boldsymbol{X}|<\frac{4\lambda_o H_T^2}{(a+T_{\mathrm{tot}}|\boldsymbol{V}_T|)^2}$ ($\sim$ 50 cm) and for $|\boldsymbol{V}_T-\boldsymbol{V}|<\frac{\lambda_o H_T^2}{T_{\mathrm{tot}}(a+T_{\mathrm{tot}}|\boldsymbol{V}_T|)^2}$ ($\sim$ 1.1 10^{-2} m/s).

From (4.1), assuming $B\le\omega_o$, $\boldsymbol{V}_T\perp\boldsymbol{Y}_T$, and $\boldsymbol{X}_R\perp\boldsymbol{Y}_T$, we can assume that our frame is such that $e_3=\frac{\boldsymbol{Y}_T}{|\boldsymbol{Y}_T|}$, $e_2=\frac{\boldsymbol{V}_T}{|\boldsymbol{V}_T|}$, and set e_1 to be such that (e_1,e_2,e_3) is a direct orthonormal

Copyright © by SIAM. Unauthorized reproduction of this article is prohibited.

Table 2
Resolution estimates for the matched-filter imaging function.

Y_1	$\dfrac{\lambda_o H_T}{a}$	9 cm
Y_2	$\lambda_o \left(\dfrac{H_T}{a} \wedge \dfrac{H_T}{2\lvert \boldsymbol{V}_T \rvert T_{\rm tot}} \right)$	$9\text{ cm} \wedge 9.7\text{ cm} = 9\text{ cm}$
Y_3	$\dfrac{c_o}{2B} \wedge \lambda_o \dfrac{H_T^2}{2\lvert \boldsymbol{V}_T \rvert T_{\rm tot} a}$	$25\text{ cm} \wedge 29\text{ cm} = 25\text{ cm}$
V_1	$\dfrac{\lambda_o H_T}{a T_{\rm tot}}$	$8.2 \cdot 10^{-3}$ m/s
V_2	$\dfrac{\lambda_o}{T_{\rm tot}} \left(\dfrac{H_T}{a} \wedge \dfrac{H_T}{2\lvert \boldsymbol{V}_T \rvert T_{\rm tot}} \right)$	$8.2 \cdot 10^{-3}\text{ m/s} \wedge 8.9 \cdot 10^{-3}\text{ m/s} = 8.2 \cdot 10^{-3}\text{ m/s}$
V_3	$\dfrac{\lambda_o}{2T_{\rm tot}}$	$1.4 \cdot 10^{-3}$ m/s

basis of $\mathbb{R}^3$. Consequently, we obtain the resolution estimates summarized in Table 2. We note an ISAR influence in the resolution of Y_2 and V_2 seen as the dependence of the resolution on $|\boldsymbol{V}_T|T_{\rm tot}$, coming solely from the fact that the reflector is moving. We also note that the resolution in Y_1 and V_1 (and part of the resolution in Y_2 and V_2) depends only on the physical aperture covered by the receivers, that is, the parameter a. As for Y_3, the resolution obtained stems mainly from the fact that our signal has a substantial bandwidth together with a mixed ISAR/physical aperture effect. We call the mixed ISAR/physical aperture effect the terms of the type $\lambda_o \frac{H_T^2}{2|\boldsymbol{V}_T|T_{\rm tot} a}$, where both the physical aperture, a, and the ISAR aperture, $|\boldsymbol{V}_T|T_{\rm tot}$, appear. They are indicated in the the phase $\Phi_{\mathcal{I}^{\rm MF}}$ definition (4.2) by the term "mixed aperture effect." We see that a small bandwidth will lead to Y_3 recovered only by the mixed ISAR/physical aperture effect, while a large bandwidth would lead to a sharp point spread function in $(Y_T)_3$ determined by the term $c_o/(2B)$.

Remark 2. If we relax our assumptions $\boldsymbol{V}_T \perp \boldsymbol{Y}_T$ and $\boldsymbol{X}_R \perp \boldsymbol{Y}_T$, then we would obtain the corresponding ISAR and physical aperture terms in Y_3 and V_3 as well.

Remark 3. In (4.1), the Doppler compensation appears only in the term $\epsilon_{\mathcal{I}^{\rm MF}}$. This is because in the matched-filter (MF) imaging function we have accounted for the Doppler effect by dividing by the factor $\gamma_{\rm s}(\boldsymbol{X}, \boldsymbol{V}, \boldsymbol{X}_R)$ as can be seen in (3.3). This is adequate compensation since it cancels the corresponding factor appearing in (2.10) for $\boldsymbol{X}$ and $\boldsymbol{V}$ in the vicinity of the true values $\boldsymbol{X}_T(s)$ and $\boldsymbol{V}_T$. Therefore Doppler effects are mitigated and do not appear to play any role in the resolution of the imaging function. We should note however that without accounting and correcting for the Doppler effects the image would have been biased and not focused at the correct target location. The same is true for the correlation-based imaging function.

Copyright © by SIAM. Unauthorized reproduction of this article is prohibited.

Downloaded 11/28/17 to 171.67.216.21. Redistribution subject to SIAM license or copyright; see http://www.siam.org/journals/ojsa.php

Downloaded 11/28/17 to 171.67.216.21. Redistribution subject to SIAM license or copyright; see http://www.siam.org/journals/ojsa.php

4.2. The correlation-based imaging function. We use the expression (2.10) of the scattered field and write the partial imaging function (3.5) in the Fourier domain

$$\begin{aligned}\mathcal{I}_j^{\mathrm{CC}}(\boldsymbol{X},\boldsymbol{V}) = \frac{k_o^4\rho^2}{(4\pi|\boldsymbol{X}_T|)^4}\frac{1}{2\pi N^2}\sum_{R,R'=1}^{N}\int_{\mathbb{R}} d\omega\,\overline{\widehat{f}\Big(\frac{\omega\gamma_{\mathrm{s}}(\boldsymbol{X},\boldsymbol{V},\boldsymbol{X}_R)}{\gamma_{\mathrm{s}}(\boldsymbol{X}_T,\boldsymbol{V}_T,\boldsymbol{X}_R)}\Big)}\,\widehat{f}\left(\frac{\omega\gamma_{\mathrm{s}}(\boldsymbol{X},\boldsymbol{V},\boldsymbol{X}_{R'})}{\gamma_{\mathrm{s}}(\boldsymbol{X}_T,\boldsymbol{V}_T,\boldsymbol{X}_{R'})}\right)\\ \times\exp\left(i\frac{\omega}{c_o}\Big((|\boldsymbol{X}-\boldsymbol{X}_R|-|\boldsymbol{X}_T-\boldsymbol{X}_R|)\gamma_{\mathrm{s}}(\boldsymbol{X},\boldsymbol{V},\boldsymbol{X}_R)\right.\\ \left.+|\boldsymbol{X}-\boldsymbol{X}_E|-|\boldsymbol{X}_T-\boldsymbol{X}_E|\frac{\gamma_{\mathrm{s}}(\boldsymbol{X},\boldsymbol{V},\boldsymbol{X}_R)}{\gamma_{\mathrm{s}}(\boldsymbol{X}_T,\boldsymbol{V}_T,\boldsymbol{X}_R)}\Big)\right)\\ \times\exp\left(-i\frac{\omega}{c_o}\Big((|\boldsymbol{X}-\boldsymbol{X}_{R'}|-|\boldsymbol{X}_T-\boldsymbol{X}_{R'}|)\gamma_{\mathrm{s}}(\boldsymbol{X},\boldsymbol{V},\boldsymbol{X}_{R'})\right.\\ \left.+|\boldsymbol{X}-\boldsymbol{X}_E|-|\boldsymbol{X}_T-\boldsymbol{X}_E|\frac{\gamma_{\mathrm{s}}(\boldsymbol{X},\boldsymbol{V},\boldsymbol{X}_{R'})}{\gamma_{\mathrm{s}}(\boldsymbol{X}_T,\boldsymbol{V}_T,\boldsymbol{X}_{R'})}\Big)\right)\end{aligned}$$

with $\boldsymbol{X}_T$ defined as before by $\boldsymbol{X}_T = \boldsymbol{X}_T(S_j) = \boldsymbol{Y}_T + \boldsymbol{V}_T S_j$. It is immediate to see that $\mathcal{I}_j^{\mathrm{CC}}(\boldsymbol{X},\boldsymbol{V})$ reduces to

$$\begin{aligned}\mathcal{I}_j^{\mathrm{CC}}(\boldsymbol{X},\boldsymbol{V}) = \frac{k_o^4\rho^2}{(4\pi|\boldsymbol{X}_T|)^4}\frac{1}{2\pi N^2}\sum_{R,R'=1}^{N}\int_{\mathbb{R}} d\omega\,\overline{\widehat{f}\Big(\frac{\omega\gamma_{\mathrm{s}}(\boldsymbol{X},\boldsymbol{V},\boldsymbol{X}_R)}{\gamma_{\mathrm{s}}(\boldsymbol{X}_T,\boldsymbol{V}_T,\boldsymbol{X}_R)}\Big)}\,\widehat{f}\left(\frac{\omega\gamma_{\mathrm{s}}(\boldsymbol{X},\boldsymbol{V},\boldsymbol{X}_{R'})}{\gamma_{\mathrm{s}}(\boldsymbol{X}_T,\boldsymbol{V}_T,\boldsymbol{X}_{R'})}\right)\\ \times\exp\left(i\frac{\omega}{c_o}\big(|\boldsymbol{X}-\boldsymbol{X}_R|-|\boldsymbol{X}_T-\boldsymbol{X}_R|\big)\gamma_{\mathrm{s}}(\boldsymbol{X},\boldsymbol{V},\boldsymbol{X}_R)\right)\\ \times\exp\left(-i\frac{\omega}{c_o}\big(|\boldsymbol{X}-\boldsymbol{X}_{R'}|-|\boldsymbol{X}_T-\boldsymbol{X}_{R'}|\big)\gamma_{\mathrm{s}}(\boldsymbol{X},\boldsymbol{V},\boldsymbol{X}_{R'})\right)\\ \times\exp\left(i\frac{\omega}{c_o}|\boldsymbol{X}_T-\boldsymbol{X}_E|\left(\frac{\gamma_{\mathrm{s}}(\boldsymbol{X},\boldsymbol{V},\boldsymbol{X}_{R'})}{\gamma_{\mathrm{s}}(\boldsymbol{X}_T,\boldsymbol{V}_T,\boldsymbol{X}_{R'})}-\frac{\gamma_{\mathrm{s}}(\boldsymbol{X},\boldsymbol{V},\boldsymbol{X}_R)}{\gamma_{\mathrm{s}}(\boldsymbol{X}_T,\boldsymbol{V}_T,\boldsymbol{X}_R)}\right)\right).\end{aligned}$$

Our second main result is the following expression which determines the resolution of the correlation-based imaging function,

(4.3)
$$\begin{aligned}\mathcal{I}^{\mathrm{CC}}(\boldsymbol{X},\boldsymbol{V}) = \frac{k_o^4\rho^2}{(4\pi|\boldsymbol{X}_T|)^4 2\pi B a^4 T_{\mathrm{tot}}}\int_{-T_{\mathrm{tot}}/2}^{T_{\mathrm{tot}}/2} ds\int_{\mathbb{R}} d\tilde{\omega}|\widehat{F}(\tilde{\omega})|^2\\ \times\left|\int_{\mathbb{R}^2} d\boldsymbol{x}_R p\left(\frac{\boldsymbol{x}_R}{a}\right)\exp\left(i(\psi_{\mathcal{I}^{\mathrm{CC}}}+\epsilon_{\mathcal{I}^{\mathrm{CC}}})(\boldsymbol{Y}-\boldsymbol{Y}_T,\boldsymbol{V}-\boldsymbol{V}_T,\boldsymbol{X}_R,s,\tilde{\omega})\right)\right|^2,\end{aligned}$$

Copyright © by SIAM. Unauthorized reproduction of this article is prohibited.

Table 3
Resolution estimates for the correlation-based imaging function.

$\boldsymbol{Y}_\perp$	$\dfrac{\lambda_o H_T}{a}$	9.2 cm
Y_3	$\lambda_o \left(\dfrac{H_T^2}{a^2} \wedge \dfrac{2H_T^2}{a\lvert \boldsymbol{V}_T \rvert T_{\rm tot}} \right)$	27 cm $\wedge$ 1.2m $=$ 27 cm
$\boldsymbol{V}_\perp$	$\dfrac{\lambda_o H_T}{a T_{\rm tot}}$	$8.2 \cdot 10^{-3}$ m/s
V_3	$\dfrac{\lambda_o}{T_{\rm tot}} \left(\dfrac{H_T^2}{a^2} \wedge \dfrac{2H_T^2}{a\lvert \boldsymbol{V}_T \rvert T_{\rm tot}} \right)$	$2.5 \cdot 10^{-2}$m/s $\wedge$ $1.1 \cdot 10^{-1}$ m/s $= 2.5 \cdot 10^{-2}$ m/s

where the phase $\psi_{\mathcal{I}^{\rm CC}}$ is defined by

$$
\begin{aligned}
&\psi_{\mathcal{I}^{\rm CC}}(\boldsymbol{Y}-\boldsymbol{Y}_T, \boldsymbol{V}-\boldsymbol{V}_T, \boldsymbol{X}_R, s, \tilde{\omega}) \\
&\quad = \frac{\omega_o + B\tilde{\omega}}{c_o} \left(\frac{1}{H_T} \underbrace{\langle \boldsymbol{Y}-\boldsymbol{Y}_T, -\boldsymbol{X}_R \rangle_\perp}_{\boldsymbol{Y}_T \text{ physical aperture effect}} \right. \\
&\qquad - \frac{1}{2H_T^2} \underbrace{(\boldsymbol{Y}-\boldsymbol{Y}_T)_3}_{Y_3 \text{ physical aperture effect}} |\boldsymbol{X}_R|_\perp^2 + \frac{s}{H_T} \underbrace{\langle \boldsymbol{V}-\boldsymbol{V}_T, -\boldsymbol{X}_R \rangle_\perp}_{\boldsymbol{V}_T \text{ ISAR effect}} \\
&\qquad + \frac{s}{2H_T^2} \underbrace{(\boldsymbol{Y}-\boldsymbol{Y}_T)_3}_{Y_3 \text{ mixed aperture effect}} \langle \boldsymbol{V}_T, \boldsymbol{X}_R \rangle_\perp \\
&\qquad \left. + \frac{s^2}{2H_T^2} \underbrace{(\boldsymbol{V}-\boldsymbol{V}_T)_3}_{V_3 \text{ mixed effect}} \langle \boldsymbol{V}_T, \boldsymbol{X}_R \rangle_\perp + \frac{s}{2H_T^2} \underbrace{(\boldsymbol{V}-\boldsymbol{V}_T)_3}_{V_3 \text{ mixed effect}} |\boldsymbol{X}_R|_\perp^2 \right).
\end{aligned}
\tag{4.4}
$$

The details of the derivation are given in Appendix B.3. As for the MF, we call the "physical aperture effect" the terms where the physical aperture a appears, the "ISAR effect" the terms where the synthetic ISAR aperture due to the movement of the object $|\boldsymbol{V}_T|T_{\rm tot}$ appears, and "mixed ISAR/physical aperture effect" the terms where the product $|\boldsymbol{V}_T|T_{\rm tot}a$ of the physical aperture and the ISAR aperture appears. This expression is obtained under the following hypotheses, which are verified for the typical values of the parameters shown in Table 1, as discussed below.

Hypothesis 2 (correlation-based imaging). *Our resolution analysis for the correlation-based imaging function is valid under the following assumptions:*

- $\frac{a+T_{\rm tot}|\boldsymbol{V}_T|}{H_T} = o(1)$, *this is the same as for the MF imaging.*
- $\frac{|\boldsymbol{V}_T|}{c_o} \ll \frac{a+T_{\rm tot}|\boldsymbol{V}_T|}{H_T}$, *which is true since* $2.3 \cdot 10^{-5} \ll 0.5$.

Under the above assumptions, we get $\epsilon_{\mathcal{I}^{\rm CC}}(\boldsymbol{Y}-\boldsymbol{Y}_T, \boldsymbol{V}-\boldsymbol{V}_T, \boldsymbol{X}_R, s, \tilde{\omega}) = o(\psi_{\mathcal{I}^{\rm CC}}(\boldsymbol{Y}-\boldsymbol{Y}_T, \boldsymbol{V}-\boldsymbol{V}_T, \boldsymbol{X}_R, s, \tilde{\omega}))$. Similarly to the previous section, our analysis is valid in the vicinity of the true target location and velocity, that is, for $|\boldsymbol{X}_T - \boldsymbol{X}| < 2\lambda_o(\frac{H_T}{a+T_{\rm tot}|\boldsymbol{V}_T|})^2$ ($\sim$ 40 cm) and for $|\boldsymbol{V}_T - \boldsymbol{V}| < \frac{\lambda_o H_T^2}{(a+|\boldsymbol{V}_T|T_{\rm tot})^2 T_{\rm tot}}$ ($\sim$ $1.1 \cdot 10^{-2}$ m/s). Our resolution estimates are summarized in Table 3.

Copyright © by SIAM. Unauthorized reproduction of this article is prohibited.

Downloaded 11/28/17 to 171.67.216.21. Redistribution subject to SIAM license or copyright; see http://www.siam.org/journals/ojsa.php

Downloaded 11/28/17 to 171.67.216.21. Redistribution subject to SIAM license or copyright; see http://www.siam.org/journals/ojsa.php

As for the MF imaging function, the Doppler compensation does not play any role in our resolution estimates because $\frac{|\boldsymbol{V}_T|}{c_o}$ is very small. Note also that the direction of $\boldsymbol{V}_T$ does not appear in the resolution estimates as those terms always cancel out at first order due to the antisymmetric roles played by $\boldsymbol{X}_R$ and $\boldsymbol{X}_{R'}$. Because of this antisymmetry, the terms in $(Y)_3\frac{B}{c_o}$ also cancel out. Similar cancellation effects occur for $(V)_3$, which explains the difference in the resolution estimates for this coordinate between the MF and the correlation-based imaging function.

We note that in this case the ISAR aperture created by the moving scatterer plays a role only in the range coordinate that is parallel to the direction from the scatterer to the receivers/emitter. The cross-range resolution in position and velocity is similar to the one of the MF imaging function. Only the range resolution in velocity is reduced compared to the one provided by the MF imaging function.

Remark 4. The correlation-based imaging method cannot exploit the available bandwidth since it relies on travel time differences. This is an important difference between MF and correlation-based imaging which does not really penalize the correlation-based methodology except for the resolution in V_3.

5. Numerical results.

5.1. Parameter regime for the numerical simulations. In the numerical simulations, the target to be imaged is located at the reference slow time $s = 0$ at $\boldsymbol{Y}_T = (0, 0, H_T)$ and it moves with constant speed $\boldsymbol{V}_T = (0, V_T, 0)$. The target motion therefore defines a synthetic aperture $A_T = V_T T_{\text{tot}}$ over the duration T_{tot} of the data gather. We have verified the theoretical resolution estimates for both the matched field $\mathcal{I}^{\text{MF}}(\boldsymbol{Y}, \boldsymbol{V})$, defined by (3.1), and the correlation-based imaging function $\mathcal{I}^{\text{CC}}(\boldsymbol{Y}, \boldsymbol{V})$, defined by (3.4), using different values for H_T, V_T, T_{tot}, and the aperture a covered by the receivers. Our numerical simulations are carried out in the X-band regime. The results shown in this section correspond to the following (realistic) values: The altitude of the moving target is $H_T = 500$ km. This height corresponds to an LEO, which includes objects orbiting at an altitude between 160 km and 2,000 km. It is well known that the altitude of an orbiting object is related to its speed by the second Kepler law. At the altitude of $H_T = 200$ km the speed for maintaining a stable orbit is 7.79 km/s and it decreases as the altitude of the orbit increases. In our numerical setup with $H_T = 500$ km the velocity for a stable orbit is $V_T = 7{,}610$ km/s. The total duration of the recordings is $T_{\text{tot}} = 22.5$ s which allows for a target synthetic aperture of $A_T = 171$ km.

The data for the scattered field are computed by a discretization of the theoretical expression (2.9). The probing pulse is (we consider that the Gaussian and, consequently, the pulse, is zero for $t \geq 3/B$ and $t \leq -3/B$)

$$f(t) = \cos(2\pi f_o t) \exp\left(-\frac{B^2 t^2}{2}\right),$$

with the central frequency $f_o = 9.6$ GHz and the bandwidth $B = 622$ MHz. This gives the central wavelength $\lambda_o = 3$ cm. The bandwidth is 6% of the central frequency and these values for f_o and B correspond to the operating Gotcha radar system [4]. The pulse repetition rate is $\Delta s = 0.015$ s. The probing pulses are emitted from a transmitter on the ground, at position

Copyright © by SIAM. Unauthorized reproduction of this article is prohibited.

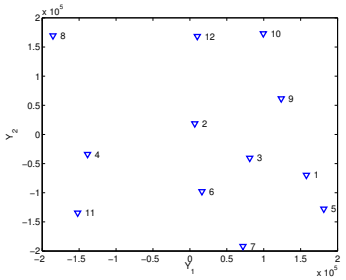

Figure 2. *Receiver distribution in a square with side $a = 400$ km. The blue triangles denote the receiver locations and the labels correspond to each receiver's number, an integer from 1 to 12. The units are in km.*

Table 4
MF resolution estimates.

		X-band	S-band
Y_1	$\frac{\lambda_o H_T}{a}$	3.75 cm	18.75 cm
Y_2	$\lambda_o \left(\frac{H_T}{a} \wedge \frac{H_T}{2V_T T_{\rm tot}} \right)$	3.75 cm $\wedge$ 4.4 cm = 3.75 cm	18.75 cm
Y_3	$\frac{c_o}{2B} \wedge \lambda_o \frac{H_T^2}{2V_T T_{\rm tot} a}$	23 cm $\wedge$ 5.5 cm = 5.5 cm	27.5 cm
V_1	$\frac{\lambda_o H_T}{a T_{\rm tot}}$	0.17 cm/s	0.85 cm/s
V_2	$\frac{\lambda_o}{T_{\rm tot}} \left(\frac{H_T}{a} \wedge \frac{H_T}{2V_T T_{\rm tot}} \right)$	0.17 cm/s $\wedge$ 0.19 cm/s = 0.17 cm/s	0.85 cm/s
V_3	$\frac{\lambda_o}{2T_{\rm tot}}$	0.07 cm/s	0.35 cm/s

$\boldsymbol{X}_E = (5, 5, 0)$ m. We have simulated data for the scattered field for 12 receivers, distributed in a square with side $a = 400$ km as illustrated in Figure 2.

5.2. Resolution estimates for the numerical simulation setup. In Tables 4 and 5 we have evaluated the resolution estimates corresponding to the parameters used in our numerical simulations. We observe that for our numerical setup the two imaging functions provide similar resolution except for V_3, the velocity in the vertical direction, in which case the results obtained by the MF imaging function are better. These conclusions are more general and do not apply only to the selected values of parameters. Similar results have been obtained for a range of realistic parameters for $a \in [100, 400]$ km and $T_{\rm tot} \in [10, 30]$ s. The central frequency, f_o, will affect the results in an obvious way since all resolution estimates are proportional to the wavelength λ_o. The bandwidth B appears only in the resolution estimate for Y_3. However, we should not forget that these expressions have been obtained under the assumption of relatively large bandwidth assuming $\frac{c_o}{2B} < \frac{4\lambda_o H_T^2}{(a+T_{\rm tot}V_T)^2}$ and $2\pi B \le \omega_o$.

Our numerical simulations are in the X-band regime. The currently planned Space Surveillance System [12] is in the S-band regime, with a central frequency of 2 GHz, which gives a 15 cm wavelength. The resolution limits in this section can be converted to the S-band sys-

Copyright © by SIAM. Unauthorized reproduction of this article is prohibited.

Downloaded 11/28/17 to 171.67.216.21. Redistribution subject to SIAM license or copyright; see http://www.siam.org/journals/ojsa.php

Table 5
Correlation-based imaging resolution estimates.

		X-band	S-band
$\boldsymbol{Y}_\perp$	$\dfrac{\lambda_o H_T}{a}$	3.75 cm	18.75 cm
Y_3	$\lambda_o \left(\dfrac{H_T^2}{a^2} \wedge \dfrac{2H_T^2}{aV_T T_{\rm tot}} \right)$	4.7 cm $\wedge$ 22 cm = 4.7 cm	23.5 cm
$\boldsymbol{V}_\perp$	$\dfrac{\lambda_o H_T}{aT_{\rm tot}}$	0.17 cm/s	0.85 cm/s
V_3	$\dfrac{\lambda_o}{T_{\rm tot}} \left(\dfrac{H_T^2}{a^2} \wedge \dfrac{2H_T^2}{aV_T T_{\rm tot}} \right)$	0.2 cm/s $\wedge$ 1 cm/s = 0.2 cm/s	1 cm/s

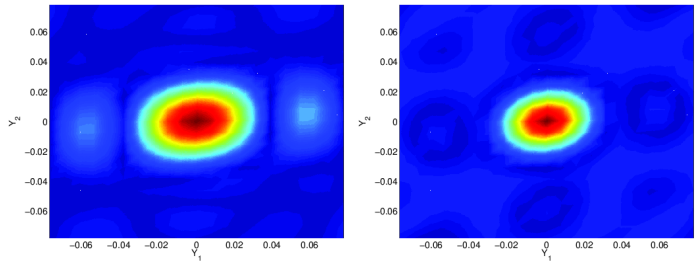

Figure 3. *Cross section of the image in the plane* (Y_1, Y_2)*:* $\mathcal{I}^{\rm MF}(\boldsymbol{Y}, \boldsymbol{V})$ *is shown on the left and* $\mathcal{I}^{\rm CC}(\boldsymbol{Y}, \boldsymbol{V})$ *on the right. The origin corresponds to the true values, which are* $Y_1 = 0$ *and* $Y_2 = 0$*. The abscissa is for* Y_1 *and the ordinate for* Y_2*. The units are in m.*

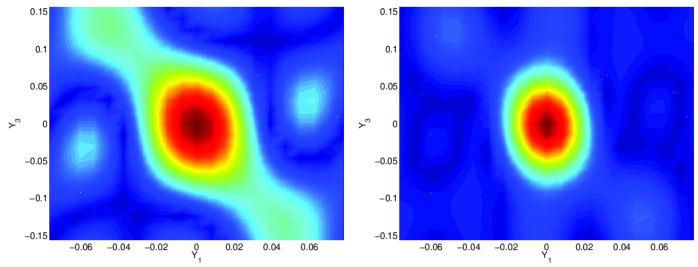

Figure 4. *Cross section of the image in the plane* (Y_1, Y_3)*:* $\mathcal{I}^{\rm MF}(\boldsymbol{Y}, \boldsymbol{V})$ *is shown on the left and* $\mathcal{I}^{\rm CC}(\boldsymbol{Y}, \boldsymbol{V})$ *on the right. The origin corresponds to the true values, which are* $Y_1 = 0$ *and* $Y_3 = H_T$*. The abscissa is for* Y_1 *and the ordinate for* Y_3*. The units are in m.*

tem by changing the 3 cm wavelength to 15 cm and the bandwidth from 622 MHz to around 125 MHz. In Tables 4 and 5 we summarize the resolution estimates for both X-band and S-band systems.

5.3. Imaging results with twelve receivers. Let us focus now on the imaging results obtained using the 12 receiver configuration shown in Figure 2. To reduce computational cost and memory requirements instead of computing the six-dimensional imaging functions, we have computed two-dimensional images by fixing four of the six unknowns to their true values. Figures 3 to 5 concern the location variable, $\boldsymbol{Y}$, while Figures 6 to 8 concern the velocity, $\boldsymbol{V}$, of the moving target.

Copyright © by SIAM. Unauthorized reproduction of this article is prohibited.

Downloaded 11/28/17 to 171.67.216.21. Redistribution subject to SIAM license or copyright; see http://www.siam.org/journals/ojsa.php

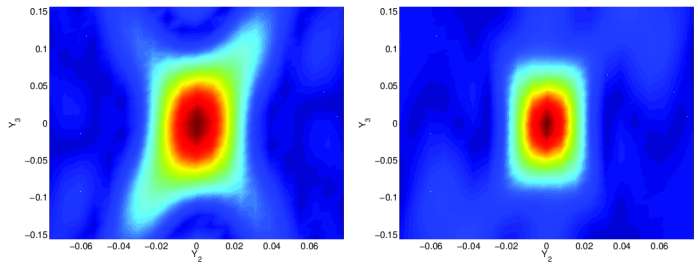

Figure 5. *Cross section of the image in the plane* (Y_2, Y_3)*:* $\mathcal{I}^{\mathrm{MF}}(\boldsymbol{Y}, \boldsymbol{V})$ *is shown on the left and* $\mathcal{I}^{\mathrm{CC}}(\boldsymbol{Y}, \boldsymbol{V})$ *on the right. The origin corresponds to the true values, which are* $Y_2 = 0$ *and* $Y_3 = H_T$*. The abscissa is for* Y_2 *and the ordinate for* Y_3*. The units are in m.*

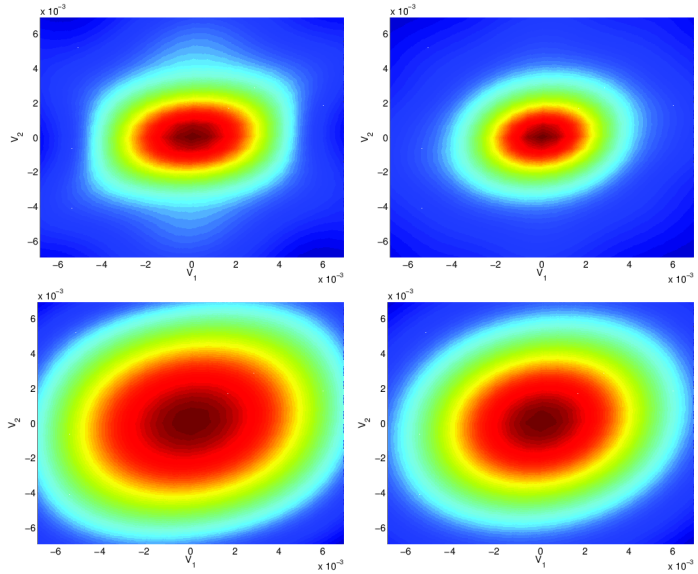

Figure 6. *Cross section of the image in the plane* (V_1, V_2)*:* $\mathcal{I}^{\mathrm{MF}}(\boldsymbol{Y}, \boldsymbol{V})$ *is shown on the left and* $\mathcal{I}^{\mathrm{CC}}(\boldsymbol{Y}, \boldsymbol{V})$ *on the right. The origin corresponds to the true values, which are* $V_1 = 0$ *and* $V_2 = V_T$*. The abscissa is for* V_1 *and the ordinate for* V_2*. The units are in m/s. The results on the top row are for* $T_{\mathrm{tot}} = 22.5$ *s while we have considered* $T_{\mathrm{tot}} = 11.25$ *s for the images in the bottom row.*

The MF and the correlation-based images in the plane (Y_1, Y_2) are shown in Figure 3. Given the estimates of Tables 1 and 2 we expect a resolution of the order of $\lambda_o H_T/a$ for both Y_1 and Y_2 which equals 3.75 cm. This is consistent with the results of Figure 3. The resolution appears to be slightly better for the correlation-based imaging function. We believe that this is due to the small number of receivers used and the fact that the MF image is obtained by adding N images each corresponding to a single receiver, while for the cross-correlation (CC) imaging function we add N^2 images each corresponding to a receiver couple (R, R'). The numerical simulations suggest that the CC imaging function converges faster to the theoretical resolution estimates, which are obtained for a dense network of receivers. This is also visible in the images of Figure 4 where we observe that the MF image shown on

Copyright © by SIAM. Unauthorized reproduction of this article is prohibited.

Downloaded 11/28/17 to 171.67.216.21. Redistribution subject to SIAM license or copyright; see http://www.siam.org/journals/ojsa.php

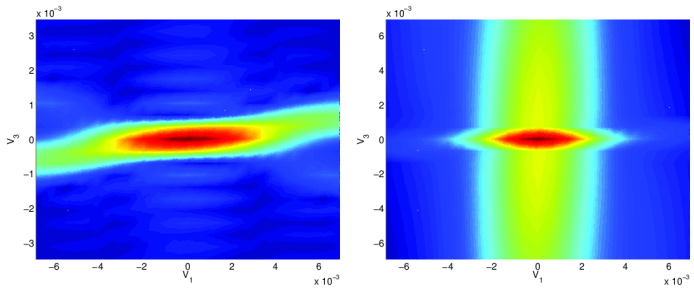

Figure 7. *Cross section of the image in the plane* (V_1, V_3)*:* $\mathcal{I}^{\mathrm{MF}}(\boldsymbol{Y}, \boldsymbol{V})$ *is shown on the left and* $\mathcal{I}^{\mathrm{CC}}(\boldsymbol{Y}, \boldsymbol{V})$ *on the right. The origin corresponds to the true values, which are* $V_1 = 0$ *and* $V_3 = 0$*. The abscissa is for* V_1 *and the ordinate for* V_3*. The units are in m/s.*

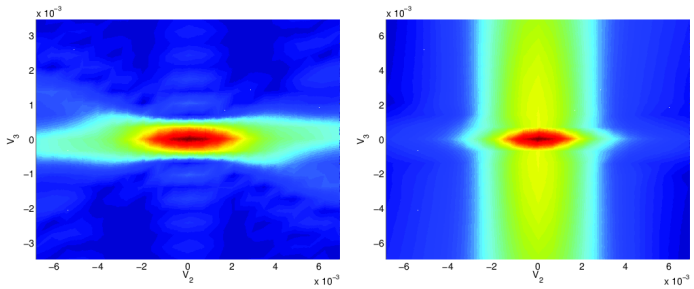

Figure 8. *Cross section of the image in the plane* (V_2, V_3)*:* $\mathcal{I}^{\mathrm{MF}}(\boldsymbol{Y}, \boldsymbol{V})$ *is shown on the left and* $\mathcal{I}^{\mathrm{CC}}(\boldsymbol{Y}, \boldsymbol{V})$ *on the right. The origin corresponds to the true values, which are* $V_2 = V_T$ *and* $V_3 = 0$*. The abscissa is for* V_1 *and the ordinate for* V_2*. The units are in m/s.*

the left has persistent side lobes while the corresponding CC image shown on the right has a resolution similar to MF but without any visible side lobes. We note that our theoretical resolution analysis gives estimates that concern the main peak of the imaging function and does not provide information about the side lobes.

The resolution in the Y_3 direction is given by $\lambda_o \frac{H_T^2}{2V_T T_{\mathrm{tot}} a}$ for the MF imaging function and by $\lambda_o \frac{H_T^2}{a^2}$ for the CC which equals 5.5 cm and 4.7 cm, respectively. This is consistent with the results of Figures 4 and 5, where Y_3 is the ordinate. Again we observe that the quality of the CC image is better with no observable side lobes in the imaging window.

The imaging results in the plane (V_1, V_2) are illustrated in Figure 6. The size of the focal spot is in agreement with the theoretical resolution estimates given by $\frac{\lambda_o H_T}{a T_{\mathrm{tot}}}$ which equals 0.17 cm/s for both V_1 and V_2 (for $T_{\mathrm{tot}} = 22.5$ s). This is a remarkably precise estimate recalling that the velocity of the moving target is large, 7610 m/s. As suggested by the theory, resolution in the target's velocity is inversely proportional to the duration of the data gather T_{tot}. This is nicely illustrated by the images in the bottom row of Figure 6 where we observe a doubling in the size of the focal spot by reducing T_{tot} from 22.5 s to 11.25 s.

As can be observed in the images shown in Figures 7 and 8 the results for the variable V_3 are better for the MF imaging function. The resolution estimates are $\frac{\lambda_o}{2T_{\mathrm{tot}}}$ for $\mathcal{I}^{\mathrm{MF}}(\boldsymbol{Y}, \boldsymbol{V})$ and $\frac{\lambda_o}{T_{\mathrm{tot}}} \frac{H_T^2}{a^2}$ for $\mathcal{I}^{\mathrm{CC}}(\boldsymbol{Y}, \boldsymbol{V})$. This equals 0.07 cm/s and 0.2 cm/s, respectively. Although the

Copyright © by SIAM. Unauthorized reproduction of this article is prohibited.

Downloaded 11/28/17 to 171.67.216.21. Redistribution subject to SIAM license or copyright; see http://www.siam.org/journals/ojsa.php

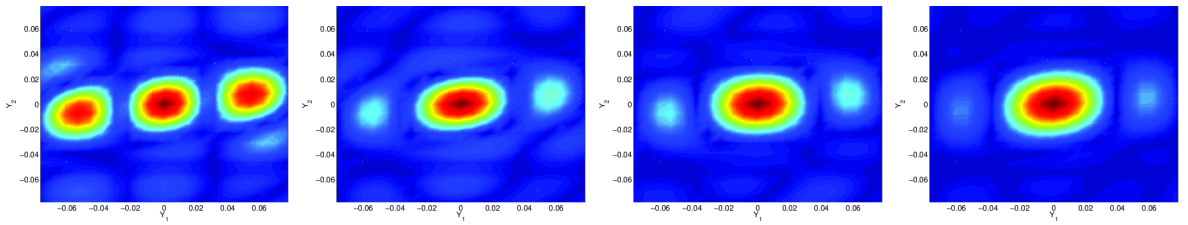

Figure 9. *Cross section of the image* $\mathcal{I}^{\mathrm{MF}}(\boldsymbol{Y},\boldsymbol{V})$ *in the plane* (Y_1,Y_2) *obtained using* 4, 6, 9, *and* 12 *receivers, respectively. The origin corresponds to the true values, which are* $Y_1=0$ *and* $Y_2=0$. *The abscissa is for* Y_1 *and the ordinate for* Y_2. *The units are in m.*

resolution of 0.2 cm/s provided by $\mathcal{I}^{\mathrm{CC}}(\boldsymbol{Y},\boldsymbol{V})$ is similar to the one obtained for the variables V_1 and V_2, the quality of the $\mathcal{I}^{\mathrm{CC}}(\boldsymbol{Y},\boldsymbol{V})$ image is not as good in the direction V_3 as seen by a vertical large side lobe in the images. Other than this, the results obtained by the correlation-based imaging function are very good, which suggests that correlation-based imaging can be used for effective imaging of fast moving targets.

As already mentioned, the correlation-based imaging function does not require either knowledge of the pulse or of the location of the source, which is an advantage. On the other hand, $\mathcal{I}^{\mathrm{CC}}(\boldsymbol{Y},\boldsymbol{V})$ is computationally more intensive than $\mathcal{I}^{\mathrm{MF}}(\boldsymbol{Y},\boldsymbol{V})$ since the cost of the imaging function is quadratic in the number of receivers instead of linear. A rather surprising result is that we do not need a dense network of receivers in order to obtain good resolution. This is true for both imaging functions although our numerical simulations suggest that the side lobes decrease faster for correlation-based imaging. We show in the next section some results obtained with a limited number of receivers.

5.4. Imaging results for a sparse receiver network. Our data are the same as before, that is, we have computed the scattered field for the 12 receiver configuration shown in Figure 2. We want to use part of these data corresponding to subsets of receivers with cardinality 4, 6, 9, and 12.

For each number of receivers used we selected the receiver set so that they span the whole square aperture (see Figure 2) as best as possible given our initial set of 12 receivers. We made the following choices: when using **4** receivers we selected the receivers with labels 5, 8, 10, and 11. Let us denote the receiver set $\mathcal{S}^4=\{5,8,10,11\}$. Then we increased the number of receivers to **6** by adding receivers 7 and 12, so that $\mathcal{S}^6=\{5,7,8,10,11,12\}$. In the case of **9** receivers we took $\mathcal{S}^9=\{2,4,5,7,8,9,10,11,12\}$ and $\mathcal{S}^{12}$ is the set containing all available receivers.

The images shown in Figures 9 and 10 are the $\mathcal{I}^{\mathrm{MF}}(\boldsymbol{Y},\boldsymbol{V})$ and $\mathcal{I}^{\mathrm{CC}}(\boldsymbol{Y},\boldsymbol{V})$ images in the plane (Y_1,Y_2) obtained using the receiver sets $\mathcal{S}^4$, $\mathcal{S}^6$, $\mathcal{S}^9$, and $\mathcal{S}^{12}$ from left to right, respectively. The image obtained using the receiver set $\mathcal{S}^4$ is not good and has important side lobes for both the MF and the correlation-based imaging functions. However, the quality of both $\mathcal{I}^{\mathrm{MF}}(\boldsymbol{Y},\boldsymbol{V})$ and $\mathcal{I}^{\mathrm{CC}}(\boldsymbol{Y},\boldsymbol{V})$ images increases rapidly with the number of receivers and very good results are obtained using just 9 receivers. For all considered configurations, we observed a faster side lobe decrease as the number of receivers increases in the case of the correlation-based images compared to the MF images. We also observe that the resolution

Copyright © by SIAM. Unauthorized reproduction of this article is prohibited.

Downloaded 11/28/17 to 171.67.216.21. Redistribution subject to SIAM license or copyright; see http://www.siam.org/journals/ojsa.php

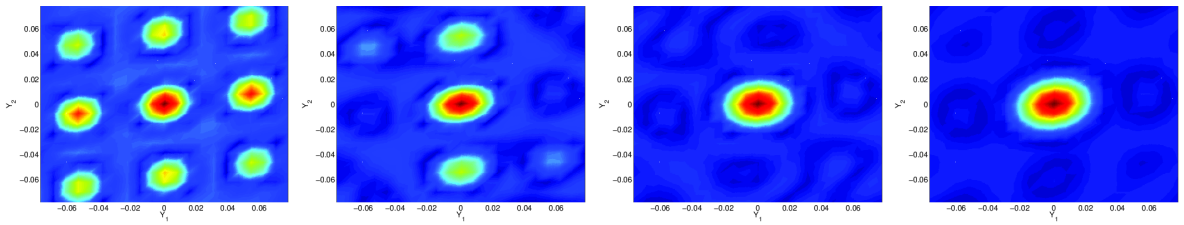

Figure 10. *Cross section of the image* $\mathcal{I}^{\mathrm{CC}}(\boldsymbol{Y},\boldsymbol{V})$ *in the plane* (Y_1,Y_2) *obtained using* 4, 6, 9, *and* 12 *receivers, respectively. The origin corresponds to the true values, which are* $Y_1=0$ *and* $Y_2=0$. *The abscissa is for* Y_1 *and the ordinate for* Y_2. *The units are in m.*

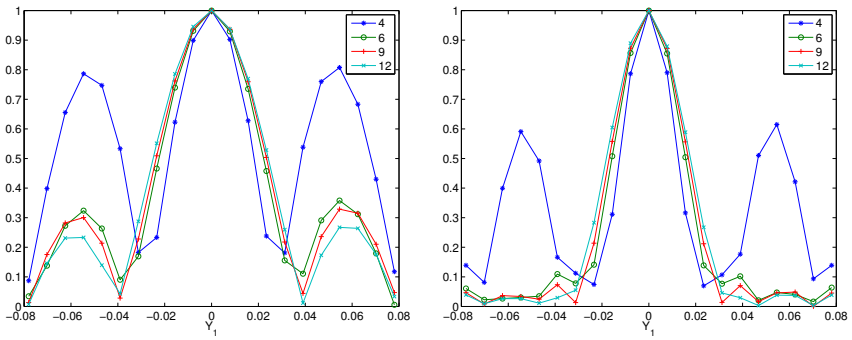

Figure 11. *Cross section of the images in the direction* Y_1 *obtained using* 4, 6, 9, *and* 12 *receivers, respectively. On the left we plot the MF* $\mathcal{I}^{\mathrm{MF}}(\boldsymbol{Y},\boldsymbol{V})$ *and on the right the correlation-based imaging function* $\mathcal{I}^{\mathrm{CC}}(\boldsymbol{Y},\boldsymbol{V})$. *The origin corresponds to the true value, which is* $Y_1=0$. *The abscissa is for* Y_1 *(the units are in m) and the ordinate is normalized by its max.*

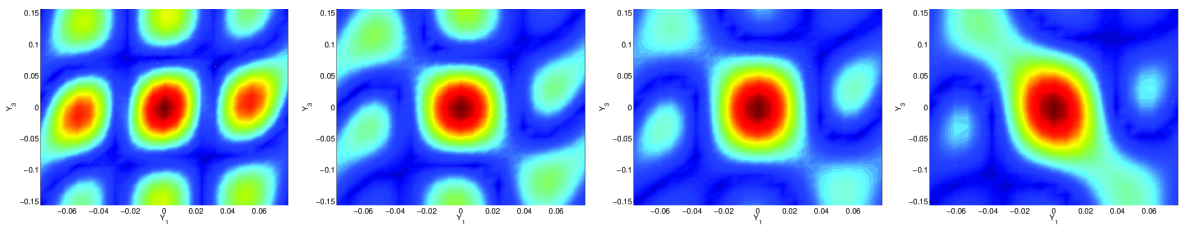

Figure 12. *Cross section of the image* $\mathcal{I}^{\mathrm{MF}}(\boldsymbol{Y},\boldsymbol{V})$ *in the plane* (Y_1,Y_3) *obtained using* 4, 6, 9, *and* 12 *receivers, respectively. The origin corresponds to the true values, which are* $Y_1=0$ *and* $Y_3=H_T$. *The abscissa is for* Y_1 *and the ordinate for* Y_3. *The units are in m.*

of the images is stable and does not vary significantly with the number of receivers used. It is mainly the side lobes that are affected by the number of receivers used. This is better illustrated in Figure 11 where we plot the $\mathcal{I}^{\mathrm{MF}}(\boldsymbol{Y},\boldsymbol{V})$ and $\mathcal{I}^{\mathrm{CC}}(\boldsymbol{Y},\boldsymbol{V})$ images as a function of Y_1 obtained using 4, 6, 9, and 12 receivers. On the left we plot the results for the MF and on the right for the correlation-based imaging.

We presented here results only for the location variables in the planes (Y_1,Y_2) and (Y_1,Y_3) (shown in Figures 12 and 13). However, similar results (not shown here) are obtained for the

Downloaded 11/28/17 to 171.67.216.21. Redistribution subject to SIAM license or copyright; see http://www.siam.org/journals/ojsa.php

Copyright © by SIAM. Unauthorized reproduction of this article is prohibited.

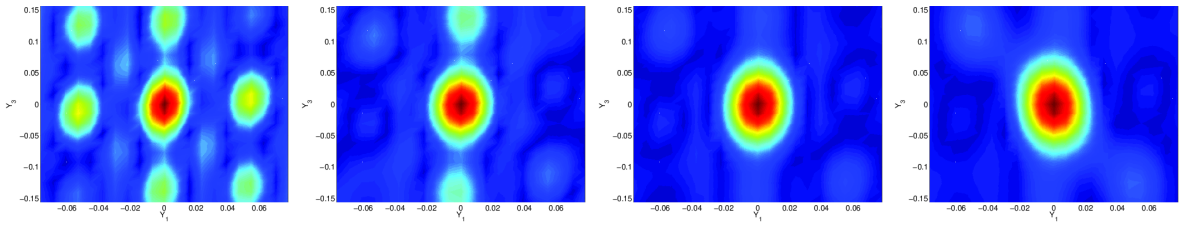

Figure 13. *Cross section of the image* $\mathcal{I}^{\mathrm{CC}}(\boldsymbol{Y},\boldsymbol{V})$ *in the plane* (Y_1,Y_3) *obtained using* 4, 6, 9, *and* 12 *receivers, respectively. The origin corresponds to the true values, which are* $Y_1=0$ *and* $Y_3=H_T$. *The abscissa is for* Y_1 *and the ordinate for* Y_3. *The units are in m.*

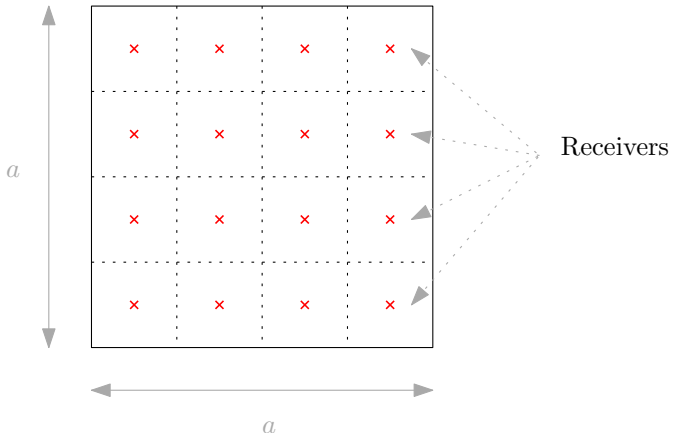

Figure 14. *Schematic representation of a regular square grid of receivers.*

velocity unknowns. A theoretical analysis that helps explain these rather surprising findings is considered in the next section.

6. Theoretical analysis of the required number of receivers. The numerical simulation results are surprising because they suggest that only a small number of receivers (around 10) is sufficient to observe the point spread function of the two imaging methods. In this section, we will analyze theoretically the role that the number of receivers plays on the imaging function. We will show that, for a regular grid of receivers, indeed, around 10 receivers are enough to observe a point spread function that is similar to the one that would have been obtained using a very large number of receivers. This is our third main result of the paper.

By regular grid we mean a regular mesh for a square of size a such that the covering is optimal for $\|.\|_\infty$. In this case, the asymptotic density of receivers p is the uniform distribution on the square as illustrated in Figure 14.

Considering the summation formula in the imaging methods, it is natural to think about the required number of receivers so as to approximate well an integral by a discretized sum. Consequently, the strategy followed here consists in deriving approximation bounds on the differences between the mean of the partial imaging functions $\tilde{I}_N^{\mathrm{MF}}$ or $\tilde{I}_N^{\mathrm{CC}}$, defined below, and the asymptotic imaging functions $\mathcal{I}^{\mathrm{MF}}$ or $\mathcal{I}^{\mathrm{CC}}$.

Copyright © by SIAM. Unauthorized reproduction of this article is prohibited.

Downloaded 11/28/17 to 171.67.216.21. Redistribution subject to SIAM license or copyright; see http://www.siam.org/journals/ojsa.php

Downloaded 11/28/17 to 171.67.216.21. Redistribution subject to SIAM license or copyright; see http://www.siam.org/journals/ojsa.php

Let us introduce the following notation for the MF imaging function at each receiver $\boldsymbol{X}_R$,

$$I_j^{\mathrm{MF}}(\boldsymbol{X},\boldsymbol{V},\boldsymbol{X}_R)=\int f(t)u_{\mathrm{s},R}\left(S_j+\frac{|\boldsymbol{X}-\boldsymbol{X}_R|}{c_o}+\frac{t+\frac{|\boldsymbol{X}-\boldsymbol{X}_E|}{c_o}}{\gamma_{\mathrm{s}}(\boldsymbol{X},\boldsymbol{V},\boldsymbol{X}_R)}\right)dt,$$

$$I^{\mathrm{MF}}(\boldsymbol{Y},\boldsymbol{V},\boldsymbol{X}_R)=\frac{1}{N_E}\sum_{j=1}^{N_E}I_j(\boldsymbol{X}(S_j),\boldsymbol{V},\boldsymbol{X}_R).$$

Recall that $\boldsymbol{X}$ and $\boldsymbol{X}_T$ still depend on the slow time. With calculations similar to the ones carried out in section 4, by passing to the Fourier domain and doing some approximations we get

$$\begin{aligned}I_j^{\mathrm{MF}}(\boldsymbol{X},\boldsymbol{V},\boldsymbol{X}_R)=&\frac{k_o^2\rho}{32\pi^3|\boldsymbol{X}_T(S_j)|^2}\int_{\mathbb{R}}d\tilde{\omega}|\hat{F}(\tilde{\omega})|^2\\&\times\exp\Bigg(i\frac{\omega}{c_o}\big(|\boldsymbol{X}_T-\boldsymbol{X}_E|+|\boldsymbol{X}_T-\boldsymbol{X}_R|-|\boldsymbol{X}(S_j)-\boldsymbol{X}_E|-|\boldsymbol{X}-\boldsymbol{X}_R|\\&\quad+|\boldsymbol{X}_T-\boldsymbol{X}_E|+|\boldsymbol{X}_T-\boldsymbol{X}_E|\frac{\boldsymbol{V}_T}{c_o}\cdot\left(\frac{\boldsymbol{X}_T-\boldsymbol{X}_R}{|\boldsymbol{X}_T-\boldsymbol{X}_R|}+\frac{\boldsymbol{X}_T-\boldsymbol{X}_E}{|\boldsymbol{X}_T-\boldsymbol{X}_E|}\right)\\&\quad-|\boldsymbol{X}-\boldsymbol{X}_E|\frac{\boldsymbol{V}}{c_o}\cdot\left(\frac{\boldsymbol{X}-\boldsymbol{X}_R}{|\boldsymbol{X}-\boldsymbol{X}_R|}+\frac{\boldsymbol{X}-\boldsymbol{X}_E}{|\boldsymbol{X}-\boldsymbol{X}_E|}\right)\Bigg).\end{aligned}$$

Assuming that the number of slow times N_E is big enough, we can approximate I^{MF} by its asymptotic version,

$$\begin{aligned}\tilde{I}^{\mathrm{MF}}(\boldsymbol{Y},\boldsymbol{V},\boldsymbol{X}_R)=&\int_{-T_{\mathrm{tot}}/2}^{T_{\mathrm{tot}}/2}ds\frac{k_o^2\rho}{32\pi^3|\boldsymbol{X}_T(s)|^2T_{\mathrm{tot}}}\int_{\mathbb{R}}d\tilde{\omega}|\hat{F}(\tilde{\omega})|^2\\&\times\exp\Bigg(i\frac{\omega}{c_o}\big(|\boldsymbol{X}_T-\boldsymbol{X}_E|+|\boldsymbol{X}_T-\boldsymbol{X}_R|-|\boldsymbol{X}(s)-\boldsymbol{X}_E|-|\boldsymbol{X}-\boldsymbol{X}_R|\\&\quad+|\boldsymbol{X}_T-\boldsymbol{X}_E|+|\boldsymbol{X}_T-\boldsymbol{X}_E|\frac{\boldsymbol{V}_T}{c_o}\cdot\left(\frac{\boldsymbol{X}_T-\boldsymbol{X}_R}{|\boldsymbol{X}_T-\boldsymbol{X}_R|}+\frac{\boldsymbol{X}_T-\boldsymbol{X}_E}{|\boldsymbol{X}_T-\boldsymbol{X}_E|}\right)\\&\quad-|\boldsymbol{X}-\boldsymbol{X}_E|\frac{\boldsymbol{V}}{c_o}\cdot\left(\frac{\boldsymbol{X}-\boldsymbol{X}_R}{|\boldsymbol{X}-\boldsymbol{X}_R|}+\frac{\boldsymbol{X}-\boldsymbol{X}_E}{|\boldsymbol{X}-\boldsymbol{X}_E|}\right)\Bigg),\end{aligned}$$

and in the Fourier domain, we obtain using the same calculations as for (4.1),

$$\begin{aligned}&\tilde{I}^{\mathrm{MF}}(\boldsymbol{Y},\boldsymbol{V},\boldsymbol{X}_R)\\&=C\int_{-T_{\mathrm{tot}}/2}^{T_{\mathrm{tot}}/2}ds\int_{\mathbb{R}}d\tilde{\omega}|\hat{F}(\tilde{\omega})|^2\exp\Big(i(\Phi_{\mathcal{I}^{\mathrm{MF}}}+\epsilon_{\mathcal{I}^{\mathrm{MF}}})(\boldsymbol{Y}-\boldsymbol{Y}_T,\boldsymbol{V}-\boldsymbol{V}_T,\boldsymbol{X}_R,s,\omega)\Big).\end{aligned}\tag{6.1}$$

Now we want to show that

$$\tilde{I}_N^{\mathrm{MF}}(\boldsymbol{Y},\boldsymbol{V})=\frac{1}{N}\sum_{R=1}^{N}\tilde{I}^{\mathrm{MF}}(\boldsymbol{Y},\boldsymbol{V},\boldsymbol{X}_R)$$

Copyright © by SIAM. Unauthorized reproduction of this article is prohibited.

Downloaded 11/28/17 to 171.67.216.21. Redistribution subject to SIAM license or copyright; see http://www.siam.org/journals/ojsa.php

has indeed a shape similar to its asymptotic version $\mathcal{I}^{\mathrm{MF}}(\boldsymbol{Y},\boldsymbol{V}) = \int \frac{d\boldsymbol{x}}{a^2} p(\frac{\boldsymbol{x}}{a}) \tilde{I}^{\mathrm{MF}}(\boldsymbol{Y},\boldsymbol{V},\boldsymbol{x})$, at least for $\boldsymbol{Y},\boldsymbol{V}$ close to the true target location, in a vicinity that is of the order of the resolution. Note that by Fubini's theorem this definition of $\mathcal{I}^{\mathrm{MF}}$ coincides with the one in (3.1).

Following the same reasoning, we define the correlation-based imaging function, corresponding to a couple of receivers located at $\boldsymbol{X}_{R_1}$, $\boldsymbol{X}_{R_2}$,

$$I_j^{\mathrm{CC}}(\boldsymbol{X},\boldsymbol{V},\boldsymbol{X}_{R_1},\boldsymbol{X}_{R_2}) = \int u_{\mathrm{s},R_1}\left(S_j + \frac{|\boldsymbol{X}-\boldsymbol{X}_{R_1}|}{c_o} + \frac{t+\frac{|\boldsymbol{X}-\boldsymbol{X}_E|}{c_o}}{\gamma_{\mathrm{s}}(\boldsymbol{X},\boldsymbol{V},\boldsymbol{X}_{R_1})}\right) \times u_{\mathrm{s},R_2}\left(S_j + \frac{|\boldsymbol{X}-\boldsymbol{X}_{R_2}|}{c_o} + \frac{t+\frac{|\boldsymbol{X}-\boldsymbol{X}_E|}{c_o}}{\gamma_{\mathrm{s}}(\boldsymbol{X},\boldsymbol{V},\boldsymbol{X}_{R_2})}\right) dt,$$

$$I^{\mathrm{CC}}(\boldsymbol{Y},\boldsymbol{V},\boldsymbol{X}_{R_1},\boldsymbol{X}_{R_2}) = \frac{1}{N_E}\sum_{j=1}^{N_E} I_j^{\mathrm{CC}}(\boldsymbol{X}(S_j),\boldsymbol{V},\boldsymbol{X}_{R_1},\boldsymbol{X}_{R_2}).$$

When N_E is big, I^{CC} can be approximated by

$$\begin{aligned}&\tilde{I}^{\mathrm{CC}}(\boldsymbol{X},\boldsymbol{V},\boldsymbol{X}_{R_1},\boldsymbol{X}_{R_2})\\ &= C\int_{-T_{\mathrm{tot}}/2}^{T_{\mathrm{tot}}/2} ds \int_{\mathbb{R}} d\tilde{\omega}|\hat{F}(\tilde{\omega})|^2 \exp\left(i(\Psi_{\mathcal{I}^{\mathrm{MF}}}+\epsilon_{\mathcal{I}^{\mathrm{MF}}})(\boldsymbol{Y}-\boldsymbol{Y}_T,\boldsymbol{V}-\boldsymbol{V}_T,\boldsymbol{X}_{R_1},s,\omega)\right)\\ &\quad\times\exp\left(-i(\Psi_{\mathcal{I}^{\mathrm{MF}}}+\epsilon_{\mathcal{I}^{\mathrm{MF}}})(\boldsymbol{Y}-\boldsymbol{Y}_T,\boldsymbol{V}-\boldsymbol{V}_T,\boldsymbol{X}_{R_2},s,\omega)\right).\end{aligned}$$

We also define the average quantity

$$\tilde{I}_N^{\mathrm{CC}}(\boldsymbol{Y},\boldsymbol{V}) = \frac{1}{N^2}\sum_{R_1=1}^{N}\sum_{R_2=1}^{N}\tilde{I}^{\mathrm{CC}}(\boldsymbol{Y},\boldsymbol{V},\boldsymbol{X}_{R_1},\boldsymbol{X}_{R_2}),$$

which is to converge to $\mathcal{I}^{\mathrm{CC}}(\boldsymbol{Y},\boldsymbol{V})$ as $N\to\infty$.

We next study in which sense the discrete versions $\tilde{I}_N^{\mathrm{MF}}$ and $\tilde{I}_N^{\mathrm{CC}}$ are good approximations of their continuous analogues $\mathcal{I}^{\mathrm{MF}}$ and $\mathcal{I}^{\mathrm{CC}}$.

6.1. MF resolution for a regular grid of receivers. We will assume in the following that we have a square grid of receivers, each side containing M receivers (hence $N=M^2$). However, the results can be easily adapted to any bounded regular configuration of receivers.

The key idea is to notice that both $\tilde{I}_N^{\mathrm{MF}}$ and $\mathcal{I}^{\mathrm{MF}}$ admit their maximum at the true target location and velocity $(\boldsymbol{Y}_T,\boldsymbol{V}_T)$, and that for a number of receivers sufficiently small, we can bound $|\tilde{I}_N^{\mathrm{MF}}(\boldsymbol{Y},\boldsymbol{V}) - \mathcal{I}^{\mathrm{MF}}(\boldsymbol{Y},\boldsymbol{V})|$ by an envelope function for $(\boldsymbol{Y},\boldsymbol{V})$ in the resolution set (see definition below).

Definition 6.1 (resolution set). *Given a six-dimensional vector $\boldsymbol{r}=(r_1,\dots,r_6)$ of positive coordinates called hereafter the reference width vector, we define the resolution set $\mathcal{R}_{\boldsymbol{Y}_T,\boldsymbol{V}_T,q,\boldsymbol{r}}$ as*

$$\begin{pmatrix}\boldsymbol{Y}_T\\ \boldsymbol{V}_T\end{pmatrix} + q\big([-r_1,r_1]\times\cdots\times[-r_6,r_6]\big),$$

where $\times$ stands for the Cartesian product of intervals.

Copyright © by SIAM. Unauthorized reproduction of this article is prohibited.

Downloaded 11/28/17 to 171.67.216.21. Redistribution subject to SIAM license or copyright; see http://www.siam.org/journals/ojsa.php

The width vector $\boldsymbol{r}$ will be equal in each dimension to the corresponding resolution estimates of the imaging method under investigation. For the MF, we have

$$
\begin{aligned}
r_1 &= \frac{\lambda_o H_T}{a}, & r_4 &= \frac{\lambda_o H_T}{a T_{\text{tot}}},\\
r_2 &= \lambda_o \left(\frac{H_T}{a} \wedge \frac{H_T}{2|\boldsymbol{V}_T|_\perp T_{\text{tot}}} \right), & r_5 &= \frac{\lambda_o}{T_{\text{tot}}} \left(\frac{H_T}{a} \wedge \frac{H_T}{2|\boldsymbol{V}_T|_\perp T_{\text{tot}}} \right),\\
r_3 &= \frac{c_o}{2B} \wedge \lambda_o \frac{H_T^2}{2|\boldsymbol{V}_T|_\perp T_{\text{tot}} a}, & r_6 &= \frac{\lambda_o}{2T_{\text{tot}}}.
\end{aligned} \tag{6.2}
$$

In other words, the resolution set is a subspace of $\mathbb{R}^6$ centered at $(\boldsymbol{Y}_T, \boldsymbol{V}_T)$, and for which the width in each dimension corresponds to a fixed proportion q of the resolution in this dimension. As we focus mainly on two-dimensional images, allowing only 2 coordinates of the $(\boldsymbol{Y}, \boldsymbol{V})$ vector to vary, we need to introduce the notion of a two-dimensional partial image which we call a 2-sliced image.

Definition 6.2 (2-sliced resolution set). *Given the reference width vector $\boldsymbol{r} = (r_1, \dots, r_6)$ of positive coordinates, we define the 2-sliced resolution set $\mathcal{R}^{j,k}_{\boldsymbol{Y}_T, \boldsymbol{V}_T, q, \boldsymbol{r}}$ as*

$$
\begin{pmatrix} \boldsymbol{Y}_T \\ \boldsymbol{V}_T \end{pmatrix} + q[-r_j, r_j]\boldsymbol{e}_j + q[-r_k, r_k]\boldsymbol{e}_k
$$

with $(\boldsymbol{e}_i)_{i=1,\dots,6}$ the canonical base of $\mathbb{R}^6$.

Let us denote $\mathcal{C}_R$ the square centered at $\boldsymbol{X}_R$ and of size $\frac{a}{\sqrt{N}}$ (recall $M = \sqrt{N}$). The difference between the discrete and the continuous MF imaging function can be written as

$$
\begin{aligned}
&\mathcal{I}^{\text{MF}}(\boldsymbol{Y}, \boldsymbol{V}) - \tilde{I}^{\text{MF}}_N(\boldsymbol{Y}, \boldsymbol{V})\\
&\quad = \frac{1}{a^2} \sum_{R=1}^{N} \int_{\mathcal{C}_R} d\boldsymbol{x} \left(\tilde{I}^{\text{MF}}(\boldsymbol{Y}, \boldsymbol{V}, \boldsymbol{x}) - \tilde{I}^{\text{MF}}(\boldsymbol{Y}, \boldsymbol{V}, \boldsymbol{X}_R) \right)\\
&\quad = \frac{1}{a^2} \sum_{R=1}^{N} \int_{\mathcal{C}_R} d\boldsymbol{x} \nabla_{\boldsymbol{X}_R} \tilde{I}^{\text{MF}}(\boldsymbol{Y}, \boldsymbol{V}, \boldsymbol{X}_R) \cdot (\boldsymbol{x} - \boldsymbol{X}_R)\\
&\qquad + \frac{1}{2} \int_0^1 dt\, (\boldsymbol{x} - \boldsymbol{X}_R) \cdot \nabla^2_{\boldsymbol{X}_R} \tilde{I}^{\text{MF}}(\boldsymbol{Y}, \boldsymbol{V}, (1-t)\boldsymbol{X}_R + t\boldsymbol{x}) \cdot (\boldsymbol{x} - \boldsymbol{X}_R).
\end{aligned}
$$

The first integral

$$
\int_{\mathcal{C}_R} d\boldsymbol{x} \nabla_{\boldsymbol{X}_R} \tilde{I}^{\text{MF}}(\boldsymbol{Y}, \boldsymbol{V}, \boldsymbol{X}_R) \cdot (\boldsymbol{x} - \boldsymbol{X}_R) = 0
$$

because of symmetry since $\boldsymbol{X}_R$ is the center of each square $\mathcal{C}_R$. Thus, expressing

Copyright © by SIAM. Unauthorized reproduction of this article is prohibited.

Downloaded 11/28/17 to 171.67.216.21. Redistribution subject to SIAM license or copyright; see http://www.siam.org/journals/ojsa.php

$\nabla^2_{\boldsymbol{X}_R}\tilde{I}^{\mathrm{MF}}(\boldsymbol{Y},\boldsymbol{V},\boldsymbol{X}_R)$ as an integral, and computing upper bounds inside this integral, we have ultimately that for $(\boldsymbol{Y},\boldsymbol{V}) \in \mathcal{R}^{k,l}_{\boldsymbol{Y}_T,\boldsymbol{V}_T,q,\boldsymbol{r}}$ with $q = O(1)$, (the calculation details are presented in Appendix C.1),

$$\begin{aligned}(6.3)\quad &\left|\mathcal{I}^{\mathrm{MF}}(\boldsymbol{Y},\boldsymbol{V}) - \tilde{I}^{\mathrm{MF}}_N(\boldsymbol{Y},\boldsymbol{V})\right| \\ &\qquad \le \|\mathcal{I}^{\mathrm{MF}}\|_\infty \left(\frac{H^1_p(\boldsymbol{Y},\boldsymbol{V})}{\sqrt{N}} \wedge \left(\frac{H^2_p(\boldsymbol{Y},\boldsymbol{V})}{2N} + \frac{1}{2N}o(1)\left(H^2_p(\boldsymbol{Y},\boldsymbol{V}) + H^1_p(\boldsymbol{Y},\boldsymbol{V}\right)\right)\right)\end{aligned}$$

with the envelope functions $H^1_p(\boldsymbol{Y},\boldsymbol{V})$ and $H^2_p(\boldsymbol{Y},\boldsymbol{V})$ defined by

$$\begin{aligned}(6.4)\quad H^1_p(\boldsymbol{Y},\boldsymbol{V}) \overset{(def)}{=}\ & 2\frac{|(\boldsymbol{Y}-\boldsymbol{Y}_T)_3|}{r_3} + 2^{\frac{1}{p^*}}\sqrt[p]{\frac{|(\boldsymbol{Y}-\boldsymbol{Y}_T)_1|^p}{r_1^p} + \frac{|(\boldsymbol{Y}-\boldsymbol{Y}_T)_2|^p}{r_2^p}} \\ &+ 2\frac{|(\boldsymbol{V}-\boldsymbol{V}_T)_3|}{r_6} + 2^{\frac{1}{p^*}}\sqrt[p]{\frac{|(\boldsymbol{V}-\boldsymbol{V}_T)_1|^p}{r_4^p} + \frac{|(\boldsymbol{V}-\boldsymbol{V}_T)_2|^p}{r_5^p}}\end{aligned}$$

for $p < \infty$ and

$$\begin{aligned}(6.5)\quad H^1_\infty(\boldsymbol{Y},\boldsymbol{V}) \overset{(def)}{=}\ & 2\frac{|(\boldsymbol{Y}-\boldsymbol{Y}_T)_3|}{r_3} + 2\left(\frac{|(\boldsymbol{Y}-\boldsymbol{Y}_T)_1|}{r_1} \wedge \frac{|(\boldsymbol{Y}-\boldsymbol{Y}_T)_2|}{r_2}\right) \\ &+ 2\frac{|(\boldsymbol{V}-\boldsymbol{V}_T)_3|}{r_6} + 2\left(\frac{|(\boldsymbol{V}-\boldsymbol{V}_T)_1|}{r_4} \wedge \frac{|(\boldsymbol{V}-\boldsymbol{V}_T)_2|}{r_5}\right)\end{aligned}$$

for $p = \infty$, and

$$(6.6)\qquad H^2_p(\boldsymbol{Y},\boldsymbol{V}) \overset{(def)}{=} \left(H^1_p(\boldsymbol{Y},\boldsymbol{V})\right)^2.$$

Here p and p^* are such that $\frac{1}{p} + \frac{1}{p^*} = 1$. Futhermore $o(1)$ here means a small quantity with respect to 1 according to Hypothesis 1 (section 4.1), $(\boldsymbol{Y},\boldsymbol{V}) \in \mathcal{R}^{k,l}_{\boldsymbol{Y}_T,\boldsymbol{V}_T,q,\boldsymbol{r}}$, and $q = O(1)$. A simple corollary could be stated in the following terms.

Theorem 6.3. *For any 2-sliced resolution $\mathcal{R}^{j,k}_{\boldsymbol{Y}_T,\boldsymbol{V}_T,q,\boldsymbol{r}}$, we have*

$$\frac{\left|\mathcal{I}^{\mathrm{MF}}(\boldsymbol{Y},\boldsymbol{V}) - \tilde{I}^{\mathrm{MF}}_N(\boldsymbol{Y},\boldsymbol{V})\right|}{\|\mathcal{I}^{\mathrm{MF}}\|_\infty} \le \sqrt{\frac{16q^2}{N}} \wedge \frac{8q^2}{N}$$

for all $(\boldsymbol{Y},\boldsymbol{V}) \in \mathcal{R}^{j,k}_{\boldsymbol{Y}_T,\boldsymbol{V}_T,q,\boldsymbol{r}}$.

This result is a direct consequence of inequality (6.3) with $p^* = \infty$ and $p = 1$. Note that better bounds can be obtained in some specific cases, for instance, with $\mathcal{R}^{1,2}_{\boldsymbol{Y}_T,\boldsymbol{V}_T,q,\boldsymbol{r}}$ or $\mathcal{R}^{4,5}_{\boldsymbol{Y}_T,\boldsymbol{V}_T,q,\boldsymbol{r}}$, we would have a bound in $\sqrt{\frac{4}{N}}q \wedge \frac{2q^2}{N}$. Depending on the 2-sliced resolution considered and the particular values of the the ratios $\frac{aT_{\mathrm{tot}}r_5}{H_T}$, $\frac{ar_1}{H_T}$, $\frac{aT_{\mathrm{tot}}|\boldsymbol{V}_T|_\perp r_3}{H_T^2}$, $\frac{aT^2_{\mathrm{tot}}|\boldsymbol{V}_T|_\perp r_6}{H_T^2}$, tighter bounds could be obtained.

To give a specific example, let us consider the (Y_1, Y_2) slice and $N = 4$. Assuming $\mathcal{I}^{\mathrm{MF}}(\boldsymbol{Y},\boldsymbol{V}) = o(\|\mathcal{I}^{\mathrm{MF}}\|_\infty)$ for $(\boldsymbol{Y},\boldsymbol{V}) \in \partial\mathcal{R}^{1,2}_{\boldsymbol{Y}_T,\boldsymbol{V}_T,q,\boldsymbol{r}}$, we can apply the previous bound

Copyright © by SIAM. Unauthorized reproduction of this article is prohibited.

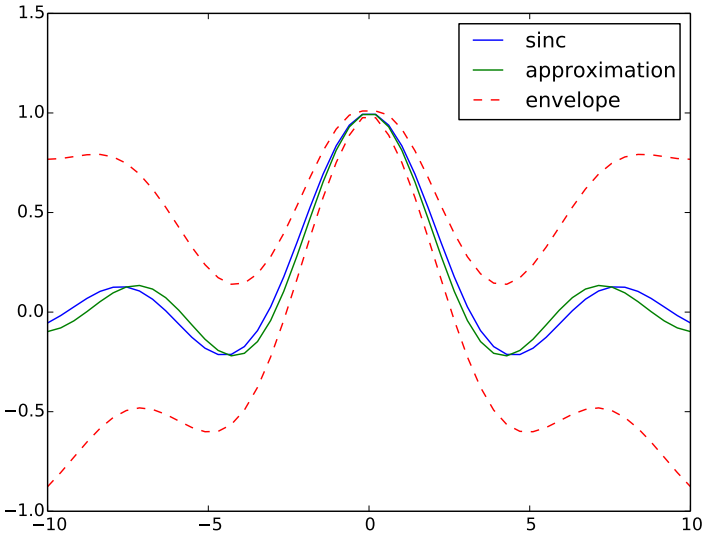

Figure 15. *Schematic illustration of the envelope functions.*

$(\sqrt{\frac{4}{N}}q \wedge \frac{2q^2}{N})$ for $q = 1$ and obtain $\tilde{I}_N^{\mathrm{MF}}(\boldsymbol{Y}, \boldsymbol{V}) = \|\mathcal{I}^{\mathrm{MF}}\|_\infty(\frac{1}{2} + o(1))$ for $(\boldsymbol{Y}, \boldsymbol{V}) \in \partial\mathcal{R}^{1,2}_{\boldsymbol{Y}_T, \boldsymbol{V}_T, q, \boldsymbol{r}}$. Achieving the same result on the resolution set $\mathcal{R}^{3,6}_{\boldsymbol{Y}_T, \boldsymbol{V}_T, q, \boldsymbol{r}}$ (the worst case) would require $N = 16$.

In Figure 15 we illustrate with a schematic how the envelope functions can be used to qualitatively explain the good imaging results obtained with a limited number of receivers in our numerical simulations. The blue curve would be the continuous imaging function obtained with an infinite number of receivers while the green curve would correspond to the discrete imaging function obtained with a limited number of receivers. The red dashed curves denote the envelope functions which are our bounds on the error, that is the difference between the continuous and the discrete imaging functions. Both functions admit their maximum at the correct target location. The error between them is zero at this location and remains a small fraction of the maximal value for points inside the resolution set.

6.2. Correlation-based imaging resolution for a regular grid of receivers. Here we follow the same steps as for the MF. We also use the resolution set and 2-sliced resolution set definitions but with a different reference width vector, $\boldsymbol{r}$, defined by the resolution estimates of the correlation-based imaging function

$$
\begin{aligned}
r_1 &= \frac{\lambda_o H_T}{a}, & r_4 &= \frac{\lambda_o H_T}{a T_{\mathrm{tot}}},\\
r_2 &= \frac{\lambda_o H_T}{a}, & r_5 &= \frac{\lambda_o H_T}{a T_{\mathrm{tot}}},\\
r_3 &= \lambda_o \left(\frac{H_T^2}{a^2} \wedge \frac{2H_T^2}{a|\boldsymbol{V}_T|_\perp T_{\mathrm{tot}}} \right), & r_6 &= \frac{\lambda_o}{T_{\mathrm{tot}}} \left(\frac{H_T^2}{a^2} \wedge \frac{2H_T^2}{a|\boldsymbol{V}_T|_\perp T_{\mathrm{tot}}} \right).
\end{aligned}
\tag{6.7}
$$

Copyright © by SIAM. Unauthorized reproduction of this article is prohibited.

Downloaded 11/28/17 to 171.67.216.21. Redistribution subject to SIAM license or copyright; see http://www.siam.org/journals/ojsa.php

Mutatis mutandis, we obtain the following results (see Appendix C.2 for calculation details),

(6.8)
$$\left|\mathcal{I}^{\mathrm{CC}}(\boldsymbol{Y},\boldsymbol{V})-\tilde{I}_N^{\mathrm{CC}}(\boldsymbol{Y},\boldsymbol{V})\right| \le 2\|\mathcal{I}^{\mathrm{MF}}\|_\infty \left(\frac{G_p^1(\boldsymbol{Y},\boldsymbol{V})}{\sqrt{N}} \wedge \frac{G_p^2(\boldsymbol{Y},\boldsymbol{V})}{2N} + \frac{1}{2N}o(1)G_p^2(\boldsymbol{Y},\boldsymbol{V})\right)$$

with

$$G_p^1(\boldsymbol{Y},\boldsymbol{V}) \overset{(def)}{=} 2\left(4\frac{|(\boldsymbol{Y}-\boldsymbol{Y}_T)_3|}{r_3} + 2^{\frac{1}{p^*}}\sqrt[p]{\frac{|(\boldsymbol{Y}-\boldsymbol{Y}_T)_1|^p}{r_1^p}+\frac{|(\boldsymbol{Y}-\boldsymbol{Y}_T)_2|^p}{r_2^p}}4\frac{|(\boldsymbol{V}-\boldsymbol{V}_T)_3|}{r_6} + 2^{\frac{1}{p^*}}\sqrt[p]{\frac{|(\boldsymbol{V}-\boldsymbol{V}_T)_1|^p}{r_4^p}+\frac{|(\boldsymbol{V}-\boldsymbol{V}_T)_2|^p}{r_5^p}}\right)$$

for $p<\infty$, and

$$G_\infty^1(\boldsymbol{Y},\boldsymbol{V}) \overset{(def)}{=} 2\left(4\frac{|(\boldsymbol{Y}-\boldsymbol{Y}_T)_3|}{r_3} + 2\left(\frac{|(\boldsymbol{Y}-\boldsymbol{Y}_T)_1|}{r_1}\wedge\frac{|(\boldsymbol{Y}-\boldsymbol{Y}_T)_2|}{r_2}\right)4\frac{|(\boldsymbol{V}-\boldsymbol{V}_T)_3|}{r_6} + 2\left(\frac{|(\boldsymbol{V}-\boldsymbol{V}_T)_1|^p}{r_4}\wedge\frac{|(\boldsymbol{V}-\boldsymbol{V}_T)_2|}{r_5}\right)\right)$$

for $p=\infty$, and

$$G_p^2(\boldsymbol{Y},\boldsymbol{V}) \overset{(def)}{=} 4\frac{|(\boldsymbol{V}-\boldsymbol{V}_T)_3|}{r_6} + 4\frac{|(\boldsymbol{Y}-\boldsymbol{Y}_T)_3|}{r_3} + G_p^1(\boldsymbol{Y},\boldsymbol{V})^2$$

for p, p^* such that $\frac{1}{p}+\frac{1}{p^*}=1$ and $p,p^*\in[1,\infty]$. Here also $o(1)$ means a small quantity with respect to 1 according to Hypothesis 2 (section 4.2), $(\boldsymbol{Y},\boldsymbol{V})\in\mathcal{R}^{k,l}_{\boldsymbol{Y}_T,\boldsymbol{V}_T,q,\boldsymbol{r}}$, and $q=O(1)$. Thus, we have the following theorem.

Theorem 6.4. *For any 2-sliced resolution $\mathcal{R}^{j,k}_{\boldsymbol{Y}_T,\boldsymbol{V}_T,q,\boldsymbol{r}}$, we have*

$$\frac{\left|\mathcal{I}^{\mathrm{CC}}(\boldsymbol{Y},\boldsymbol{V})-\tilde{I}_N^{\mathrm{CC}}(\boldsymbol{Y},\boldsymbol{V})\right|}{\|\mathcal{I}^{\mathrm{CC}}\|_\infty} \le \sqrt{\frac{256}{N}}\,q \wedge \frac{128q^2+2q}{N}$$

for all $(\boldsymbol{Y},\boldsymbol{V})\in\mathcal{R}^{j,k}_{\boldsymbol{Y}_T,\boldsymbol{V}_T,q,\boldsymbol{r}}$.

This bound seems really pessimistic compared to the results obtained in the simulations. However, this large number is only due to the vertical direction that concerns the Y_3 and V_3 estimation. For the MF, we could retrieve the third coordinate of the position using the bandwidth while the bandwidth is not helping us in the CC case. Also, for the MF we were able to retrieve the third coordinate of the speed by the ISAR effect, that is, the synthetic

Downloaded 11/28/17 to 171.67.216.21. Redistribution subject to SIAM license or copyright; see http://www.siam.org/journals/ojsa.php

Copyright © by SIAM. Unauthorized reproduction of this article is prohibited.

Downloaded 11/28/17 to 171.67.216.21. Redistribution subject to SIAM license or copyright; see http://www.siam.org/journals/ojsa.php

aperture created by the moving object, while in CC the ISAR effects cancel out, and only terms involving $\boldsymbol{X}_R$ remain. Thus we have a factor 8 because of the two *mixed effects* that appear in the range direction. However, if we consider partial images $\mathcal{R}^{1,2}_{\boldsymbol{Y}_T,\boldsymbol{V}_T,q,\boldsymbol{r}}$ and $\mathcal{R}^{4,5}_{\boldsymbol{Y}_T,\boldsymbol{V}_T,q,\boldsymbol{r}}$, we will obtain a bound of $\sqrt{\frac{16}{N}}q \wedge \frac{8q^2}{N}$ which is tighter.

The derived upper bounds suggest that more receivers could be required for correlation-based imaging compared to MF. For example, to achieve the same precision in the horizontal components (Y_1, Y_2, V_1, V_2), then the CC image would require 4 times more receivers than the MF. However, we should not forget that these are just upper bounds and therefore they should not be mistaken for necessary conditions. Moreover, our numerical simulations indicate that correlation-based imaging converges more rapidly than MF to the asymptotic point spread function since the side lobes decrease faster as the number of receivers increases.

Remark 5. As shown in section 4, the resolution for both imaging methods depends on the carrier frequency but our analysis shows that a small number of receivers is needed to obtain the theoretical imaging results established in the limit of a continuous distribution of receivers. The error bound between the continuous and the discrete function is obtained in an area that is proportional to the resolution $q\times[-r_j, r_j]$ with r_j the resolution estimate in variable $j = 1, \ldots, 6$. Because the area depends on the resolution a fixed number of receivers is needed independent of the carrier frequency. If however the area is fixed and is not proportional to the resolution, more receivers will be needed as the carrier frequency increases.

7. Conclusions. In this paper we consider methods for imaging a fast moving object orbiting the earth and analyze their resolutions. Our imaging system consists of a passive network of receivers and one powerful emitter located on the ground. We carry out a detailed resolution analysis from first principles for two imaging methods: the well-established MF and a correlation-based imaging method. For simplicity we assume that the receivers are also located on the ground. It would be more interesting for the correlation-based imaging method to have high-flying airborne receivers. Since, however, the speed of the receivers is low, and much lower than that of a satellite in LEO, we expect our theory to generalize to this case. Airborne receivers are of interest because they can fly above the turbulent atmosphere, in which case we expect the correlation-based imaging method to be robust relative to atmospheric turbulence effects. Robustness of correlation-based imaging to propagation medium fluctuations was shown in [9, 10, 11] for stationary receiver arrays. We also expect correlation-based imaging to be robust to additive measurement noise since we cross-correlate signals recorded at different receivers. For both imaging methods, we obtain nearly optimal resolution results that are of the order of the wavelength, which is 3 cm for the X-band surveillance system. Our analysis shows that even for a fast moving object such as a low-orbit satellite ($V_T \sim 7000$ m/s), the Doppler correction does not affect the resolution but needs to be taken into consideration in the imaging functions. We also show that a sparse configuration of about 10 uniformly distributed receivers over an area of diameter 400 kilometers is sufficient so as to have a point spread function with a similar shape (same maximum located at the same point and same decreasing width, which means same resolution) to the one obtained with a dense set of receivers. Extensive numerical simulations clearly support and confirm the theory developed in this paper. Our resolution analysis can be used for assessing the performance of MF and correlation-based imaging in the case of well-separated pointlike

Copyright © by SIAM. Unauthorized reproduction of this article is prohibited.

scatterers. For extended objects and/or nearby reflectors a careful analysis of the side lobes of the point spread function presented here should be carried out.

Appendix A. Other imaging functions for CC. If the pulse emission profile remains the same throughout the experiment, one could also think about cross correlating and migrating signals corresponding to different pairs of receivers and different pulses. This would require sending the signals to a base station and then cross correlating at a later time the NN_E recordings $(u_{\mathrm{s},R}(S_j+t))_t$, $j=1,\dots,N_E$, $R=1,\dots,N$. This is indeed possible if we know the relative emission times, ΔT_E, and the emitter location, $\boldsymbol{X}_E$, by considering the following imaging function,

$$\widetilde{\mathcal{I}}^{\mathrm{CC}}(\boldsymbol{Y},\boldsymbol{V})=\frac{1}{N_E^2}\sum_{j,j'=1}^{N_E}\widetilde{\mathcal{I}}^{\mathrm{CC}}_{j,j'}(\boldsymbol{Y}+\boldsymbol{V}S_j,\boldsymbol{Y}+\boldsymbol{V}S_{j'},\boldsymbol{V}), \tag{A.1}$$

$$\begin{aligned}\widetilde{\mathcal{I}}^{\mathrm{CC}}_{j,j'}(\boldsymbol{X},\boldsymbol{X}',\boldsymbol{V})=\frac{1}{N^2}\sum_{R,R'=1}^{N}\int u_{\mathrm{s},R}\left(S_j+\frac{|\boldsymbol{X}-\boldsymbol{X}_R|}{c_o}+\frac{t+\frac{|\boldsymbol{X}-\boldsymbol{X}_E|}{c_o}}{\gamma_{\mathrm{s}}(\boldsymbol{X},\boldsymbol{V},\boldsymbol{X}_R)}\right)\\ \times u_{\mathrm{s},R'}\left(S_{j'}+\frac{|\boldsymbol{X}'-\boldsymbol{X}_{R'}|}{c_o}+\frac{t+\frac{|\boldsymbol{X}'-\boldsymbol{X}_E|}{c_o}}{\gamma_{\mathrm{s}}(\boldsymbol{X}',\boldsymbol{V},\boldsymbol{X}_{R'})}\right)dt.\end{aligned} \tag{A.2}$$

In the same setting, we can consider another imaging function,

$$\widehat{\mathcal{I}}^{\mathrm{CC}}(\boldsymbol{Y},\boldsymbol{V})=\frac{1}{N_E^2}\sum_{j,j'=1}^{N_E}\widehat{\mathcal{I}}^{\mathrm{CC}}_{j,j'}(\boldsymbol{Y}+\boldsymbol{V}S_j,\boldsymbol{Y}+\boldsymbol{V}S_{j'},\boldsymbol{V}), \tag{A.3}$$

$$\begin{aligned}\widehat{\mathcal{I}}^{\mathrm{CC}}_{j,j'}(\boldsymbol{X},\boldsymbol{X}',\boldsymbol{V})=\frac{1}{N}\sum_{R=1}^{N}\int u_{\mathrm{s},R}\left(S_j+\frac{|\boldsymbol{X}-\boldsymbol{X}_R|}{c_o}+\frac{t+\frac{|\boldsymbol{X}-\boldsymbol{X}_E|}{c_o}}{\gamma_{\mathrm{s}}(\boldsymbol{X},\boldsymbol{V},\boldsymbol{X}_R)}\right)\\ \times u_{\mathrm{s},R}\left(S_{j'}+\frac{|\boldsymbol{X}'-\boldsymbol{X}_R|}{c_o}+\frac{t+\frac{|\boldsymbol{X}'-\boldsymbol{X}_E|}{c_o}}{\gamma_{\mathrm{s}}(\boldsymbol{X}',\boldsymbol{V},\boldsymbol{X}_R)}\right)dt.\end{aligned} \tag{A.4}$$

In this case processing can be carried out by each receiver, and then the images are stacked,

$$\widehat{\mathcal{I}}^{\mathrm{CC}}(\boldsymbol{Y},\boldsymbol{V})=\frac{1}{N}\sum_{R=1}^{N}\widehat{\mathcal{I}}^{\mathrm{CC}}_{R}(\boldsymbol{Y},\boldsymbol{V}), \tag{A.5}$$

$$\widehat{\mathcal{I}}^{\mathrm{CC}}_{R}(\boldsymbol{Y},\boldsymbol{V})=\frac{1}{N_E^2}\sum_{j,j'=1}^{N_E}\widehat{\mathcal{I}}^{\mathrm{CC}}_{j,j',R}(\boldsymbol{Y}+\boldsymbol{V}S_j,\boldsymbol{Y}+\boldsymbol{V}S_{j'},\boldsymbol{V}), \tag{A.6}$$

$$\begin{aligned}\widehat{\mathcal{I}}^{\mathrm{CC}}_{j,j',R}(\boldsymbol{X},\boldsymbol{X}',\boldsymbol{V})=\int u_{\mathrm{s},R}\left(S_j+\frac{|\boldsymbol{X}-\boldsymbol{X}_R|}{c_o}+\frac{t+\frac{|\boldsymbol{X}-\boldsymbol{X}_E|}{c_o}}{\gamma_{\mathrm{s}}(\boldsymbol{X},\boldsymbol{V},\boldsymbol{X}_R)}\right)\\ \times u_{\mathrm{s},R}\left(S_{j'}+\frac{|\boldsymbol{X}'-\boldsymbol{X}_R|}{c_o}+\frac{t+\frac{|\boldsymbol{X}'-\boldsymbol{X}_E|}{c_o}}{\gamma_{\mathrm{s}}(\boldsymbol{X}',\boldsymbol{V},\boldsymbol{X}_R)}\right)dt.\end{aligned} \tag{A.7}$$

Downloaded 11/28/17 to 171.67.216.21. Redistribution subject to SIAM license or copyright; see http://www.siam.org/journals/ojsa.php

Copyright © by SIAM. Unauthorized reproduction of this article is prohibited.

Downloaded 11/28/17 to 171.67.216.21. Redistribution subject to SIAM license or copyright; see http://www.siam.org/journals/ojsa.php

This latter imaging functional cross correlates the scattered signals recorded at each receiver separately and corresponding to different emission times. Therefore, less communication with the base station is required since each receiver can store and process the N_E signals $(u_{s,R}(S_j+t))_t$, $j=1,\dots,N_E$, that it records. The individual receiver contributions $\widehat{\mathcal{I}}_R^{\mathrm{CC}}(\boldsymbol{Y},\boldsymbol{V})$ should be send to the base station where the averaging over all receivers as in (A.5) would be performed.

Appendix B. Resolution analysis.

B.1. Preliminary considerations.

In general we have the following Taylor expansion,

$$|\boldsymbol{X}+\boldsymbol{\delta}| = |\boldsymbol{X}| + \boldsymbol{m}_{\boldsymbol{X}}\cdot\boldsymbol{\delta} + \frac{1}{2}{}^t\boldsymbol{\delta}\frac{\mathbf{P}_{\boldsymbol{X}}^{\perp}}{|\boldsymbol{X}|^2}\boldsymbol{\delta} - \frac{1}{2}{}^t\boldsymbol{\delta}\frac{\mathbf{P}_{\boldsymbol{X}}^{\perp}}{|\boldsymbol{X}|^3}\boldsymbol{\delta}(\boldsymbol{m}_{\boldsymbol{X}}\cdot\boldsymbol{\delta}) + O\left(\frac{|\boldsymbol{\delta}|^4}{|\boldsymbol{X}|^3}\right).$$

Thus, especially with $\boldsymbol{X}=\boldsymbol{Y}_T$, we get,

$$|\boldsymbol{Y}_T+\boldsymbol{\delta}| = |\boldsymbol{Y}_T| + (\boldsymbol{\delta})_3 + \frac{1}{2}\frac{|\boldsymbol{\delta}_\perp|^2}{|\boldsymbol{Y}_T|}\left(1-\frac{(\boldsymbol{\delta})_3}{|\boldsymbol{Y}_T|}\right) + O\left(\frac{|\boldsymbol{\delta}|^4}{|\boldsymbol{Y}_T|^3}\right).$$

We also have the Taylor expansion,

$$\boldsymbol{m}_{\boldsymbol{X}+\boldsymbol{\delta}} = \boldsymbol{m}_{\boldsymbol{X}} + \mathbf{P}_{\boldsymbol{X}}^{\perp}\frac{\boldsymbol{\delta}}{|\boldsymbol{X}|} - \frac{1}{2|\boldsymbol{X}|^2}\left(\boldsymbol{m}_{\boldsymbol{X}}\ \left({}^t\boldsymbol{\delta}\mathbf{P}_{\boldsymbol{X}}^{\perp}\boldsymbol{\delta}\right) + 2(\boldsymbol{m}_{\boldsymbol{X}}\cdot\boldsymbol{\delta})\mathbf{P}_{\boldsymbol{X}}^{\perp}\boldsymbol{\delta}\right) + O\left(\frac{|\boldsymbol{\delta}|^3}{|\boldsymbol{X}|^3}\right),$$

which for $\boldsymbol{X}=\boldsymbol{Y}_T$ reduces to

$$\boldsymbol{m}_{\boldsymbol{Y}_T+\boldsymbol{\delta}} = \boldsymbol{m}_{\boldsymbol{Y}_T} + \frac{\boldsymbol{\delta}_\perp}{|\boldsymbol{Y}_T|} - \frac{1}{2|\boldsymbol{Y}_T|^2}\left(\boldsymbol{m}_{\boldsymbol{Y}_T}\ |\boldsymbol{\delta}|_\perp^2 + 2(\boldsymbol{\delta})_3\boldsymbol{\delta}_\perp\right) + O\left(\frac{|\boldsymbol{\delta}|^3}{|\boldsymbol{Y}_T|^3}\right).$$

B.2. Matched filter case.

For the matched filter resolution analysis, we want to use these expansions for the difference $|\boldsymbol{X}_T-\boldsymbol{X}_E|+|\boldsymbol{X}_T-\boldsymbol{X}_R|-|\boldsymbol{X}-\boldsymbol{X}_E|-|\boldsymbol{X}-\boldsymbol{X}_R|$. Expanding first with respect to $|\boldsymbol{X}-\boldsymbol{X}_T|$, and then with respect to $\boldsymbol{X}_R$ and $\boldsymbol{X}_E$, and using that $|\boldsymbol{X}_T-\boldsymbol{X}|+|\boldsymbol{X}_R|+|\boldsymbol{X}_E|+T_{\mathrm{tot}}|\boldsymbol{V}_T|\ll|\boldsymbol{X}_T|$, we get

$$\begin{aligned}
&|\boldsymbol{X}_T-\boldsymbol{X}_E|+|\boldsymbol{X}_T-\boldsymbol{X}_R|-|\boldsymbol{X}-\boldsymbol{X}_E|-|\boldsymbol{X}-\boldsymbol{X}_R| \\
&\quad= (\boldsymbol{X}-\boldsymbol{X}_T)\cdot(-\boldsymbol{m}_{\boldsymbol{X}_T-\boldsymbol{X}_R}-\boldsymbol{m}_{\boldsymbol{X}_T-\boldsymbol{X}_E}) + O\left(\frac{|\boldsymbol{X}-\boldsymbol{X}_T|^2}{H_T}\right) \\
&\quad= (\boldsymbol{X}-\boldsymbol{X}_T)\cdot\Bigg(-2\boldsymbol{m}_{\boldsymbol{Y}_T} + \frac{\mathbf{P}_{\boldsymbol{Y}_T}^{\perp}}{|\boldsymbol{Y}_T|}(\boldsymbol{X}_R+\boldsymbol{X}_E-2S_j\boldsymbol{V}_T) \\
&\qquad\qquad + \frac{1}{2|\boldsymbol{Y}_T|^2}\big(\boldsymbol{m}_{\boldsymbol{Y}_T}\ |S_j\boldsymbol{V}_T-\boldsymbol{X}_R|_\perp^2 + 2(S_j\boldsymbol{V}_T-\boldsymbol{X}_R)_3(S_j\boldsymbol{V}_T-\boldsymbol{X}_R)_\perp \\
&\qquad\qquad\qquad + \boldsymbol{m}_{\boldsymbol{Y}_T}\ |S_j\boldsymbol{V}_T-\boldsymbol{X}_E|_\perp^2 + 2(S_j\boldsymbol{V}_T-\boldsymbol{X}_E)_3(S_j\boldsymbol{V}_T-\boldsymbol{X}_E)_\perp\big) \\
&\qquad\qquad + O\left(\frac{|S_j\boldsymbol{V}_T|^3+|\boldsymbol{X}_R|^3+|\boldsymbol{X}_E|^3}{H_T^3}\right)\Bigg) + O\left(\frac{|\boldsymbol{X}-\boldsymbol{X}_T|^2}{H_T}\right)
\end{aligned}$$

Copyright © by SIAM. Unauthorized reproduction of this article is prohibited.

$$
\begin{aligned}
&= -2(\boldsymbol{X}-\boldsymbol{X}_T)_3 + \frac{1}{H_T}\langle \boldsymbol{X}-\boldsymbol{X}_T, \boldsymbol{X}_R+\boldsymbol{X}_E-2S_j\boldsymbol{V}_T\rangle_\perp \\
&\quad + \frac{1}{2H_T^2}(\boldsymbol{X}-\boldsymbol{X}_T)_3\left(2|S_j\boldsymbol{V}_T|_\perp^2 - 2\langle S_j\boldsymbol{V}_T, \boldsymbol{X}_R+\boldsymbol{X}_E\rangle_\perp + |\boldsymbol{X}_R|_\perp^2 + |\boldsymbol{X}_E|_\perp^2\right) \\
&\quad + \frac{1}{H_T^2}\langle \boldsymbol{X}-\boldsymbol{X}_T, (S_j\boldsymbol{V}_T-\boldsymbol{X}_E)_3(S_j\boldsymbol{V}_T-\boldsymbol{X}_E) + (S_j\boldsymbol{V}_T-\boldsymbol{X}_R)_3(S_j\boldsymbol{V}_T-\boldsymbol{X}_R)\rangle_\perp \\
&\quad + O\left(\frac{(a+T_{\rm tot}|\boldsymbol{V}_T|)^3}{H_T^3}|\boldsymbol{X}-\boldsymbol{X}_T| + \frac{|\boldsymbol{X}-\boldsymbol{X}_T|^2}{H_T}\right),
\end{aligned}
$$

where in the second equality, we have also differentiated some terms with respect to $S_j\boldsymbol{V}_T$. Moreover,

$$
\begin{aligned}
&|\boldsymbol{X}_T-\boldsymbol{X}_E|\boldsymbol{V}_T\cdot\frac{\boldsymbol{X}_T-\boldsymbol{X}_E}{|\boldsymbol{X}_T-\boldsymbol{X}_E|} - |\boldsymbol{X}-\boldsymbol{X}_E|\boldsymbol{V}\cdot\frac{\boldsymbol{X}-\boldsymbol{X}_E}{|\boldsymbol{X}-\boldsymbol{X}_E|} \\
&\quad = \boldsymbol{V}_T\cdot(\boldsymbol{X}_T-\boldsymbol{X}_E) - \boldsymbol{V}\cdot(\boldsymbol{X}-\boldsymbol{X}_E) \\
&\quad = (\boldsymbol{V}_T-\boldsymbol{V})\cdot(\boldsymbol{X}_T-\boldsymbol{X}_E) + \boldsymbol{V}\cdot(\boldsymbol{X}_T-\boldsymbol{X}) \\
&\quad = (\boldsymbol{V}_T-\boldsymbol{V})\cdot(\boldsymbol{X}_T-\boldsymbol{X}_E) + \boldsymbol{V}_T\cdot(\boldsymbol{X}_T-\boldsymbol{X}) + O(|\boldsymbol{X}_T-\boldsymbol{X}||\boldsymbol{V}_T-\boldsymbol{V}|) \\
&\quad = H_T(\boldsymbol{V}_T-\boldsymbol{V})_3 + \boldsymbol{V}_T\cdot(\boldsymbol{X}_T-\boldsymbol{X}) + O(|\boldsymbol{X}_T-\boldsymbol{X}||\boldsymbol{V}_T-\boldsymbol{V}| + (a+T_{\rm tot}|\boldsymbol{V}_T|)|\boldsymbol{V}_T-\boldsymbol{V}|).
\end{aligned}
$$

We also have

$$
\begin{aligned}
&|\boldsymbol{X}_T-\boldsymbol{X}_E|\boldsymbol{V}_T\cdot\frac{\boldsymbol{X}_T-\boldsymbol{X}_R}{|\boldsymbol{X}_T-\boldsymbol{X}_R|} - |\boldsymbol{X}-\boldsymbol{X}_E|\boldsymbol{V}\cdot\frac{\boldsymbol{X}-\boldsymbol{X}_R}{|\boldsymbol{X}-\boldsymbol{X}_R|} \\
&\quad = |\boldsymbol{X}_T-\boldsymbol{X}_E|(\boldsymbol{V}_T-\boldsymbol{V})\cdot\boldsymbol{m}_{TR} + \boldsymbol{m}_{TE}\cdot(\boldsymbol{X}_T-\boldsymbol{X})\boldsymbol{V}_T\cdot\boldsymbol{m}_{TR} \\
&\qquad + |\boldsymbol{X}_T-\boldsymbol{X}_E|^t\boldsymbol{V}_T\frac{\mathbf{P}_{TR}^\perp}{|\boldsymbol{X}_T-\boldsymbol{X}_R|}(\boldsymbol{X}_T-\boldsymbol{X}) + O\left(\frac{|\boldsymbol{X}_T-\boldsymbol{X}|^2||\boldsymbol{V}_T|}{H_T}\right) \\
&\quad = H_T(\boldsymbol{V}_T-\boldsymbol{V})_3 + \boldsymbol{V}_T\cdot(\boldsymbol{X}_T-\boldsymbol{X}) \\
&\qquad + O\left(\frac{|\boldsymbol{X}_T-\boldsymbol{X}|^2||\boldsymbol{V}_T|}{H_T} + \frac{a+T_{\rm tot}|\boldsymbol{V}_T|}{H_T}|\boldsymbol{V}_T||\boldsymbol{X}_T-\boldsymbol{X}|\right. \\
&\qquad\qquad \left. + |\boldsymbol{V}_T-\boldsymbol{V}|(a+T_{\rm tot}|\boldsymbol{V}_T|)\frac{|\boldsymbol{X}_T-\boldsymbol{X}|+a+T_{\rm tot}|\boldsymbol{V}_T|}{H_T}\right).
\end{aligned}
$$

To neglect the $O()$ expressions in the phase terms we need

- for the first expansion, that $\frac{\omega_o}{c_o}\frac{(a+T_{\rm tot}|\boldsymbol{V}_T|)^3}{H_T^3}|\boldsymbol{X}-\boldsymbol{X}_T| = o(1)$ and $\frac{\omega_o|\boldsymbol{X}_T-\boldsymbol{X}|^2}{H_Tc_o} = o(1)$;
- for the second expansion that $\frac{\omega_o}{c_o^2}(a+T_{\rm tot}|\boldsymbol{V}_T|)|\boldsymbol{V}_T-\boldsymbol{V}| = o(1)$ and $\frac{\omega_o|\boldsymbol{X}_T-\boldsymbol{X}||\boldsymbol{V}_T-\boldsymbol{V}|}{c_o^2} = o(1)$;
- for the third expansion that $\frac{\omega_o}{c_o^2}\frac{a+T_{\rm tot}|\boldsymbol{V}_T|}{H_T}(H_T|\boldsymbol{V}_T-\boldsymbol{V}| + |\boldsymbol{V}_T||\boldsymbol{X}_T-\boldsymbol{X}|) = o(1)$, that $\frac{\omega_o|\boldsymbol{X}_T-\boldsymbol{X}|^2||\boldsymbol{V}_T|}{H_Tc_o^2} = o(1)$, and $\frac{\omega_o}{c_o^2}|\boldsymbol{V}_T-\boldsymbol{V}|(a+T_{\rm tot}|\boldsymbol{V}_T|)\frac{|\boldsymbol{X}_T-\boldsymbol{X}|+a+T_{\rm tot}|\boldsymbol{V}_T|}{H_T} = o(1)$.

Downloaded 11/28/17 to 171.67.216.21. Redistribution subject to SIAM license or copyright; see http://www.siam.org/journals/ojsa.php

Copyright © by SIAM. Unauthorized reproduction of this article is prohibited.

Downloaded 11/28/17 to 171.67.216.21. Redistribution subject to SIAM license or copyright; see http://www.siam.org/journals/ojsa.php

More precisely, let us assume that

$$\frac{a+T_{\rm tot}|\boldsymbol{V}_T|}{H_T}=o(1),\quad \frac{V_T}{c_o}\ll\left(\frac{a+T_{\rm tot}|\boldsymbol{V}_T|}{H_T}\right)^2,\quad \frac{H_T^2}{c_o(a+T_{\rm tot}|\boldsymbol{V}_T|)T_{\rm tot}}\ll 1,\quad \frac{\lambda_o}{H_T}\ll 16\left(\frac{a+T_{\rm tot}|\boldsymbol{V}_T|}{H_T}\right)^4,$$

and

$$|\boldsymbol{X}_T-\boldsymbol{X}|<\frac{4\lambda_o H_T^2}{(a+T_{\rm tot}|\boldsymbol{V}_T|)^2},\quad |\boldsymbol{V}_T-\boldsymbol{V}|<\frac{\lambda_o H_T^2}{T_{\rm tot}(a+T_{\rm tot}|\boldsymbol{V}_T|)^2},\quad \frac{c_o}{2B}<\frac{4\lambda_o H_T^2}{(a+T_{\rm tot}|\boldsymbol{V}_T|)^2}.$$

Then it follows that $\frac{\omega_o}{c_o}|\boldsymbol{X}_T-\boldsymbol{X}|(\frac{a+T_{\rm tot}|\boldsymbol{V}_T|}{H_T})^3<o(1)$ and $\frac{\omega_o}{c_o^2}(a+T_{\rm tot}|\boldsymbol{V}_T|)|\boldsymbol{V}_T-\boldsymbol{V}|\le\frac{H_T^2}{c_o(a+T_{\rm tot}|\boldsymbol{V}_T|)T_{\rm tot}}=o(1)$. Moreover, $\frac{\omega_o|\boldsymbol{X}_T-\boldsymbol{X}|^2}{c_oH_T}\ll 1$, and the other requirement are also satisfied. Consequently, all the expressions in $O()$ can be neglected in the phase terms. Moreover, our assumptions also imply that

$$|\boldsymbol{V}_T-\boldsymbol{V}|\ll\frac{c_o^2}{H_TB}\text{ and }|\boldsymbol{X}_T-\boldsymbol{X}|\ll\frac{c_o^2}{|\boldsymbol{V}_T|B}.$$

Or, equivalently, $\frac{|\boldsymbol{V}_T-\boldsymbol{V}|}{|\boldsymbol{V}_T|}$ and $\frac{|\boldsymbol{X}_T-\boldsymbol{X}|}{H_T}\ll\frac{c_o^2}{|\boldsymbol{V}_T|BH_T}$ ($\sim$4.3%). This allows us to keep only the travel time terms in the centered bandwidth integral.

The condition $\frac{c_o}{2B}<\frac{4\lambda_oH_T^2}{(a+T_{\rm tot}|\boldsymbol{V}_T|)^2}$ is only needed so as to have a consistent and simple reasoning. We can remove this assumption using higher order expansions. For a general B, we would need to assume that $|\boldsymbol{X}_T-\boldsymbol{X}|<\lambda_o\frac{4\lambda_oH_T^p}{(a+T_{\rm tot}|\boldsymbol{V}_T|)^p}$ with $p>\frac{\log(\frac{\omega_o}{8B\lambda_o})}{\log(\frac{H_T}{a+T_{\rm tot}|\boldsymbol{V}_T|})}$, this means doing p-order expansions of travel times. Under these assumptions we obtain

$$\begin{aligned}
&\mathcal{I}_j^{\rm MF}(\boldsymbol{X},\boldsymbol{V})\\
&\sim\frac{k_o^2\rho}{32\pi^3H_T^2Ba^2}\int_{\mathbb{R}^2}d\boldsymbol{x}_R p\Big(\frac{\boldsymbol{x}_R}{a}\Big)\\
&\quad\times\exp\Big(i\frac{\omega_o}{c_o}\Big(-2(\boldsymbol{X}-\boldsymbol{X}_T)_3+\frac{1}{H_T}\langle\boldsymbol{X}-\boldsymbol{X}_T,\boldsymbol{X}_R+\boldsymbol{X}_E-2S_j\boldsymbol{V}_T\rangle_\perp\\
&\quad+\frac{1}{2H_T^2}(\boldsymbol{X}-\boldsymbol{X}_T)_3(2|S_j\boldsymbol{V}_T|_\perp^2-2\langle S_j\boldsymbol{V}_T,\boldsymbol{X}_R+\boldsymbol{X}_E\rangle_\perp+|\boldsymbol{X}_R|_\perp^2+|\boldsymbol{X}_E|_\perp^2)\\
&\quad+\frac{1}{H_T^2}\langle\boldsymbol{X}-\boldsymbol{X}_T,(S_j\boldsymbol{V}_T-\boldsymbol{X}_E)_3(S_j\boldsymbol{V}_T-\boldsymbol{X}_E)+(S_j\boldsymbol{V}_T-\boldsymbol{X}_R)_3(S_j\boldsymbol{V}_T-\boldsymbol{X}_R)\rangle_\perp\Big)\Big)\\
&\quad\times\Big[\int_{\mathbb{R}}|\hat F(\tilde\omega)|^2\exp\Big(i\frac{B}{c_o}\tilde\omega\Big(-2(\boldsymbol{X}-\boldsymbol{X}_T)_3+\frac{1}{H_T}\langle\boldsymbol{X}-\boldsymbol{X}_T,\boldsymbol{X}_R+\boldsymbol{X}_E-2S_j\boldsymbol{V}_T\rangle_\perp\\
&\quad+\frac{1}{2H_T^2}(\boldsymbol{X}-\boldsymbol{X}_T)_3(2|S_j\boldsymbol{V}_T|_\perp^2-2\langle S_j\boldsymbol{V}_T,\boldsymbol{X}_R+\boldsymbol{X}_E\rangle_\perp+|\boldsymbol{X}_R|_\perp^2+|\boldsymbol{X}_E|_\perp^2)\\
&\quad+\frac{1}{H_T^2}\langle\boldsymbol{X}-\boldsymbol{X}_T,(S_j\boldsymbol{V}_T-\boldsymbol{X}_E)_3(S_j\boldsymbol{V}_T-\boldsymbol{X}_E)+(S_j\boldsymbol{V}_T-\boldsymbol{X}_R)_3(S_j\boldsymbol{V}_T-\boldsymbol{X}_R)\rangle_\perp\Big)\Big)d\tilde\omega\Big]\\
&\quad\times\exp\Big(i\frac{2\omega_o}{c_o^2}\big(H_T(\boldsymbol{V}_T-\boldsymbol{V})_3+\boldsymbol{V}_T\cdot(\boldsymbol{X}_T-\boldsymbol{X})\big)\Big)\Big)
\end{aligned}$$

Copyright © by SIAM. Unauthorized reproduction of this article is prohibited.

with $\boldsymbol{X}_R = (\boldsymbol{x}_R, 0)$. Consequently, summing up over slow time, we get

$$
\begin{aligned}
&\mathcal{I}^{\mathrm{MF}}(\boldsymbol{X},\boldsymbol{V}) \\
&= \frac{k_o^2\rho}{32\pi^3 H_T^2 B N_E}\sum_{j=1}^{N_E}\int_{\mathbb{R}} d\tilde{\omega}|\hat{F}(\tilde{\omega})|^2\frac{1}{a^2}\int_{\mathbb{R}^2} d\boldsymbol{x}_R p\Big(\frac{\boldsymbol{x}_R}{a}\Big) \\
&\quad\times\exp\Big(i\frac{\omega_o+B\tilde{\omega}}{c_o}\Big(-2(\boldsymbol{X}-\boldsymbol{X}_T)_3+\frac{1}{H_T}\langle \boldsymbol{X}-\boldsymbol{X}_T, \boldsymbol{X}_R+\boldsymbol{X}_E-2S_j\boldsymbol{V}_T\rangle_\perp \\
&\quad+\frac{1}{2H_T^2}(\boldsymbol{X}-\boldsymbol{X}_T)_3(2|S_j\boldsymbol{V}_T|_\perp^2-2\langle S_j\boldsymbol{V}_T,\boldsymbol{X}_R+\boldsymbol{X}_E\rangle_\perp+|\boldsymbol{X}_R|^2+|\boldsymbol{X}_E|_\perp^2) \\
&\quad+\frac{1}{H_T^2}\langle \boldsymbol{X}-\boldsymbol{X}_T,(S_j\boldsymbol{V}_T-\boldsymbol{X}_E)_3(S_j\boldsymbol{V}_T-\boldsymbol{X}_E)+(S_j\boldsymbol{V}_T-\boldsymbol{X}_R)_3(S_j\boldsymbol{V}_T-\boldsymbol{X}_R)\rangle_\perp\Big)\Big) \\
&\quad\times\exp\Big(i\frac{2\omega_o}{c_o^2}\big(H_T(\boldsymbol{V}_T-\boldsymbol{V})_3+\boldsymbol{V}_T\cdot(\boldsymbol{X}_T-\boldsymbol{X})\big)\Big),
\end{aligned}
$$

which becomes

$$
\begin{aligned}
&\mathcal{I}^{\mathrm{MF}}(\boldsymbol{X},\boldsymbol{V}) \\
&= \frac{k_o^2\rho}{32\pi^3 H_T^2 B N_E}\sum_{j=1}^{N_E}\int_{\mathbb{R}} d\tilde{\omega}|\hat{F}(\tilde{\omega})|^2\frac{1}{a^2}\int_{\mathbb{R}^2} d\boldsymbol{x}_R p\Big(\frac{\boldsymbol{x}_R}{a}\Big) \\
&\quad\times\exp\Big(i\frac{\omega_o+\tilde{\omega}B}{c_o}\Big(\frac{-2S_j}{H_T}\langle \boldsymbol{V}-\boldsymbol{V}_T,\boldsymbol{X}_R+\boldsymbol{X}_E\rangle_\perp \\
&\qquad-\frac{2}{H_T^2}\langle S_j\boldsymbol{V}_T,\boldsymbol{X}_R+\boldsymbol{X}_E\rangle_\perp((\boldsymbol{Y}-\boldsymbol{Y}_T)_3+S_j(\boldsymbol{V}-\boldsymbol{V}_T)_3) \\
&\qquad+\frac{-1}{H_T^2}\langle \boldsymbol{Y}-\boldsymbol{Y}_T+S_j(\boldsymbol{V}_T-\boldsymbol{V}),(\boldsymbol{X}_E+\boldsymbol{X}_R)_3(\boldsymbol{V}_T)+(\boldsymbol{V}_T)_3(\boldsymbol{X}_E+\boldsymbol{X}_R)\rangle_\perp \\
&\qquad+S_j(\boldsymbol{V}_T-\boldsymbol{V})_3\frac{|\boldsymbol{X}_R|^2+|\boldsymbol{X}_E|_\perp^2}{H_T^2}+\frac{S_j}{H_T^2}\langle \boldsymbol{V}-\boldsymbol{V}_T,(\boldsymbol{X}_E)_3(\boldsymbol{X}_E)+(\boldsymbol{X}_R)_3(\boldsymbol{X}_R)\rangle_\perp\Big)\Big) \\
&\quad\times\exp\Big(i\frac{\omega_o+\tilde{\omega}B}{c_o}\Big(\frac{1}{H_T}\langle \boldsymbol{Y}-\boldsymbol{Y}_T,\boldsymbol{X}_R+\boldsymbol{X}_E\rangle_\perp \\
&\qquad+\frac{1}{H_T^2}\langle \boldsymbol{Y}-\boldsymbol{Y}_T,(\boldsymbol{X}_E)_3(\boldsymbol{X}_E)+(\boldsymbol{X}_R)_3(\boldsymbol{X}_R)\rangle_\perp \\
&\qquad+(\boldsymbol{Y}_T-\boldsymbol{Y})_3\frac{|\boldsymbol{X}_R|^2+|\boldsymbol{X}_E|_\perp^2}{H_T^2}\Big)\Big) \\
&\quad\times\exp\Big(i\frac{\omega_o+\tilde{\omega}B}{c_o}\Big(-2S_j(\boldsymbol{V}-\boldsymbol{V}_T)_3+\frac{-2S_j}{H_T}\langle \boldsymbol{Y}-\boldsymbol{Y}_T,\boldsymbol{V}_T\rangle_\perp+\frac{-2S_j^2}{H_T}\langle \boldsymbol{V}-\boldsymbol{V}_T,\boldsymbol{V}_T\rangle_\perp \\
&\qquad+\frac{S_j^2|\boldsymbol{V}_T|_\perp^2(\boldsymbol{Y}-\boldsymbol{Y}_T)_3+S_j^3|\boldsymbol{V}_T|_\perp^2(\boldsymbol{V}-\boldsymbol{V}_T)_3}{H_T^2} \\
&\qquad+\frac{2}{H_T^2}\langle \boldsymbol{Y}-\boldsymbol{Y}_T+S_j(\boldsymbol{V}-\boldsymbol{V}_T),(S_j\boldsymbol{V}_T)_3(S_j\boldsymbol{V}_T)\rangle_\perp+S_j\frac{\boldsymbol{V}_T}{c_o}\cdot(\boldsymbol{V}_T-\boldsymbol{V})\Big)\Big) \\
&\quad\times\exp\Big(-2i\frac{\tilde{\omega}B}{c_o}(\boldsymbol{Y}-\boldsymbol{Y}_T)_3\Big) \\
&\quad\times\exp\Big(i\frac{\omega_o}{c_o}\Big(-2(\boldsymbol{Y}-\boldsymbol{Y}_T)_3+\frac{H_T}{c_o}(\boldsymbol{V}_T-\boldsymbol{V})_3+\frac{\boldsymbol{V}_T}{c_o}\cdot(\boldsymbol{Y}_T-\boldsymbol{Y})\Big)\Big).
\end{aligned}
$$

Downloaded 11/28/17 to 171.67.216.21. Redistribution subject to SIAM license or copyright; see http://www.siam.org/journals/ojsa.php

Copyright © by SIAM. Unauthorized reproduction of this article is prohibited.

Downloaded 11/28/17 to 171.67.216.21. Redistribution subject to SIAM license or copyright; see http://www.siam.org/journals/ojsa.php

Some comments on the terms in the last equality:

- The first exponential contains cross terms with dependence in $\boldsymbol{X}_R$ and S_j and $\tilde{\omega}$.
- The second exponential contains terms with dependence only in $\boldsymbol{X}_R$ and $\tilde{\omega}$.
- The third exponential contains terms with dependence only in S_j and $\tilde{\omega}$.
- The fourth exponential contains terms with dependence only in $\tilde{\omega}$.
- The sixth exponential contains terms independent from all the summation integrations indices. Therefore, it can be taken out of the summations and has no effect on the modulus of the imaging function.

Taking the modulus of this expression, and approximating $\frac{1}{N_E}\sum_{j=1}^{N_E}$ by $\frac{1}{T_{\text{tot}}}\int_{-T_{\text{tot}}/2}^{T_{\text{tot}}/2} ds$, we obtain

$$
\begin{aligned}
&\left|\mathcal{I}^{\text{MF}}(\boldsymbol{X},\boldsymbol{V})\right| \\
&= \frac{k_o^2\rho}{32\pi^3 H_T^2 B T_{\text{tot}}}\Big|\int_{-T_{\text{tot}}/2}^{T_{\text{tot}}/2} ds \int_{\mathbb{R}} d\tilde{\omega}|\hat{F}(\tilde{\omega})|^2 \frac{1}{a^2}\int_{\mathbb{R}^2} d\boldsymbol{x}_R p\Big(\frac{\boldsymbol{x}_R}{a}\Big) \\
&\quad\times \exp\Big(i\frac{\omega_o+\tilde{\omega}B}{c_o}\Big(\frac{s}{H_T}\langle \boldsymbol{V}-\boldsymbol{V}_T, \boldsymbol{X}_R+\boldsymbol{X}_E\rangle_\perp \\
&\qquad -\frac{2}{H_T^2}\langle s\boldsymbol{V}_T, \boldsymbol{X}_R+\boldsymbol{X}_E\rangle_\perp((\boldsymbol{Y}-\boldsymbol{Y}_T)_3 + s(\boldsymbol{V}-\boldsymbol{V}_T)_3) \\
&\qquad +\frac{-1}{H_T^2}\langle \boldsymbol{Y}-\boldsymbol{Y}_T+s(\boldsymbol{V}_T-\boldsymbol{V}), (\boldsymbol{X}_E+\boldsymbol{X}_R)_3(\boldsymbol{V}_T)+(\boldsymbol{V}_T)_3(\boldsymbol{X}_E+\boldsymbol{X}_R)\rangle_\perp \\
&\qquad +s(\boldsymbol{V}_T-\boldsymbol{V})_3\frac{|\boldsymbol{X}_R|^2+|\boldsymbol{X}_E|_\perp^2}{H_T^2}+\frac{s}{H_T^2}\langle \boldsymbol{V}-\boldsymbol{V}_T, (\boldsymbol{X}_E)_3(\boldsymbol{X}_E)+(\boldsymbol{X}_R)_3(\boldsymbol{X}_R)\rangle_\perp\Big)\Big) \\
&\quad\times \exp\Big(i\frac{\omega_o+\tilde{\omega}B}{c_o}\Big(\frac{1}{H_T}\langle \boldsymbol{Y}-\boldsymbol{Y}_T, \boldsymbol{X}_R+\boldsymbol{X}_E\rangle_\perp \\
&\qquad +\frac{1}{H_T^2}\langle \boldsymbol{Y}-\boldsymbol{Y}_T, (\boldsymbol{X}_E)_3(\boldsymbol{X}_E)+(\boldsymbol{X}_R)_3(\boldsymbol{X}_R)\rangle_\perp \\
&\qquad +(\boldsymbol{Y}_T-\boldsymbol{Y})_3\frac{|\boldsymbol{X}_R|^2+|\boldsymbol{X}_E|_\perp^2}{H_T^2}\Big)\Big) \\
&\quad\times \exp\Big(i\frac{\omega_o+\tilde{\omega}B}{c_o}\Big(-2s(\boldsymbol{V}-\boldsymbol{V}_T)_3+\frac{-2s}{H_T}\langle \boldsymbol{Y}-\boldsymbol{Y}_T, \boldsymbol{V}_T\rangle_\perp+\frac{-2s^2}{H_T}\langle \boldsymbol{V}-\boldsymbol{V}_T, \boldsymbol{V}_T\rangle_\perp \\
&\qquad +\frac{s^2|\boldsymbol{V}_T|_\perp^2(\boldsymbol{Y}-\boldsymbol{Y}_T)_3+s^3|\boldsymbol{V}_T|_\perp^2(\boldsymbol{V}-\boldsymbol{V}_T)_3}{H_T^2} \\
&\qquad +\frac{2}{H_T^2}\langle \boldsymbol{Y}-\boldsymbol{Y}_T+s(\boldsymbol{V}-\boldsymbol{V}_T), (s\boldsymbol{V}_T)_3(s\boldsymbol{V}_T)\rangle_\perp + s\frac{\boldsymbol{V}_T}{c_o}\cdot(\boldsymbol{V}_T-\boldsymbol{V})\Big)\Big) \\
&\quad\times \exp\Big(-2i\frac{\tilde{\omega}B}{c_o}(\boldsymbol{Y}-\boldsymbol{Y}_T)_3\Big)\Big|.
\end{aligned}
$$

We can show that

$$
\begin{aligned}
\left|\mathcal{I}^{\text{MF}}(\boldsymbol{X},\boldsymbol{V})\right| = \frac{k_o^2\rho}{32\pi^3 H_T^2 B T_{\text{tot}}}\Big|&\int_{-T_{\text{tot}}/2}^{T_{\text{tot}}/2} ds \int_{\mathbb{R}} d\tilde{\omega}|\hat{F}(\tilde{\omega})|^2 \frac{1}{a^2}\int_{\mathbb{R}^2} d\boldsymbol{x}_R p\Big(\frac{\boldsymbol{x}_R}{a}\Big) \\
&\times \exp\left(i(\Phi_{\mathcal{I}^{\text{MF}}}+\epsilon_{\mathcal{I}^{\text{MF}}})(\boldsymbol{Y}-\boldsymbol{Y}_T, \boldsymbol{V}-\boldsymbol{V}_T, \boldsymbol{X}_R, s, \tilde{\omega})\right)\Big|,
\end{aligned}
\tag{B.1}
$$

Copyright © by SIAM. Unauthorized reproduction of this article is prohibited.

Downloaded 11/28/17 to 171.67.216.21. Redistribution subject to SIAM license or copyright; see http://www.siam.org/journals/ojsa.php

with the phases defined as

$$
\begin{aligned}
&\Phi_{\mathcal{I}^{\mathrm{MF}}}(\boldsymbol{Y}-\boldsymbol{Y}_T,\boldsymbol{V}-\boldsymbol{V}_T,\boldsymbol{X}_R,s,\tilde{\omega})\\
&\quad=\frac{\omega_o+\tilde{\omega}B}{c_o}\left(\frac{s}{H_T}\underbrace{\langle \boldsymbol{V}-\boldsymbol{V}_T,\boldsymbol{X}_R+\boldsymbol{X}_E\rangle_\perp}_{(\boldsymbol{V}_T)_\perp\text{resolution}}+\frac{1}{H_T}\underbrace{\langle \boldsymbol{Y}-\boldsymbol{Y}_T,\boldsymbol{X}_R+\boldsymbol{X}_E\rangle_\perp}_{\boldsymbol{Y}_\perp\text{ physical aperture effect}}\right.\\
&\qquad-\frac{2}{H_T^2}\langle s\boldsymbol{V}_T,\boldsymbol{X}_R+\boldsymbol{X}_E\rangle_\perp\left(\underbrace{(\boldsymbol{Y}-\boldsymbol{Y}_T)_3}_{Y_3\text{ mixed aperture effect}}+s\underbrace{(\boldsymbol{V}-\boldsymbol{V}_T)_3}_{V_3\text{ mixed aperture effect}}\right)\\
&\qquad-2s\underbrace{(\boldsymbol{V}-\boldsymbol{V}_T)_3}_{V_3\text{ ISAR effect}}+\frac{-2s}{H_T}\underbrace{\langle \boldsymbol{Y}-\boldsymbol{Y}_T,\boldsymbol{V}_T\rangle_\perp}_{Y_2\text{ ISAR effect}}+\frac{-2s^2}{H_T}\underbrace{\langle \boldsymbol{V}-\boldsymbol{V}_T,\boldsymbol{V}_T\rangle_\perp}_{V_2\text{ ISAR effect}}\\
&\qquad\left.-2\frac{\tilde{\omega}B}{c_o}\underbrace{(\boldsymbol{Y}-\boldsymbol{Y}_T)_3}_{Y_3\text{ bandwidth effect}}\right),
\end{aligned}
$$

and

$$
\begin{aligned}
&\epsilon_{\mathcal{I}^{\mathrm{MF}}}(\boldsymbol{Y}-\boldsymbol{Y}_T,\boldsymbol{V}-\boldsymbol{V}_T,\boldsymbol{X}_R,s,\tilde{\omega})\\
&\quad=\frac{\omega_o+\tilde{\omega}B}{c_o}\left(-\frac{1}{H_T^2}\langle \boldsymbol{Y}-\boldsymbol{Y}_T+s(\boldsymbol{V}_T-\boldsymbol{V}),(\boldsymbol{X}_E+\boldsymbol{X}_R)_3(\boldsymbol{V}_T)+(\boldsymbol{V}_T)_3(\boldsymbol{X}_E+\boldsymbol{X}_R)\rangle_\perp\right.\\
&\qquad+s(\boldsymbol{V}_T-\boldsymbol{V})_3\frac{|\boldsymbol{X}_R|^2+|\boldsymbol{X}_E|_\perp^2}{H_T^2}+\frac{s}{H_T^2}\langle \boldsymbol{V}-\boldsymbol{V}_T,(\boldsymbol{X}_E)_3(\boldsymbol{X}_E)+(\boldsymbol{X}_R)_3(\boldsymbol{X}_R)\rangle_\perp\\
&\qquad+\frac{1}{H_T^2}\langle \boldsymbol{Y}-\boldsymbol{Y}_T,(\boldsymbol{X}_E)_3(\boldsymbol{X}_E)+(\boldsymbol{X}_R)_3(\boldsymbol{X}_R)\rangle_\perp+(\boldsymbol{Y}_T-\boldsymbol{Y})_3\frac{|\boldsymbol{X}_R|^2+|\boldsymbol{X}_E|_\perp^2}{H_T^2}\\
&\qquad+\frac{s^2|\boldsymbol{V}_T|_\perp^2(\boldsymbol{Y}-\boldsymbol{Y}_T)_3+s^3|\boldsymbol{V}_T|_\perp^2(\boldsymbol{V}-\boldsymbol{V}_T)_3}{H_T^2}\\
&\qquad+\frac{2}{H_T^2}\langle \boldsymbol{Y}-\boldsymbol{Y}_T+s(\boldsymbol{V}-\boldsymbol{V}_T),(s\boldsymbol{V}_T)_3(s\boldsymbol{V}_T)\rangle_\perp\\
&\qquad\left.+\underbrace{s\frac{\boldsymbol{V}_T}{c_o}\cdot(\boldsymbol{V}_T-\boldsymbol{V})}_{\text{stems from the Doppler compensation}}\right).
\end{aligned}
$$

Furthermore, under our assumptions we have $\epsilon_{\mathcal{I}^{\mathrm{MF}}}=o(\Phi_{\mathcal{I}^{\mathrm{MF}}})$.

B.3. Correlation-based imaging function. If the number of receivers is large enough, then we can approximate the partial imaging function by its continuum approximation in space and replace $\frac{1}{N^2}\sum_{R,R'=1}^{N}$ by $\frac{1}{a^2}\int_{\mathbb{R}^2\times\mathbb{R}^2}d\boldsymbol{x}_R d\boldsymbol{x}_{R'}p(\boldsymbol{x}_R/a)p(\boldsymbol{x}_{R'}/a)$. Then we find

Copyright © by SIAM. Unauthorized reproduction of this article is prohibited.

Downloaded 11/28/17 to 171.67.216.21. Redistribution subject to SIAM license or copyright; see http://www.siam.org/journals/ojsa.php

$$
\begin{aligned}
&\mathcal{I}_j^{\mathrm{CC}}(\boldsymbol{X},\boldsymbol{V})\\
&\quad=\frac{k_o^4\rho^2}{(4\pi|\boldsymbol{X}_T|)^4 2\pi B a^4}\int_{\mathbb{R}^2} d\boldsymbol{x}_R p\left(\frac{\boldsymbol{x}_R}{a}\right)\int_{\mathbb{R}^2} d\boldsymbol{x}_{R'} p\left(\frac{\boldsymbol{x}_{R'}}{a}\right)\\
&\qquad\times\exp\left(i\frac{\omega_o}{c_o}\left(|\boldsymbol{X}-\boldsymbol{X}_R|-|\boldsymbol{X}-\boldsymbol{X}_{R'}|-|\boldsymbol{X}_T-\boldsymbol{X}_R|+|\boldsymbol{X}_T-\boldsymbol{X}_{R'}|\right)\right)\\
&\qquad\times\left[\int_{\mathbb{R}}|\hat{F}(\tilde{\omega})|^2\exp\left(i\frac{B}{c_o}\tilde{\omega}\left(|\boldsymbol{X}-\boldsymbol{X}_R|-|\boldsymbol{X}-\boldsymbol{X}_{R'}|-|\boldsymbol{X}_T-\boldsymbol{X}_R|+|\boldsymbol{X}_T-\boldsymbol{X}_{R'}|\right)\right)d\tilde{\omega}\right]\\
&\qquad\times\exp\left(i\frac{\omega_o}{c_o}(|\boldsymbol{X}_T-\boldsymbol{X}_R|-|\boldsymbol{X}-\boldsymbol{X}_R|)\frac{\boldsymbol{V}}{c_o}\cdot\left(\frac{\boldsymbol{X}-\boldsymbol{X}_R}{|\boldsymbol{X}-\boldsymbol{X}_R|}+\frac{\boldsymbol{X}-\boldsymbol{X}_E}{|\boldsymbol{X}-\boldsymbol{X}_E|}\right)\right)\\
&\qquad\times\exp\left(-i\frac{\omega_o}{c_o}(|\boldsymbol{X}_T-\boldsymbol{X}_{R'}|-|\boldsymbol{X}-\boldsymbol{X}_{R'}|)\frac{\boldsymbol{V}}{c_o}\cdot\left(\frac{\boldsymbol{X}-\boldsymbol{X}_{R'}}{|\boldsymbol{X}-\boldsymbol{X}_{R'}|}+\frac{\boldsymbol{X}-\boldsymbol{X}_E}{|\boldsymbol{X}-\boldsymbol{X}_E|}\right)\right)\\
&\qquad\times\exp\left(i\frac{\omega_o}{c_o}|\boldsymbol{X}_T-\boldsymbol{X}_E|\frac{\boldsymbol{V}}{c_o}\cdot\left(\frac{\boldsymbol{X}-\boldsymbol{X}_R}{|\boldsymbol{X}-\boldsymbol{X}_R|}-\frac{\boldsymbol{X}-\boldsymbol{X}_{R'}}{|\boldsymbol{X}-\boldsymbol{X}_{R'}|}\right)\right)\\
&\qquad\times\exp\left(-i\frac{\omega_o}{c_o}|\boldsymbol{X}_T-\boldsymbol{X}_E|\frac{\boldsymbol{V}_T}{c_o}\cdot\left(\frac{\boldsymbol{X}_T-\boldsymbol{X}_R}{|\boldsymbol{X}_T-\boldsymbol{X}_R|}-\frac{\boldsymbol{X}_T-\boldsymbol{X}_{R'}}{|\boldsymbol{X}_T-\boldsymbol{X}_{R'}|}\right)\right)
\end{aligned}
$$

with $\boldsymbol{X}_R=(\boldsymbol{x}_R,0)$. Forcing $\boldsymbol{V}_T=\boldsymbol{V}_T+\boldsymbol{V}-\boldsymbol{V}_T$ we have

$$
\begin{aligned}
&\mathcal{I}_j^{\mathrm{CC}}(\boldsymbol{X},\boldsymbol{V})\\
&\quad=\frac{k_o^4\rho^2}{(4\pi|\boldsymbol{X}_T|)^4 2\pi B a^4}\int_{\mathbb{R}^2} d\boldsymbol{x}_R p\left(\frac{\boldsymbol{x}_R}{a}\right)\int_{\mathbb{R}^2} d\boldsymbol{x}_{R'} p\left(\frac{\boldsymbol{x}_{R'}}{a}\right)\\
&\qquad\times\exp\left(i\frac{\omega_o}{c_o}\left(|\boldsymbol{X}-\boldsymbol{X}_R|-|\boldsymbol{X}-\boldsymbol{X}_{R'}|-|\boldsymbol{X}_T-\boldsymbol{X}_R|+|\boldsymbol{X}_T-\boldsymbol{X}_{R'}|\right)\right)\\
&\qquad\times\left[\int_{\mathbb{R}}|\hat{F}(\tilde{\omega})|^2\exp\left(i\frac{B}{c_o}\tilde{\omega}\left(|\boldsymbol{X}-\boldsymbol{X}_R|-|\boldsymbol{X}-\boldsymbol{X}_{R'}|-|\boldsymbol{X}_T-\boldsymbol{X}_R|+|\boldsymbol{X}_T-\boldsymbol{X}_{R'}|\right)\right)d\tilde{\omega}\right]\\
&\qquad\times\exp\left(i\frac{\omega_o}{c_o}(|\boldsymbol{X}_T-\boldsymbol{X}_R|-|\boldsymbol{X}-\boldsymbol{X}_R|)\frac{\boldsymbol{V}-\boldsymbol{V}_T}{c_o}\cdot\left(\frac{\boldsymbol{X}-\boldsymbol{X}_R}{|\boldsymbol{X}-\boldsymbol{X}_R|}+\frac{\boldsymbol{X}-\boldsymbol{X}_E}{|\boldsymbol{X}-\boldsymbol{X}_E|}\right)\right)\\
&\qquad\times\exp\left(i\frac{\omega_o}{c_o}(|\boldsymbol{X}_T-\boldsymbol{X}_R|-|\boldsymbol{X}-\boldsymbol{X}_R|)\frac{\boldsymbol{V}_T}{c_o}\cdot\left(\frac{\boldsymbol{X}-\boldsymbol{X}_R}{|\boldsymbol{X}-\boldsymbol{X}_R|}+\frac{\boldsymbol{X}-\boldsymbol{X}_E}{|\boldsymbol{X}-\boldsymbol{X}_E|}\right)\right)\\
&\qquad\times\exp\left(-i\frac{\omega_o}{c_o}(|\boldsymbol{X}_T-\boldsymbol{X}_{R'}|-|\boldsymbol{X}-\boldsymbol{X}_{R'}|)\frac{\boldsymbol{V}-\boldsymbol{V}_T}{c_o}\cdot\left(\frac{\boldsymbol{X}-\boldsymbol{X}_{R'}}{|\boldsymbol{X}-\boldsymbol{X}_{R'}|}+\frac{\boldsymbol{X}-\boldsymbol{X}_E}{|\boldsymbol{X}-\boldsymbol{X}_E|}\right)\right)\\
&\qquad\times\exp\left(-i\frac{\omega_o}{c_o}(|\boldsymbol{X}_T-\boldsymbol{X}_{R'}|-|\boldsymbol{X}-\boldsymbol{X}_{R'}|)\frac{\boldsymbol{V}_T}{c_o}\cdot\left(\frac{\boldsymbol{X}-\boldsymbol{X}_{R'}}{|\boldsymbol{X}-\boldsymbol{X}_{R'}|}+\frac{\boldsymbol{X}-\boldsymbol{X}_E}{|\boldsymbol{X}-\boldsymbol{X}_E|}\right)\right)\\
&\qquad\times\exp\left(i\frac{\omega_o}{c_o}|\boldsymbol{X}_T-\boldsymbol{X}_E|\frac{\boldsymbol{V}-\boldsymbol{V}_T}{c_o}\cdot\left(\frac{\boldsymbol{X}-\boldsymbol{X}_R}{|\boldsymbol{X}-\boldsymbol{X}_R|}-\frac{\boldsymbol{X}-\boldsymbol{X}_{R'}}{|\boldsymbol{X}-\boldsymbol{X}_{R'}|}\right)\right)\\
&\qquad\times\exp\left(-i\frac{\omega_o}{c_o}|\boldsymbol{X}_T-\boldsymbol{X}_E|\frac{\boldsymbol{V}_T}{c_o}\cdot\left(\frac{\boldsymbol{X}_T-\boldsymbol{X}_R}{|\boldsymbol{X}_T-\boldsymbol{X}_R|}-\frac{\boldsymbol{X}_T-\boldsymbol{X}_{R'}}{|\boldsymbol{X}_T-\boldsymbol{X}_{R'}|}-\frac{\boldsymbol{X}-\boldsymbol{X}_R}{|\boldsymbol{X}-\boldsymbol{X}_R|}+\frac{\boldsymbol{X}-\boldsymbol{X}_{R'}}{|\boldsymbol{X}-\boldsymbol{X}_{R'}|}\right)\right).
\end{aligned}
$$

If we assume that $\frac{\omega_o}{c_o^2}|\boldsymbol{X}_T-\boldsymbol{X}|\times|\boldsymbol{V}_T-\boldsymbol{V}|=o(1)$ (which is proven to be true under assumptions stated further), we have

Copyright © by SIAM. Unauthorized reproduction of this article is prohibited.

$$
\begin{aligned}
&\mathcal{I}_j^{\mathrm{CC}}(\boldsymbol{X},\boldsymbol{V})\\
&\quad=\frac{k_o^4\rho^2}{(4\pi|\boldsymbol{X}_T|)^4 2\pi B a^4}\int_{\mathbb{R}^2} d\boldsymbol{x}_R p\left(\frac{\boldsymbol{x}_R}{a}\right)\int_{\mathbb{R}^2} d\boldsymbol{x}_{R'} p\left(\frac{\boldsymbol{x}_{R'}}{a}\right)\\
&\qquad\times\exp\left(i\frac{\omega_o}{c_o}\left(|\boldsymbol{X}-\boldsymbol{X}_R|-|\boldsymbol{X}-\boldsymbol{X}_{R'}|-|\boldsymbol{X}_T-\boldsymbol{X}_R|+|\boldsymbol{X}_T-\boldsymbol{X}_{R'}|\right)\right)\\
&\qquad\times\left[\int_{\mathbb{R}}|\hat{F}(\tilde{\omega})|^2\exp\left(i\frac{B}{c_o}\tilde{\omega}\left(|\boldsymbol{X}-\boldsymbol{X}_R|-|\boldsymbol{X}-\boldsymbol{X}_{R'}|-|\boldsymbol{X}_T-\boldsymbol{X}_R|+|\boldsymbol{X}_T-\boldsymbol{X}_{R'}|\right)\right)d\tilde{\omega}\right]\\
&\qquad\times\exp\left(i\frac{\omega_o}{c_o}(|\boldsymbol{X}_T-\boldsymbol{X}_R|-|\boldsymbol{X}-\boldsymbol{X}_R|)\frac{\boldsymbol{V}_T}{c_o}\cdot\left(\frac{\boldsymbol{X}-\boldsymbol{X}_R}{|\boldsymbol{X}-\boldsymbol{X}_R|}+\frac{\boldsymbol{X}-\boldsymbol{X}_E}{|\boldsymbol{X}-\boldsymbol{X}_E|}\right)\right)\\
&\qquad\times\exp\left(-i\frac{\omega_o}{c_o}(|\boldsymbol{X}_T-\boldsymbol{X}_{R'}|-|\boldsymbol{X}-\boldsymbol{X}_{R'}|)\frac{\boldsymbol{V}_T}{c_o}\cdot\left(\frac{\boldsymbol{X}-\boldsymbol{X}_{R'}}{|\boldsymbol{X}-\boldsymbol{X}_{R'}|}+\frac{\boldsymbol{X}-\boldsymbol{X}_E}{|\boldsymbol{X}-\boldsymbol{X}_E|}\right)\right)\\
&\qquad\times\exp\left(i\frac{\omega_o}{c_o}|\boldsymbol{X}_T-\boldsymbol{X}_E|\frac{\boldsymbol{V}-\boldsymbol{V}_T}{c_o}\cdot\left(\frac{\boldsymbol{X}-\boldsymbol{X}_R}{|\boldsymbol{X}-\boldsymbol{X}_R|}-\frac{\boldsymbol{X}-\boldsymbol{X}_{R'}}{|\boldsymbol{X}-\boldsymbol{X}_{R'}|}\right)\right)\\
&\qquad\times\exp\left(-i\frac{\omega_o}{c_o}|\boldsymbol{X}_T-\boldsymbol{X}_E|\frac{\boldsymbol{V}_T}{c_o}\cdot\left(\frac{\boldsymbol{X}_T-\boldsymbol{X}_R}{|\boldsymbol{X}_T-\boldsymbol{X}_R|}-\frac{\boldsymbol{X}_T-\boldsymbol{X}_{R'}}{|\boldsymbol{X}_T-\boldsymbol{X}_{R'}|}-\frac{\boldsymbol{X}-\boldsymbol{X}_R}{|\boldsymbol{X}-\boldsymbol{X}_R|}+\frac{\boldsymbol{X}-\boldsymbol{X}_{R'}}{|\boldsymbol{X}-\boldsymbol{X}_{R'}|}\right)\right)
\end{aligned}
$$

up to $+cc$. Note that this formula shows that the imaging function tries basically to match the measured differences of travel times $|\boldsymbol{X}_T-\boldsymbol{X}_R|-|\boldsymbol{X}_T-\boldsymbol{X}_{R'}|$ with the candidate ones $|\boldsymbol{X}-\boldsymbol{X}_R|-|\boldsymbol{X}-\boldsymbol{X}_{R'}|$.

We want now to expand the differences $|\boldsymbol{X}-\boldsymbol{X}_R|-|\boldsymbol{X}-\boldsymbol{X}_{R'}|-|\boldsymbol{X}_T-\boldsymbol{X}_R|+|\boldsymbol{X}_T-\boldsymbol{X}_{R'}|$. Using

$$
\boldsymbol{m}_{\boldsymbol{X}+\boldsymbol{\delta}}=\boldsymbol{m}_{\boldsymbol{X}}+\mathbf{P}_{\boldsymbol{X}}^{\perp}\frac{\boldsymbol{\delta}}{|\boldsymbol{X}|}-\frac{1}{2|\boldsymbol{X}|}\left(\boldsymbol{m}_{\boldsymbol{X}}\,{}^t\boldsymbol{\delta}\frac{\mathbf{P}_{\boldsymbol{X}}^{\perp}}{|\boldsymbol{X}|}\boldsymbol{\delta}+2(\boldsymbol{m}_{\boldsymbol{X}}\cdot\boldsymbol{\delta})\frac{\mathbf{P}_{\boldsymbol{X}}^{\perp}}{|\boldsymbol{X}|}\boldsymbol{\delta}\right)+O\left(\frac{|\boldsymbol{\delta}|^3}{|\boldsymbol{X}|^3}\right),
$$

and expanding first with respect to $|\boldsymbol{X}-\boldsymbol{X}_T|$, and then with respect to $\boldsymbol{X}_R$ and $\boldsymbol{X}_E$ (using that $|\boldsymbol{X}_T-\boldsymbol{X}|+|\boldsymbol{X}_R|+|\boldsymbol{X}_{R'}|+|\boldsymbol{X}_E|+T_{\mathrm{tot}}|\boldsymbol{V}_T|\ll|\boldsymbol{Y}_T|$), and knowing that $\boldsymbol{X}_R,\ \boldsymbol{X}_{R'}\perp\boldsymbol{Y}_T$ we have

$$
\begin{aligned}
&|\boldsymbol{X}-\boldsymbol{X}_R|-|\boldsymbol{X}-\boldsymbol{X}_{R'}|-|\boldsymbol{X}_T-\boldsymbol{X}_R|+|\boldsymbol{X}_T-\boldsymbol{X}_{R'}|\\
&\quad=(\boldsymbol{X}-\boldsymbol{X}_T)\cdot\left(\boldsymbol{m}_{\boldsymbol{X}_T-\boldsymbol{X}_R}-\boldsymbol{m}_{\boldsymbol{X}_T-\boldsymbol{X}_{R'}}\right)+O\left(|\boldsymbol{X}-\boldsymbol{X}_T|^2\right)\\
&\quad=(\boldsymbol{X}-\boldsymbol{X}_T)\cdot\left(\frac{\mathbf{P}_{\boldsymbol{Y}_T}^{\perp}}{|\boldsymbol{Y}_T|}(\boldsymbol{X}_{R'}-\boldsymbol{X}_R)-\frac{\boldsymbol{m}_{\boldsymbol{Y}_T}}{2H_T^2}\left(|S_j\boldsymbol{V}_T-\boldsymbol{X}_R|_{\perp}^2-|S_j\boldsymbol{V}_T-\boldsymbol{X}_{R'}|_{\perp}^2\right)\right.\\
&\qquad\qquad\left.-\frac{1}{H_T^2}\left((S_j\boldsymbol{V}_T-\boldsymbol{X}_R)_3(S_j\boldsymbol{V}_T-\boldsymbol{X}_R)_{\perp}-(S_j\boldsymbol{V}_T-\boldsymbol{X}_{R'})_3(S_j\boldsymbol{V}_T-\boldsymbol{X}_{R'})_{\perp}\right)\right.\\
&\qquad\left.+O\left(\frac{|\boldsymbol{X}-\boldsymbol{X}_T|^2}{H_T}+\frac{(a+|\boldsymbol{V}_T|T_{\mathrm{tot}})^3}{H_T^3}|\boldsymbol{X}-\boldsymbol{X}_T|\right)\right.\\
&\quad=\frac{1}{H_T}\langle\boldsymbol{X}-\boldsymbol{X}_T,\boldsymbol{X}_{R'}-\boldsymbol{X}_R\rangle_{\perp}-\frac{1}{2H_T^2}(\boldsymbol{X}-\boldsymbol{X}_T)_3\left(S_j\langle\boldsymbol{V}_T,\boldsymbol{X}_{R'}-\boldsymbol{X}_R\rangle_{\perp}+|\boldsymbol{X}_R|_{\perp}^2-|\boldsymbol{X}_{R'}|_{\perp}^2\right)\\
&\qquad+\frac{S_j}{H_T^2}(\boldsymbol{V}_T)_3\langle\boldsymbol{X}-\boldsymbol{X}_T,\boldsymbol{X}_{R'}-\boldsymbol{X}_R\rangle_{\perp}-\frac{1}{H_T^2}\langle\boldsymbol{X}-\boldsymbol{X}_T,-(\boldsymbol{X}_{R'})_3\boldsymbol{X}_{R'}+(\boldsymbol{X}_R)_3\boldsymbol{X}_R\rangle_{\perp}\\
&\qquad+O\left(\frac{|\boldsymbol{X}-\boldsymbol{X}_T|^2}{H_T}+\frac{(a+|\boldsymbol{V}_T|T_{\mathrm{tot}})^3}{H_T^3}|\boldsymbol{X}-\boldsymbol{X}_T|\right).
\end{aligned}
$$

Downloaded 11/28/17 to 171.67.216.21. Redistribution subject to SIAM license or copyright; see http://www.siam.org/journals/ojsa.php

Copyright © by SIAM. Unauthorized reproduction of this article is prohibited.

Downloaded 11/28/17 to 171.67.216.21. Redistribution subject to SIAM license or copyright; see http://www.siam.org/journals/ojsa.php

For the fourth term in the expression of $\mathcal{I}_j^{\mathrm{CC}}(\boldsymbol{X},\boldsymbol{V})$ we have

$$
\begin{aligned}
&|\boldsymbol{X}_T-\boldsymbol{X}_E|\frac{\boldsymbol{V}-\boldsymbol{V}_T}{c_o}\cdot\left(\frac{\boldsymbol{X}-\boldsymbol{X}_R}{|\boldsymbol{X}-\boldsymbol{X}_R|}-\frac{\boldsymbol{X}-\boldsymbol{X}_{R'}}{|\boldsymbol{X}-\boldsymbol{X}_{R'}|}\right)\\
&\quad=\frac{H_T}{c_o}\left[\frac{1}{H_T}\langle\boldsymbol{V}-\boldsymbol{V}_T,\boldsymbol{X}_{R'}-\boldsymbol{X}_R\rangle_\perp-\frac{1}{2H_T^2}(\boldsymbol{V}-\boldsymbol{V}_T)_3\Big(S_j\langle\boldsymbol{V}_T,\boldsymbol{X}_{R'}-\boldsymbol{X}_R\rangle_\perp\right.\\
&\qquad\qquad\left.+|\boldsymbol{X}_R|_\perp^2-|\boldsymbol{X}_{R'}|_\perp^2\Big)+\frac{S_j}{H_T^2}(\boldsymbol{V}_T)_3(\boldsymbol{X}_R-\boldsymbol{X}_{R'})_\perp\right]\\
&\quad-\frac{1}{H_T^2}\langle\boldsymbol{X}-\boldsymbol{X}_T,-(\boldsymbol{X}_{R'})_3\boldsymbol{X}_{R'}+(\boldsymbol{X}_R)_3\boldsymbol{X}_R\rangle_\perp\\
&\quad+(S_j\boldsymbol{V}_T-\boldsymbol{X}_E)_3\frac{1}{c_oH_T}\langle\boldsymbol{V}-\boldsymbol{V}_T,\boldsymbol{X}_{R'}-\boldsymbol{X}_R\rangle_\perp.
\end{aligned}
$$

For the second term in the expression of $\mathcal{I}_j^{\mathrm{CC}}(\boldsymbol{X},\boldsymbol{V})$ we have

$$
\begin{aligned}
&(|\boldsymbol{X}_T-\boldsymbol{X}_R|-|\boldsymbol{X}-\boldsymbol{X}_R|)\frac{\boldsymbol{V}_T}{c_o}\cdot\left(\frac{\boldsymbol{X}-\boldsymbol{X}_R}{|\boldsymbol{X}-\boldsymbol{X}_R|}+\frac{\boldsymbol{X}-\boldsymbol{X}_E}{|\boldsymbol{X}-\boldsymbol{X}_E|}\right)\\
&\quad=[(\boldsymbol{X}_T-\boldsymbol{X})\cdot\boldsymbol{m}_{\boldsymbol{X}_T-\boldsymbol{X}_R}]\frac{\boldsymbol{V}_T}{c_o}\cdot(\boldsymbol{m}_{\boldsymbol{X}-\boldsymbol{X}_R}+\boldsymbol{m}_{\boldsymbol{X}-\boldsymbol{X}_E})+O\left(\frac{|\boldsymbol{V}_T|}{c_oH_T}|\boldsymbol{X}_T-\boldsymbol{X}|^2\right),
\end{aligned}
$$

and the same stands, replacing R by R'.

Consequently, neglecting the $O()$, and using the calculation of $\boldsymbol{m}_{\boldsymbol{X}_T-\boldsymbol{X}_R}-\boldsymbol{m}_{\boldsymbol{X}_T-\boldsymbol{X}_{R'}}$ already done previously and the fact that in a second order tensor space, we have

$$
(\boldsymbol{u}+\boldsymbol{a},\boldsymbol{v}+\boldsymbol{a}')-(\boldsymbol{u}+\boldsymbol{b},\boldsymbol{v}+\boldsymbol{b}')=(\boldsymbol{a}-\boldsymbol{b},\boldsymbol{v})+(\boldsymbol{u},\boldsymbol{a}'-\boldsymbol{b}')+(\boldsymbol{a},\boldsymbol{a}')-(\boldsymbol{b},\boldsymbol{b}'),
$$

and applying this with $\boldsymbol{a}=\boldsymbol{m}_{\boldsymbol{X}_T-\boldsymbol{X}_R}-\boldsymbol{m}_{\boldsymbol{Y}_T}$, $\boldsymbol{b}=\boldsymbol{m}_{\boldsymbol{X}_T-\boldsymbol{X}_{R'}}-\boldsymbol{m}_{\boldsymbol{Y}_T}$, $\boldsymbol{a}'=\boldsymbol{m}_{\boldsymbol{X}_T-\boldsymbol{X}_R}+\boldsymbol{m}_{\boldsymbol{X}_T-\boldsymbol{X}_E}-2\boldsymbol{m}_{\boldsymbol{Y}_T}$, $\boldsymbol{b}'=\boldsymbol{m}_{\boldsymbol{X}_T-\boldsymbol{X}_{R'}}+\boldsymbol{m}_{\boldsymbol{X}_T-\boldsymbol{X}_E}-2\boldsymbol{m}_{\boldsymbol{Y}_T}$, $\boldsymbol{a}'-\boldsymbol{b}'=\boldsymbol{a}-\boldsymbol{b}=\boldsymbol{m}_{\boldsymbol{X}_T-\boldsymbol{X}_R}-\boldsymbol{m}_{\boldsymbol{X}_T-\boldsymbol{X}_{R'}}$ and $\boldsymbol{u}=\boldsymbol{m}_{\boldsymbol{Y}_T}$ and $\boldsymbol{v}=2\boldsymbol{m}_{\boldsymbol{Y}_T}$, and using this algebraic formula with the bilinear form $\boldsymbol{m}_1,\boldsymbol{m}_2\in(\mathbb{R}^3)^2\to(\boldsymbol{X}_T-\boldsymbol{X})\cdot\boldsymbol{m}_1\frac{\boldsymbol{V}_T}{c_o}\cdot\boldsymbol{m}_2$ we ultimately get

$$
\begin{aligned}
&(|\boldsymbol{X}_T-\boldsymbol{X}_R|-|\boldsymbol{X}-\boldsymbol{X}_R|)\frac{\boldsymbol{V}_T}{c_o}\cdot\left(\frac{\boldsymbol{X}-\boldsymbol{X}_R}{|\boldsymbol{X}-\boldsymbol{X}_R|}+\frac{\boldsymbol{X}-\boldsymbol{X}_E}{|\boldsymbol{X}-\boldsymbol{X}_E|}\right)\\
&\quad-(|\boldsymbol{X}_T-\boldsymbol{X}_{R'}|-|\boldsymbol{X}-\boldsymbol{X}_{R'}|)\frac{\boldsymbol{V}_T}{c_o}\cdot\left(\frac{\boldsymbol{X}-\boldsymbol{X}_{R'}}{|\boldsymbol{X}-\boldsymbol{X}_{R'}|}+\frac{\boldsymbol{X}-\boldsymbol{X}_E}{|\boldsymbol{X}-\boldsymbol{X}_E|}\right)\\
&\quad=(\boldsymbol{X}_T-\boldsymbol{X})\cdot[\boldsymbol{m}_{\boldsymbol{X}_T-\boldsymbol{X}_R}]\frac{\boldsymbol{V}_T}{c_o}\cdot(\boldsymbol{m}_{\boldsymbol{X}_T-\boldsymbol{X}_R}+\boldsymbol{m}_{\boldsymbol{X}_T-\boldsymbol{X}_E})-(\boldsymbol{X}_T-\boldsymbol{X})\\
&\quad\cdot[\boldsymbol{m}_{\boldsymbol{X}_T-\boldsymbol{X}_{R'}}]\frac{\boldsymbol{V}_T}{c_o}\cdot(\boldsymbol{m}_{\boldsymbol{X}_T-\boldsymbol{X}_{R'}}+\boldsymbol{m}_{\boldsymbol{X}_T-\boldsymbol{X}_E})
\end{aligned}
$$

Copyright © by SIAM. Unauthorized reproduction of this article is prohibited.

Downloaded 11/28/17 to 171.67.216.21. Redistribution subject to SIAM license or copyright; see http://www.siam.org/journals/ojsa.php

$$
\begin{aligned}
&= 2\Bigg[\frac{1}{H_T}\langle \boldsymbol{X}-\boldsymbol{X}_T, \boldsymbol{X}_{R'}-\boldsymbol{X}_R\rangle_\perp \\
&\qquad - \frac{1}{2H_T^2}(\boldsymbol{X}-\boldsymbol{X}_T)_3\left(S_j\langle \boldsymbol{V}_T, \boldsymbol{X}_{R'}-\boldsymbol{X}_R\rangle_\perp + |\boldsymbol{X}_R|_\perp^2 - |\boldsymbol{X}_{R'}|_\perp^2\right) \\
&\qquad - \frac{1}{H_T^2}\langle \boldsymbol{X}-\boldsymbol{X}_T, -(\boldsymbol{X}_{R'})_3\boldsymbol{X}_{R'} + (\boldsymbol{X}_R)_3\boldsymbol{X}_R\rangle_\perp\Bigg]\frac{(\boldsymbol{V}_T)_3}{c_o} \\
&\quad + (\boldsymbol{X}_T-\boldsymbol{X})_3\frac{1}{c_o}\Bigg[\frac{1}{H_T}\langle \boldsymbol{V}_T, \boldsymbol{X}_{R'}-\boldsymbol{X}_R\rangle_\perp \\
&\qquad\qquad - \frac{1}{2H_T^2}(\boldsymbol{V}_T)_3\left(S_j\langle \boldsymbol{V}_T, \boldsymbol{X}_{R'}-\boldsymbol{X}_R\rangle_\perp + |\boldsymbol{X}_R|_\perp^2 - |\boldsymbol{X}_{R'}|_\perp^2\right) \\
&\qquad\qquad - \frac{1}{H_T^2}\langle \boldsymbol{V}_T, +(\boldsymbol{X}_{R'})_3\boldsymbol{X}_{R'} - (\boldsymbol{X}_R)_3\boldsymbol{X}_R\rangle_\perp\Bigg] \\
&\quad + 2\frac{1}{c_oH_T^2}\langle \boldsymbol{X}-\boldsymbol{X}_T, \boldsymbol{X}_R\rangle_\perp\langle \boldsymbol{V}_T, \boldsymbol{X}_R\rangle_\perp - 2\frac{1}{c_oH_T^2}\langle \boldsymbol{X}-\boldsymbol{X}_T, \boldsymbol{X}_{R'}\rangle_\perp\langle \boldsymbol{V}_T, \boldsymbol{X}_{R'}\rangle_\perp \\
&\quad + O\left(\frac{(a+|\boldsymbol{V}_T|T_{\rm tot})^2}{H_T^2}\frac{|\boldsymbol{V}_T|}{c_o}|\boldsymbol{X}-\boldsymbol{X}_T|\right).
\end{aligned}
$$

For the last term in the expression of $\mathcal{I}_j^{\rm CC}(\boldsymbol{X},\boldsymbol{V})$,

$$
\begin{aligned}
&|\boldsymbol{X}_T-\boldsymbol{X}_E|\frac{\boldsymbol{V}_T}{c_o}\cdot\left(\frac{\boldsymbol{X}_T-\boldsymbol{X}_R}{|\boldsymbol{X}_T-\boldsymbol{X}_R|} - \frac{\boldsymbol{X}_T-\boldsymbol{X}_{R'}}{|\boldsymbol{X}_T-\boldsymbol{X}_{R'}|} - \frac{\boldsymbol{X}-\boldsymbol{X}_R}{|\boldsymbol{X}-\boldsymbol{X}_R|} + \frac{\boldsymbol{X}-\boldsymbol{X}_{R'}}{|\boldsymbol{X}-\boldsymbol{X}_{R'}|}\right) \\
&\quad = |\boldsymbol{X}_T-\boldsymbol{X}_E|\frac{\boldsymbol{V}_T}{c_o}\cdot\left[\frac{\mathbf{P}^\perp_{\boldsymbol{X}_T-\boldsymbol{X}_{R'}}}{|\boldsymbol{X}_T-\boldsymbol{X}_{R'}|} - \frac{\mathbf{P}^\perp_{\boldsymbol{X}_T-\boldsymbol{X}_R}}{|\boldsymbol{X}_T-\boldsymbol{X}_R|}\right]\cdot(\boldsymbol{X}-\boldsymbol{X}_T) + O\left(\frac{|\boldsymbol{X}-\boldsymbol{X}_T|^2}{H_T}\right).
\end{aligned}
$$

A second order expansion of $\frac{\mathbf{P}^\perp_{\boldsymbol{X}_T-\boldsymbol{X}_{R'}}}{|\boldsymbol{X}_T-\boldsymbol{X}_{R'}|} - \frac{\mathbf{P}^\perp_{\boldsymbol{X}_T-\boldsymbol{X}_R}}{|\boldsymbol{X}_T-\boldsymbol{X}_R|}$ would be rather horrible. However, let us just mention the terms up to order $|\boldsymbol{X}-\boldsymbol{X}_T|\frac{\boldsymbol{V}_T(a+T_{\rm tot}|\boldsymbol{V}_T|)}{c_oH_T}$ (as we assumed that $\frac{|\boldsymbol{V}_T|}{c_o} \ll \frac{a}{H_T}$; we will see thereafter that indeed, we do not need to do more calculations),

$$
\begin{aligned}
&|\boldsymbol{X}_T-\boldsymbol{X}_E|\frac{\boldsymbol{V}_T}{c_o}\cdot\left(\frac{\boldsymbol{X}_T-\boldsymbol{X}_R}{|\boldsymbol{X}_T-\boldsymbol{X}_R|} - \frac{\boldsymbol{X}_T-\boldsymbol{X}_{R'}}{|\boldsymbol{X}_T-\boldsymbol{X}_{R'}|} - \frac{\boldsymbol{X}-\boldsymbol{X}_R}{|\boldsymbol{X}-\boldsymbol{X}_R|} + \frac{\boldsymbol{X}-\boldsymbol{X}_{R'}}{|\boldsymbol{X}-\boldsymbol{X}_{R'}|}\right) \\
&\quad = -\frac{H_T}{c_o}\big(\langle \boldsymbol{V}_T, \boldsymbol{X}_R-\boldsymbol{X}_{R'}\rangle_\perp(\boldsymbol{X}-\boldsymbol{X}_T)_3 + \langle \boldsymbol{X}_R-\boldsymbol{X}_{R'}, \boldsymbol{X}-\boldsymbol{X}_T\rangle_\perp(\boldsymbol{V}_T)_3 \\
&\qquad\qquad + \langle \boldsymbol{X}-\boldsymbol{X}_T, \boldsymbol{V}_T\rangle_\perp(\boldsymbol{X}_R-\boldsymbol{X}_{R'})_3\big) \\
&\qquad + O\left(|\boldsymbol{X}-\boldsymbol{X}_T|^2 + |\boldsymbol{X}-\boldsymbol{X}_T|\frac{\boldsymbol{V}_T(a+T_{\rm tot}|\boldsymbol{V}_T|)^2}{c_oH_T^2}\right).
\end{aligned}
$$

Now let us assume that

$$
\frac{a+T_{\rm tot}|\boldsymbol{V}_T|}{H_T} = o(1), \quad \frac{V_T}{c_o} \ll \left(\frac{a+T_{\rm tot}|\boldsymbol{V}_T|}{H_T}\right)^2, \quad \frac{H_T^2}{c_o(a+T_{\rm tot}|\boldsymbol{V}_T|)T_{\rm tot}} \ll 1, \quad \frac{\lambda_o}{H_T} \ll 16\left(\frac{a+T_{\rm tot}|\boldsymbol{V}_T|}{H_T}\right)^4,
$$

Copyright © by SIAM. Unauthorized reproduction of this article is prohibited.

Downloaded 11/28/17 to 171.67.216.21. Redistribution subject to SIAM license or copyright; see http://www.siam.org/journals/ojsa.php

and

$$|\boldsymbol{X}_T - \boldsymbol{X}| < \frac{4\lambda_o H_T^2}{(a + T_{\text{tot}}|\boldsymbol{V}_T|)^2}, \quad |\boldsymbol{V}_T - \boldsymbol{V}| < \frac{\lambda_o H_T^2}{T_{\text{tot}}(a + T_{\text{tot}}|\boldsymbol{V}_T|)^2}.$$

Then, under these assumptions, the $O()$ terms will be negligible in the expansions above. We can see in all the expansions that $\boldsymbol{X}_R$ and $\boldsymbol{X}_{R'}$ play an antisymmetric role in the sense that each time there is a term with $\boldsymbol{X}_R$ in the phase, the opposite term is present with $\boldsymbol{X}_{R'}$.

Consequently,

$$\begin{aligned}
&\mathcal{I}_j^{\text{CC}}(\boldsymbol{X}, \boldsymbol{V}) \\
&= \frac{k_o^4 \rho^2}{(4\pi|\boldsymbol{X}_T|)^4 2\pi B a^4} \Big[\int_{\mathbb{R}} d\tilde{\omega} |\hat{F}(\tilde{\omega})|^2 \Big| \int_{\mathbb{R}^2} d\boldsymbol{x}_R p\Big(\frac{\boldsymbol{x}_R}{a}\Big) \\
&\quad \times \exp\Big(i \frac{\omega_o + B\tilde{\omega}}{c_o} \Big(\frac{1}{H_T} \langle \boldsymbol{X} - \boldsymbol{X}_T, -\boldsymbol{X}_R \rangle_\perp - \frac{1}{2H_T^2} (\boldsymbol{X} - \boldsymbol{X}_T)_3 (S_j \langle \boldsymbol{V}_T, -\boldsymbol{X}_R \rangle_\perp + |\boldsymbol{X}_R|_\perp^2) \\
&\qquad + \frac{S_j}{H_T^2} (\boldsymbol{V}_T)_3 \langle \boldsymbol{X} - \boldsymbol{X}_T, \boldsymbol{X}_R \rangle_\perp - \frac{1}{H_T^2} \langle \boldsymbol{X} - \boldsymbol{X}_T, (\boldsymbol{X}_R)_3 \boldsymbol{X}_R \rangle_\perp \Big) \Big) \\
&\quad \times \exp\Big(i \frac{\omega_o}{c_o} \Big(2 \Big[\frac{1}{H_T} \langle \boldsymbol{X} - \boldsymbol{X}_T, -\boldsymbol{X}_R \rangle_\perp - \frac{1}{2H_T^2} (\boldsymbol{X} - \boldsymbol{X}_T)_3 (S_j \langle \boldsymbol{V}_T, -\boldsymbol{X}_R \rangle_\perp + |\boldsymbol{X}_R|_\perp^2) \\
&\qquad\quad - \frac{1}{H_T^2} \langle \boldsymbol{X} - \boldsymbol{X}_T, (\boldsymbol{X}_R)_3 \boldsymbol{X}_R \rangle_\perp \Big] \frac{(\boldsymbol{V}_T)_3}{c_o} \\
&\qquad\quad + (\boldsymbol{X}_T - \boldsymbol{X})_3 \frac{1}{c_o} \Big[\frac{1}{H_T} \langle \boldsymbol{V}_T, \boldsymbol{X}_{R'} - \boldsymbol{X}_R \rangle_\perp - \frac{1}{2H_T^2} (\boldsymbol{V}_T)_3 (S_j \langle \boldsymbol{V}_T, -\boldsymbol{X}_R \rangle_\perp + |\boldsymbol{X}_R|_\perp^2) \\
&\qquad\quad - \frac{1}{H_T^2} \langle \boldsymbol{V}_T, -(\boldsymbol{X}_R)_3 \boldsymbol{X}_R \rangle_\perp \Big] \\
&\qquad\quad + 2 \frac{1}{c_o H_T^2} \langle \boldsymbol{V}_T, \boldsymbol{X}_R \rangle_\perp \langle \boldsymbol{V}_T, \boldsymbol{X}_R \rangle_\perp \Big) \Big) \\
&\quad \times \exp\Big(i \frac{\omega_o}{c_o} \Big(\frac{H_T}{c_o} \Big[\frac{1}{H_T} \langle \boldsymbol{V} - \boldsymbol{V}_T, -\boldsymbol{X}_R \rangle_\perp - \frac{1}{2H_T^2} (\boldsymbol{V} - \boldsymbol{V}_T)_3 (S_j \langle \boldsymbol{V}_T, -\boldsymbol{X}_R \rangle_\perp + |\boldsymbol{X}_R|_\perp^2) \\
&\qquad\quad + \frac{S_j}{H_T^2} (\boldsymbol{V}_T)_3 (\boldsymbol{X}_R)_\perp \Big] - \frac{1}{H_T^2} \langle \boldsymbol{X} - \boldsymbol{X}_T, (\boldsymbol{X}_R)_3 \boldsymbol{X}_R \rangle_\perp \\
&\qquad\quad + (S_j \boldsymbol{V}_T - \boldsymbol{X}_E)_3 \frac{1}{c_o H_T} \langle \boldsymbol{V} - \boldsymbol{V}_T, -\boldsymbol{X}_R \rangle_\perp \Big) \Big) \\
&\quad \times \exp\Big(i \frac{\omega_o}{c_o} \Big(\frac{-H_T}{c_o} \big(\langle \boldsymbol{V}_T, \boldsymbol{X}_R \rangle_\perp (\boldsymbol{X} - \boldsymbol{X}_T)_3 + \langle \boldsymbol{X}_R, \boldsymbol{X} - \boldsymbol{X}_T \rangle_\perp (\boldsymbol{V}_T)_3 \\
&\qquad + \langle \boldsymbol{X} - \boldsymbol{X}_T, \boldsymbol{V}_T \rangle_\perp (\boldsymbol{X}_R - \boldsymbol{X}_{R'})_3 \big) \; + \; O\Big(|\boldsymbol{X} - \boldsymbol{X}_T| \frac{\boldsymbol{V}_T (a + T_{\text{tot}}|\boldsymbol{V}_T|)^2}{c_o H_T^2} \Big) \Big) \Big) \Big|^2 \Big],
\end{aligned}$$

and replacing $\boldsymbol{X}_T(S_j)$ by $\boldsymbol{Y}_T + S_j \boldsymbol{V}_T$ and $\boldsymbol{X}(S_j)$ by $\boldsymbol{Y} + S_j \boldsymbol{V}$ (done only in the travel time difference because we can see that all the other remaining terms would be negligible due to $\frac{V_T}{c_o}$ small), we get

Copyright © by SIAM. Unauthorized reproduction of this article is prohibited.

$$
\begin{aligned}
&\mathcal{I}_j^{\mathrm{CC}}(\boldsymbol{X},\boldsymbol{V})\\
&= \frac{k_o^4\rho^2}{(4\pi|\boldsymbol{X}_T|)^4 2\pi B a^4}\Bigg[\int_{\mathbb{R}} d\tilde{\omega}|\hat{F}(\tilde{\omega})|^2\Big|\int_{\mathbb{R}^2} d\boldsymbol{x}_R p\Big(\frac{\boldsymbol{x}_R}{a}\Big)\\
&\quad\times\exp\Big(i\frac{\omega_o+B\tilde{\omega}}{c_o}\Big(\frac{1}{H_T}\langle\boldsymbol{Y}-\boldsymbol{Y}_T,-\boldsymbol{X}_R\rangle_\perp-\frac{1}{2H_T^2}(\boldsymbol{Y}-\boldsymbol{Y}_T)_3|\boldsymbol{X}_R|_\perp^2\\
&\qquad-\frac{1}{H_T^2}\langle\boldsymbol{Y}-\boldsymbol{Y}_T,(\boldsymbol{X}_R)_3\boldsymbol{X}_R\rangle_\perp\Big)\Big)\\
&\quad\times\exp\Big(i\frac{\omega_o+B\tilde{\omega}}{c_o}\Big(\frac{S_j}{H_T}\langle\boldsymbol{V}-\boldsymbol{V}_T,-\boldsymbol{X}_R\rangle_\perp\Big)\Big)\\
&\quad\times\exp\Big(i\frac{\omega_o+B\tilde{\omega}}{c_o}\Big(\frac{S_j}{2H_T^2}(\boldsymbol{Y}-\boldsymbol{Y}_T)_3\langle\boldsymbol{V}_T,\boldsymbol{X}_R\rangle_\perp+\frac{S_j^2}{2H_T^2}(\boldsymbol{V}-\boldsymbol{V}_T)_3\langle\boldsymbol{V}_T,\boldsymbol{X}_R\rangle_\perp\\
&\qquad+\frac{S_j}{2H_T^2}(\boldsymbol{V}-\boldsymbol{V}_T)_3|\boldsymbol{X}_R|_\perp^2+\frac{S_j}{H_T^2}(\boldsymbol{V}_T)_3\langle\boldsymbol{Y}-\boldsymbol{Y}_T,\boldsymbol{X}_R\rangle_\perp+\frac{S_j^2}{H_T^2}(\boldsymbol{V}_T)_3\langle\boldsymbol{V}-\boldsymbol{V}_T,\boldsymbol{X}_R\rangle_\perp\Big)\Big)\\
&\quad\times\exp\Big(i\frac{\omega_o}{c_o}\Big(2\Big[\frac{1}{H_T}\langle\boldsymbol{X}-\boldsymbol{X}_T,-\boldsymbol{X}_R\rangle_\perp-\frac{1}{2H_T^2}(\boldsymbol{X}-\boldsymbol{X}_T)_3(S_j\langle\boldsymbol{V}_T,-\boldsymbol{X}_R\rangle_\perp+|\boldsymbol{X}_R|_\perp^2\Big)\\
&\qquad-\frac{1}{H_T^2}\langle\boldsymbol{X}-\boldsymbol{X}_T,(\boldsymbol{X}_R)_3\boldsymbol{X}_R\rangle_\perp\Big]\frac{(\boldsymbol{V}_T)_3}{c_o}\\
&\qquad+(\boldsymbol{X}_T-\boldsymbol{X})_3\frac{1}{c_o}\Big[\frac{1}{H_T}\langle\boldsymbol{V}_T,-\boldsymbol{X}_R\rangle_\perp-\frac{1}{2H_T^2}(\boldsymbol{V}_T)_3(S_j\langle\boldsymbol{V}_T,-\boldsymbol{X}_R\rangle_\perp+|\boldsymbol{X}_R|_\perp^2)\\
&\qquad-\frac{1}{H_T^2}\langle\boldsymbol{V}_T,-(\boldsymbol{X}_R)_3\boldsymbol{X}_R\rangle_\perp\Big]\\
&\qquad+2\frac{1}{c_oH_T^2}\langle\boldsymbol{X}-\boldsymbol{X}_T,\boldsymbol{X}_R\rangle_\perp\langle\boldsymbol{V}_T,\boldsymbol{X}_R\rangle_\perp\Big)\Big)\\
&\quad\times\exp\Big(i\frac{\omega_o}{c_o}\Big(\frac{H_T}{c_o}\Big[\frac{1}{H_T}\langle\boldsymbol{V}-\boldsymbol{V}_T,-\boldsymbol{X}_R\rangle_\perp-\frac{1}{2H_T^2}(\boldsymbol{V}-\boldsymbol{V}_T)_3(S_j\langle\boldsymbol{V}_T,-\boldsymbol{X}_R\rangle_\perp+|\boldsymbol{X}_R|_\perp^2\Big)\\
&\qquad+\frac{S_j}{H_T^2}(\boldsymbol{V}_T)_3(\boldsymbol{X}_R)_\perp\Big]-\frac{1}{H_T^2}\langle\boldsymbol{X}-\boldsymbol{X}_T,(\boldsymbol{X}_R)_3\boldsymbol{X}_R\rangle_\perp\\
&\qquad+(S_j\boldsymbol{V}_T-\boldsymbol{X}_E)_3\frac{1}{c_oH_T}\langle\boldsymbol{V}-\boldsymbol{V}_T,-\boldsymbol{X}_R\rangle_\perp\Big)\Big)\\
&\quad\times\exp\Big(i\frac{\omega_o}{c_o}\Big(\frac{-H_T}{c_o}\big(\langle\boldsymbol{V}_T,\boldsymbol{X}_R\rangle_\perp(\boldsymbol{X}-\boldsymbol{X}_T)_3+\langle\boldsymbol{X}_R,\boldsymbol{X}-\boldsymbol{X}_T\rangle_\perp(\boldsymbol{V}_T)_3\\
&\qquad+\langle\boldsymbol{X}-\boldsymbol{X}_T,\boldsymbol{V}_T\rangle_\perp(\boldsymbol{X}_R)_3\big)\;+\;O(|\boldsymbol{X}-\boldsymbol{X}_T|\frac{\boldsymbol{V}_T(a+T_{\mathrm{tot}}|\boldsymbol{V}_T|)^2}{c_oH_T^2}\Big)\Big)\Big)\Big|^2\Bigg].
\end{aligned}
$$

As usual, summing the partial imaging functions over j can be handled by replacing S_j by s, and $\frac{1}{N_E}\sum_{j=1}^{N_E}$ by $\frac{1}{T_{\mathrm{tot}}}\int_{-T_{\mathrm{tot}}/2}^{T_{\mathrm{tot}}/2} ds$:

Copyright © by SIAM. Unauthorized reproduction of this article is prohibited.

Downloaded 11/28/17 to 171.67.216.21. Redistribution subject to SIAM license or copyright; see http://www.siam.org/journals/ojsa.php

Downloaded 11/28/17 to 171.67.216.21. Redistribution subject to SIAM license or copyright; see http://www.siam.org/journals/ojsa.php

$$
\begin{aligned}
&\mathcal{I}^{\mathrm{CC}}(\boldsymbol{X},\boldsymbol{V})\\
&= \frac{k_o^4\rho^2}{(4\pi|\boldsymbol{X}_T|)^4 2\pi B a^4 T_{\mathrm{tot}}}\int_{-T_{\mathrm{tot}}/2}^{T_{\mathrm{tot}}/2} ds\Bigg[\int_{\mathbb{R}} d\tilde{\omega}|\hat{F}(\tilde{\omega})|^2\Big|\int_{\mathbb{R}^2} d\boldsymbol{x}_R p\Big(\frac{\boldsymbol{x}_R}{a}\Big)\\
&\quad\times\exp\Big(i\frac{\omega_o+B\tilde{\omega}}{c_o}\Big(\frac{1}{H_T}\langle\boldsymbol{Y}-\boldsymbol{Y}_T,-\boldsymbol{X}_R\rangle_\perp-\frac{1}{2H_T^2}(\boldsymbol{Y}-\boldsymbol{Y}_T)_3|\boldsymbol{X}_R|_\perp^2\\
&\qquad-\frac{1}{H_T^2}\langle\boldsymbol{Y}-\boldsymbol{Y}_T,(\boldsymbol{X}_R)_3\boldsymbol{X}_R\rangle_\perp\Big)\\
&\quad\times\exp\Big(i\frac{\omega_o+B\tilde{\omega}}{c_o}\Big(\frac{s}{H_T}\langle\boldsymbol{V}-\boldsymbol{V}_T,-\boldsymbol{X}_R\rangle_\perp\Big)\Big)\\
&\quad\times\exp\Big(i\frac{\omega_o+B\tilde{\omega}}{c_o}\Big(2\frac{s}{2H_T^2}(\boldsymbol{Y}-\boldsymbol{Y}_T)_3\langle\boldsymbol{V}_T,\boldsymbol{X}_R\rangle_\perp+\frac{s^2}{2H_T^2}(\boldsymbol{V}-\boldsymbol{V}_T)_3\langle\boldsymbol{V}_T,\boldsymbol{X}_R\rangle_\perp\\
&\qquad+\frac{s}{2H_T^2}(\boldsymbol{V}-\boldsymbol{V}_T)_3|\boldsymbol{X}_R|_\perp^2+\frac{s}{H_T^2}(\boldsymbol{V}_T)_3\langle\boldsymbol{Y}-\boldsymbol{Y}_T,\boldsymbol{X}_R\rangle_\perp+\frac{s^2}{H_T^2}(\boldsymbol{V}_T)_3\langle\boldsymbol{V}-\boldsymbol{V}_T,\boldsymbol{X}_R\rangle_\perp\Big)\Big)\\
&\quad\times\exp\Big(i\frac{\omega_o}{c_o}\Big(2\Big[\frac{1}{H_T}\langle\boldsymbol{X}-\boldsymbol{X}_T,-\boldsymbol{X}_R\rangle_\perp-\frac{1}{2H_T^2}(\boldsymbol{X}-\boldsymbol{X}_T)_3(s\langle\boldsymbol{V}_T,-\boldsymbol{X}_R\rangle_\perp+|\boldsymbol{X}_R|_\perp^2)\\
&\qquad-\frac{1}{H_T^2}\langle\boldsymbol{X}-\boldsymbol{X}_T,(\boldsymbol{X}_R)_3\boldsymbol{X}_R\rangle_\perp\Big]\frac{(\boldsymbol{V}_T)_3}{c_o}\\
&\qquad+(\boldsymbol{X}_T-\boldsymbol{X})_3\frac{1}{c_o}\Big[\frac{1}{H_T}\langle\boldsymbol{V}_T,-\boldsymbol{X}_R\rangle_\perp-\frac{1}{2H_T^2}(\boldsymbol{V}_T)_3(s\langle\boldsymbol{V}_T,-\boldsymbol{X}_R\rangle_\perp+|\boldsymbol{X}_R|_\perp^2)\\
&\qquad-\frac{1}{H_T^2}\langle\boldsymbol{V}_T,-(\boldsymbol{X}_R)_3\boldsymbol{X}_R\rangle_\perp\Big]\\
&\qquad+2\frac{1}{c_oH_T^2}\langle\boldsymbol{X}-\boldsymbol{X}_T,\boldsymbol{X}_R\rangle_\perp\langle\boldsymbol{V}_T,\boldsymbol{X}_R\rangle_\perp\Big)\Big)\\
&\quad\times\exp\Big(i\frac{\omega_o}{c_o}\Big(\frac{H_T}{c_o}\Big[\frac{1}{H_T}\langle\boldsymbol{V}-\boldsymbol{V}_T,-\boldsymbol{X}_R\rangle_\perp-\frac{1}{2H_T^2}(\boldsymbol{V}-\boldsymbol{V}_T)_3(s\langle\boldsymbol{V}_T,-\boldsymbol{X}_R\rangle_\perp+|\boldsymbol{X}_R|_\perp^2)\\
&\qquad+\frac{s}{H_T^2}(\boldsymbol{V}_T)_3(\boldsymbol{X}_R)_\perp\Big]-\frac{1}{H_T^2}\langle\boldsymbol{X}-\boldsymbol{X}_T,(\boldsymbol{X}_R)_3\boldsymbol{X}_R\rangle_\perp\\
&\qquad+(s\boldsymbol{V}_T-\boldsymbol{X}_E)_3\frac{1}{c_oH_T}\langle\boldsymbol{V}-\boldsymbol{V}_T,-\boldsymbol{X}_R\rangle_\perp\Big)\Big)\\
&\quad\times\exp\Bigg(i\frac{\omega_o}{c_o}\Big(\frac{-H_T}{c_o}\Big(\langle\boldsymbol{V}_T,\boldsymbol{X}_R\rangle_\perp(\boldsymbol{X}-\boldsymbol{X}_T)_3+\langle\boldsymbol{X}_R,\boldsymbol{X}-\boldsymbol{X}_T\rangle_\perp(\boldsymbol{V}_T)_3\\
&\qquad+\langle\boldsymbol{X}-\boldsymbol{X}_T,\boldsymbol{V}_T\rangle_\perp(\boldsymbol{X}_R-\boldsymbol{X}_{R'})_3\Big)+O(|\boldsymbol{X}-\boldsymbol{X}_T|\frac{\boldsymbol{V}_T(a+T_{\mathrm{tot}}|\boldsymbol{V}_T|)^2}{c_oH_T^2}\Big)\Big)\Bigg)\Big|^2\Bigg].
\end{aligned}
$$

Ultimately, the result can be expressed in the following form,

$$
\begin{aligned}
\mathcal{I}^{\mathrm{CC}}(\boldsymbol{X},\boldsymbol{V}) = \frac{k_o^4\rho^2}{(4\pi|\boldsymbol{X}_T|)^4 2\pi B a^4 T_{\mathrm{tot}}}\int_{-T_{\mathrm{tot}}/2}^{T_{\mathrm{tot}}/2} ds\int_{\mathbb{R}} d\tilde{\omega}|\hat{F}(\tilde{\omega})|^2\\
\Big|\int_{\mathbb{R}^2} d\boldsymbol{x}_R p\left(\frac{\boldsymbol{x}_R}{a}\right)\exp\left(i(\psi_{\mathcal{I}^{\mathrm{CC}}}+\epsilon_{\mathcal{I}^{\mathrm{CC}}})(\boldsymbol{Y}-\boldsymbol{Y}_T,\boldsymbol{V}-\boldsymbol{V}_T,\boldsymbol{X}_R,s,\tilde{\omega})\right)\Big|^2
\end{aligned}
$$

Copyright © by SIAM. Unauthorized reproduction of this article is prohibited.

with the phase terms defined by

$$\begin{aligned}
&\psi_{\mathcal{I}^{\rm CC}}(\boldsymbol{Y}-\boldsymbol{Y}_T,\boldsymbol{V}-\boldsymbol{V}_T,\boldsymbol{X}_R,s,\tilde{\omega})\\
&\quad=\frac{\omega_o+B\tilde{\omega}}{c_o}\Bigg(\frac{1}{H_T}\underbrace{\langle\boldsymbol{Y}-\boldsymbol{Y}_T,-\boldsymbol{X}_R\rangle_\perp}_{\boldsymbol{Y}_T\text{ physical aperture effect}}-\frac{1}{2H_T^2}\underbrace{(\boldsymbol{Y}-\boldsymbol{Y}_T)_3}_{Y_3\text{ physical apperture effect}}\quad|\boldsymbol{X}_R|_\perp^2\\
&\qquad+\frac{s}{H_T}\underbrace{\langle\boldsymbol{V}-\boldsymbol{V}_T,-\boldsymbol{X}_R\rangle_\perp}_{\boldsymbol{V}_T\text{ ISAR effect}}+\frac{s}{2H_T^2}\underbrace{(\boldsymbol{V}-\boldsymbol{V}_T)_3}_{V_3\text{ mixed effect}}\ |\boldsymbol{X}_R|_\perp^2\\
&\qquad+\frac{s}{2H_T^2}\underbrace{(\boldsymbol{Y}-\boldsymbol{Y}_T)_3}_{Y_3\text{ mixed apperture effect}}\quad\langle\boldsymbol{V}_T,\boldsymbol{X}_R\rangle_\perp+\frac{s^2}{2H_T^2}\underbrace{(\boldsymbol{V}-\boldsymbol{V}_T)_3}_{V_3\text{ mixed effect}}\langle\boldsymbol{V}_T,\boldsymbol{X}_R\rangle_\perp\Bigg)
\end{aligned}$$

and

$$\begin{aligned}
&\epsilon_{\mathcal{I}^{\rm CC}}(\boldsymbol{Y}-\boldsymbol{Y}_T,\boldsymbol{V}-\boldsymbol{V}_T,\boldsymbol{X}_R,s,\tilde{\omega})\\
&\quad=\frac{\omega_o+B\tilde{\omega}}{c_o}\Bigg(-\frac{1}{H_T^2}\langle\boldsymbol{Y}-\boldsymbol{Y}_T,(\boldsymbol{X}_R)_3\boldsymbol{X}_R\rangle_\perp+\frac{s}{H_T^2}(\boldsymbol{V}_T)_3\langle\boldsymbol{Y}-\boldsymbol{Y}_T,\boldsymbol{X}_R\rangle_\perp\\
&\qquad+\frac{s^2}{H_T^2}(\boldsymbol{V}_T)_3\langle\boldsymbol{V}-\boldsymbol{V}_T,\boldsymbol{X}_R\rangle_\perp-\frac{1}{H_T^2}\langle\boldsymbol{Y}-\boldsymbol{Y}_T,(\boldsymbol{X}_R)_3\boldsymbol{X}_R\rangle_\perp\\
&\qquad-\frac{s}{H_T^2}\langle\boldsymbol{V}-\boldsymbol{V}_T,(\boldsymbol{X}_R)_3\boldsymbol{X}_R\rangle_\perp\Bigg)\\
&\quad+\frac{\omega_o}{c_o}\Bigg(2\Bigg[\frac{1}{H_T}\langle\boldsymbol{X}-\boldsymbol{X}_T,-\boldsymbol{X}_R\rangle_\perp-\frac{1}{2H_T^2}(\boldsymbol{X}-\boldsymbol{X}_T)_3\left(s\langle\boldsymbol{V}_T,-\boldsymbol{X}_R\rangle_\perp+|\boldsymbol{X}_R|_\perp^2\right)\\
&\qquad-\frac{1}{H_T^2}\langle\boldsymbol{X}-\boldsymbol{X}_T,(\boldsymbol{X}_R)_3\boldsymbol{X}_R\rangle_\perp\Bigg]\frac{(\boldsymbol{V}_T)_3}{c_o}\\
&\qquad+\frac{(\boldsymbol{X}_T-\boldsymbol{X})_3}{c_o}\Bigg[\frac{1}{H_T}\langle\boldsymbol{V}_T,-\boldsymbol{X}_R\rangle_\perp-\frac{(\boldsymbol{V}_T)_3}{2H_T^2}\left(s\langle\boldsymbol{V}_T,-\boldsymbol{X}_R\rangle_\perp+|\boldsymbol{X}_R|_\perp^2\right)\\
&\qquad-\frac{1}{H_T^2}\langle\boldsymbol{V}_T,-(\boldsymbol{X}_R)_3\boldsymbol{X}_R\rangle_\perp\Bigg]\\
&\qquad+2\frac{1}{c_oH_T^2}\langle\boldsymbol{X}-\boldsymbol{X}_T,\boldsymbol{X}_R\rangle_\perp\langle\boldsymbol{V}_T,\boldsymbol{X}_R\rangle_\perp\Bigg)\\
&\quad+\frac{\omega_o}{c_o}\Bigg(\frac{H_T}{c_o}\Bigg[\frac{1}{H_T}\langle\boldsymbol{V}-\boldsymbol{V}_T,-\boldsymbol{X}_R\rangle_\perp-\frac{1}{2H_T^2}(\boldsymbol{V}-\boldsymbol{V}_T)_3\left(s\langle\boldsymbol{V}_T,-\boldsymbol{X}_R\rangle_\perp+|\boldsymbol{X}_R|_\perp^2\right)\\
&\qquad+\frac{s}{H_T^2}(\boldsymbol{V}_T)_3(\boldsymbol{X}_R)_\perp\Bigg]-\frac{1}{H_T^2}\langle\boldsymbol{X}-\boldsymbol{X}_T,(\boldsymbol{X}_R)_3\boldsymbol{X}_R\rangle_\perp\\
&\qquad+(s\boldsymbol{V}_T-\boldsymbol{X}_E)_3\frac{1}{c_oH_T}\langle\boldsymbol{V}-\boldsymbol{V}_T,-\boldsymbol{X}_R\rangle_\perp\Bigg)\\
&\quad+\frac{\omega_o}{c_o}\Bigg(\frac{-H_T}{c_o}\left(\langle\boldsymbol{V}_T,\boldsymbol{X}_R\rangle_\perp(\boldsymbol{X}-\boldsymbol{X}_T)_3+\langle\boldsymbol{X}_R,\boldsymbol{X}-\boldsymbol{X}_T\rangle_\perp(\boldsymbol{V}_T)_3+\langle\boldsymbol{X}-\boldsymbol{X}_T,\boldsymbol{V}_T\rangle_\perp(\boldsymbol{X}_R)_3\right)\Bigg).
\end{aligned}$$

Downloaded 11/28/17 to 171.67.216.21. Redistribution subject to SIAM license or copyright; see http://www.siam.org/journals/ojsa.php

Copyright © by SIAM. Unauthorized reproduction of this article is prohibited.

Note that under the above assumptions, we have $\epsilon_{\mathcal{I}^{\mathrm{CC}}}(\boldsymbol{Y}-\boldsymbol{Y}_T,\boldsymbol{V}-\boldsymbol{V}_T,\boldsymbol{X}_R,s,\tilde{\omega}) = o(\psi_{\mathcal{I}^{\mathrm{CC}}}(\boldsymbol{Y}-\boldsymbol{Y}_T,\boldsymbol{V}-\boldsymbol{V}_T,\boldsymbol{X}_R,s,\tilde{\omega}))$.

Appendix C. Bounds calculations.

C.1. MF case. To ease notation we will denote $\phi(\boldsymbol{Y},\boldsymbol{V},\boldsymbol{X}_R) = (\Phi_{\mathcal{I}^{\mathrm{MF}}}+\epsilon_{\mathcal{I}^{\mathrm{MF}}})(\boldsymbol{Y}-\boldsymbol{Y}_T,\boldsymbol{V}-\boldsymbol{V}_T,\boldsymbol{X}_R,s,\tilde{\omega})$. Indeed, for $\boldsymbol{Y},\boldsymbol{V}\in\mathcal{R}_{\boldsymbol{Y}_T,\boldsymbol{V}_T,q,\boldsymbol{r}}$, we can show that (under certain assumptions allowing us to change the order of $\int$ and $\nabla_{\boldsymbol{X}_R}$),

$$\begin{aligned}\nabla_{\boldsymbol{X}_R}\tilde{I}^{\mathrm{MF}}(\boldsymbol{Y},\boldsymbol{V},\boldsymbol{X}_R) &= C\int_{-T_{\mathrm{tot}}/2}^{T_{\mathrm{tot}}/2} ds\int_{\mathbb{R}} d\tilde{\omega}|\hat{F}(\tilde{\omega})|^2\exp\Big(i\phi(\boldsymbol{Y},\boldsymbol{V},\boldsymbol{X}_R)\Big)\\ &\qquad\times i\nabla_{\boldsymbol{X}_R}\phi(\boldsymbol{Y},\boldsymbol{V},\boldsymbol{X}_R)\\ \nabla^2_{\boldsymbol{X}_R}\tilde{I}^{\mathrm{MF}}(\boldsymbol{Y},\boldsymbol{V},\boldsymbol{X}_R) &= C\int_{-T_{\mathrm{tot}}/2}^{T_{\mathrm{tot}}/2} ds\int_{\mathbb{R}} d\tilde{\omega}|\hat{F}(\tilde{\omega})|^2\exp\Big(i\phi(\boldsymbol{Y},\boldsymbol{V},\boldsymbol{X}_R)\Big)\\ &\qquad\times\Big(i\nabla^2_{\boldsymbol{X}_R}\phi(\boldsymbol{Y},\boldsymbol{V},\boldsymbol{X}_R)-\nabla_{\boldsymbol{X}_R}\phi^t\nabla_{\boldsymbol{X}_R}\phi(\boldsymbol{Y},\boldsymbol{V},\boldsymbol{X}_R)\Big).\end{aligned}$$

As we have $(\boldsymbol{x}-\boldsymbol{X}_R)_3=0$ (but all the results can be also proven under the weaker condition $(\boldsymbol{x}-\boldsymbol{X}_R)_3=o(\|\boldsymbol{x}-\boldsymbol{X}_R\|)$) then,

$$\begin{aligned}\nabla_{\boldsymbol{X}_R}\phi(\boldsymbol{Y},\boldsymbol{V},\boldsymbol{X}_R)\cdot(\boldsymbol{x}-\boldsymbol{X}_R) &= \frac{\omega_o+B\tilde{\omega}}{c_o}\Big(\frac{s}{H_T}(\boldsymbol{V}-\boldsymbol{V}_T)_\perp-\frac{2s(\boldsymbol{V}_T)_\perp}{H_T^2}((\boldsymbol{Y}-\boldsymbol{Y}_T)_3\\ &\qquad+s(\boldsymbol{V}-\boldsymbol{V}_T)_3)+\frac{(\boldsymbol{Y}-\boldsymbol{Y}_T)_\perp}{H_T}\Big)\cdot(\boldsymbol{x}-\boldsymbol{X}_R)\\ &\quad+o(\|\nabla\phi\|\|\boldsymbol{X}_R-\boldsymbol{x}\|).\end{aligned}$$

The above term will be shown to be negligible in the following for $\|\boldsymbol{X}_R-\boldsymbol{x}\|\le\frac{a}{\sqrt{N}}$ and $(\boldsymbol{Y},\boldsymbol{V})\in\mathcal{R}^{k,l}_{\boldsymbol{Y}_T,\boldsymbol{V}_T,q,\boldsymbol{r}}$. Actually, assuming $(\boldsymbol{Y},\boldsymbol{V})\in\mathcal{R}^{k,l}_{\boldsymbol{Y}_T,\boldsymbol{V}_T,q,\boldsymbol{r}}$ (for $q=O(1)$), only the dominant terms of $\nabla\phi$ (the one related to a differentiation of the underbraced terms in (4.1)) will appear in the differentiation. For the Hessian of ϕ, we have

$${}^t(\boldsymbol{x}-\boldsymbol{X}_R)\nabla^2_{\boldsymbol{X}_R}\phi(\boldsymbol{Y},\boldsymbol{V},\boldsymbol{X}_R)(\boldsymbol{x}-\boldsymbol{X}_R)=\frac{\omega_o+B\tilde{\omega}}{c_oH_T^2}\Big(s(\boldsymbol{V}-\boldsymbol{V}_T)_3+(\boldsymbol{Y}-\boldsymbol{Y}_T)_3\Big)\|\boldsymbol{X}_R-\boldsymbol{x}\|_2^2.$$

If we further assume that $\|\boldsymbol{X}_R-\boldsymbol{x}\|\le\frac{a}{\sqrt{N}}$, we have (using a Hölder inequality with $p,p^*\in[1,\infty]$ and $\frac{1}{p}+\frac{1}{p^*}=1$ and using the fact that $\boldsymbol{x}-\boldsymbol{X}_R$ lives in a two dimensional space [3]),

$$\begin{aligned}&|\nabla_{\boldsymbol{X}_R}\phi(\boldsymbol{Y},\boldsymbol{V},\boldsymbol{X}_R)\cdot(\boldsymbol{x}-\boldsymbol{X}_R)|\\ &\quad\le\frac{\omega_o+B\tilde{\omega}}{c_o}\frac{a}{\sqrt{N}}2^{\frac{1}{p^*}}\Big(\frac{T_{\mathrm{tot}}}{H_T}\|\boldsymbol{V}-\boldsymbol{V}_T\|_{\perp,p}+\frac{\|\boldsymbol{Y}-\boldsymbol{Y}_T\|_{\perp,p}}{H_T}\\ &\qquad+\frac{2T_{\mathrm{tot}}\|\boldsymbol{V}_T\|_{\perp,\infty}2^{\frac{1}{p}}}{H_T^2}(|(\boldsymbol{Y}-\boldsymbol{Y}_T)_3|+T_{\mathrm{tot}}|(\boldsymbol{V}-\boldsymbol{V}_T)_3|)\Big)\\ &\quad\le\frac{1}{\sqrt{N}}(H^1_p(\boldsymbol{Y},\boldsymbol{V})+o(1)H^1_p(\boldsymbol{Y},\boldsymbol{V}).\end{aligned}\tag{C.1}$$

Copyright © by SIAM. Unauthorized reproduction of this article is prohibited.

Downloaded 11/28/17 to 171.67.216.21. Redistribution subject to SIAM license or copyright; see http://www.siam.org/journals/ojsa.php

Downloaded 11/28/17 to 171.67.216.21. Redistribution subject to SIAM license or copyright; see http://www.siam.org/journals/ojsa.php

Here $o(1)$ means a small quantity with respect to 1 according to Hypothesis 1 (section 4.1), $(\boldsymbol{Y},\boldsymbol{V}) \in \mathcal{R}^{k,l}_{\boldsymbol{Y}_T,\boldsymbol{V}_T,q,\boldsymbol{r}}$, and $q = O(1)$ with

$$H^1_p(\boldsymbol{Y},\boldsymbol{V}) \overset{(def)}{=} 2\frac{|(\boldsymbol{Y}-\boldsymbol{Y}_T)_3|}{r_3} + 2^{\frac{1}{p^*}}\sqrt[p]{\frac{|(\boldsymbol{Y}-\boldsymbol{Y}_T)_1|^p}{r_1^p} + \frac{|(\boldsymbol{Y}-\boldsymbol{Y}_T)_2|^p}{r_2^p}} + 2\frac{|(\boldsymbol{V}-\boldsymbol{V}_T)_3|}{r_6} + 2^{\frac{1}{p^*}}\sqrt[p]{\frac{|(\boldsymbol{V}-\boldsymbol{V}_T)_1|^p}{r_4^p} + \frac{|(\boldsymbol{V}-\boldsymbol{V}_T)_2|^p}{r_5^p}}$$

for $p < \infty$ and

$$H^1_\infty(\boldsymbol{Y},\boldsymbol{V}) \overset{(def)}{=} 2\frac{|(\boldsymbol{Y}-\boldsymbol{Y}_T)_3|}{r_3} + 2\left(\frac{|(\boldsymbol{Y}-\boldsymbol{Y}_T)_1|}{r_1} \wedge \frac{|(\boldsymbol{Y}-\boldsymbol{Y}_T)_2|}{r_2}\right) + 2\frac{|(\boldsymbol{V}-\boldsymbol{V}_T)_3|}{r_6} + 2\left(\frac{|(\boldsymbol{V}-\boldsymbol{V}_T)_1|}{r_4} \wedge \frac{|(\boldsymbol{V}-\boldsymbol{V}_T)_2|}{r_5}\right) \tag{C.2}$$

for $p = \infty$.

Note that $H^1_p(\boldsymbol{Y},\boldsymbol{V})$ is a distance between $(\boldsymbol{Y},\boldsymbol{V})$ and $(\boldsymbol{Y}_T,\boldsymbol{V}_T)$ and, therefore, for any $\delta > 0$, $H^1_p(\boldsymbol{Y}_T + \delta\Delta\boldsymbol{Y}, \boldsymbol{V}_T + \delta\Delta\boldsymbol{V}) = \delta H^1_p(\boldsymbol{Y}_T + \Delta\boldsymbol{Y}, \boldsymbol{V}_T + \Delta\boldsymbol{V})$,

$$\begin{aligned}
&\left|{}^t(\boldsymbol{x}-\boldsymbol{X}_R)\left(i\nabla^2_{\boldsymbol{X}_R}\phi(\boldsymbol{Y},\boldsymbol{V},\boldsymbol{X}_R) - \nabla_{\boldsymbol{X}_R}\phi\,{}^t\nabla_{\boldsymbol{X}_R}\phi(\boldsymbol{Y},\boldsymbol{V},\boldsymbol{X}_R)\right)(\boldsymbol{x}-\boldsymbol{X}_R)\right| \\
&\quad\le \frac{1}{N}\left(\frac{|(\boldsymbol{V}-\boldsymbol{V}_T)_3|}{r_6}\frac{a}{H_T} + \frac{|(\boldsymbol{Y}-\boldsymbol{Y}_T)_3|}{r_3}\frac{a}{H_T} + H^1_p(\boldsymbol{Y},\boldsymbol{V})^2 + o\left(H^1_p(\boldsymbol{Y},\boldsymbol{V})^2\right)\right) \\
&\quad\le \frac{1}{N}\left(H^2_p(\boldsymbol{Y},\boldsymbol{V}) + o(1)\left(H^2_p(\boldsymbol{Y},\boldsymbol{V}) + H^1_p(\boldsymbol{Y},\boldsymbol{V})\right)\right)
\end{aligned} \tag{C.3}$$

with

$$H^2_p(\boldsymbol{Y},\boldsymbol{V}) \overset{(def)}{=} H^1_p(\boldsymbol{Y},\boldsymbol{V})^2.$$

As $\|\mathcal{I}^{\mathrm{MF}}\|_\infty = \mathcal{I}^{\mathrm{MF}}(\boldsymbol{Y}_T,\boldsymbol{V}_T) = C\int ds \int_{\mathbb{R}} d\tilde{\omega}|\hat{F}(\tilde{\omega})|^2$, we ultimately have

$$\left|\mathcal{I}^{\mathrm{MF}}(\boldsymbol{Y},\boldsymbol{V}) - \tilde{I}^{\mathrm{MF}}_N(\boldsymbol{Y},\boldsymbol{V})\right| \le \frac{\|\mathcal{I}^{\mathrm{MF}}\|_\infty}{2N}\left(H^2_p(\boldsymbol{Y},\boldsymbol{V}) + o(1)\left(H^2_p(\boldsymbol{Y},\boldsymbol{V}) + H^1_p(\boldsymbol{Y},\boldsymbol{V})\right)\right).$$

However, the same reasoning could be made without using the barycenter trick (that is, having only a first order Taylor expansion to bound). In this case, we would obtain,

$$\left|\mathcal{I}^{\mathrm{MF}}(\boldsymbol{Y},\boldsymbol{V}) - \tilde{I}^{\mathrm{MF}}_N(\boldsymbol{Y},\boldsymbol{V})\right| \le \frac{\|\mathcal{I}^{\mathrm{MF}}\|_\infty}{\sqrt{N}} H^1_p(\boldsymbol{Y},\boldsymbol{V}).$$

Consequently, we have

$$\left|\mathcal{I}^{\mathrm{MF}}(\boldsymbol{Y},\boldsymbol{V}) - \tilde{I}^{\mathrm{MF}}_N(\boldsymbol{Y},\boldsymbol{V})\right| \le \|\mathcal{I}^{\mathrm{MF}}\|_\infty\left(\frac{H^1_p(\boldsymbol{Y},\boldsymbol{V})}{\sqrt{N}} \wedge \frac{H^2_p(\boldsymbol{Y},\boldsymbol{V})}{2N} + \frac{1}{2N}o(1)\left(H^2_p(\boldsymbol{Y},\boldsymbol{V}) + H^1_p(\boldsymbol{Y},\boldsymbol{V})\right)\right).$$

Copyright © by SIAM. Unauthorized reproduction of this article is prohibited.

Downloaded 11/28/17 to 171.67.216.21. Redistribution subject to SIAM license or copyright; see http://www.siam.org/journals/ojsa.php

C.2. CC case. To ease notation we will denote $\psi(\boldsymbol{Y},\boldsymbol{V},\boldsymbol{X}_R) = (\Psi_{\mathcal{I}^{\mathrm{MF}}} + \epsilon_{\mathcal{I}^{\mathrm{MF}}})(\boldsymbol{Y} - \boldsymbol{Y}_T, \boldsymbol{V} - \boldsymbol{V}_T, \boldsymbol{X}_R, s, \tilde{\omega})$;

$$
\begin{aligned}
&\mathcal{I}^{\mathrm{CC}}(\boldsymbol{Y},\boldsymbol{V}) - \tilde{I}_N^{\mathrm{CC}}(\boldsymbol{Y},\boldsymbol{V}) \\
&\quad= \frac{1}{a^4}\sum_{R_1=1}^{N}\sum_{R_2=1}^{N}\int_{\mathcal{C}_{R_1}} d\boldsymbol{x}_1 \int_{\mathcal{C}_{R_1}} d\boldsymbol{x}_2 \tilde{I}^{\mathrm{CC}}(\boldsymbol{Y},\boldsymbol{V},\boldsymbol{x}_1,\boldsymbol{x}_2) - \tilde{I}^{\mathrm{CC}}(\boldsymbol{Y},\boldsymbol{V},\boldsymbol{X}_{R_1},\boldsymbol{X}_{R_2}) \\
&\quad= \frac{1}{a^4}\sum_{R_1=1}^{N}\sum_{R_2=1}^{N}\int_{\mathcal{C}_{R_1}} d\boldsymbol{x}_1 \int_{\mathcal{C}_{R_1}} d\boldsymbol{x}_2 \nabla_{\boldsymbol{X}_{R_1},\boldsymbol{X}_{R_2}} \tilde{I}^{\mathrm{CC}}(\boldsymbol{Y},\boldsymbol{V},\boldsymbol{X}_{R_1},\boldsymbol{X}_{R_2}) \cdot \begin{pmatrix} \boldsymbol{x}_1 - \boldsymbol{X}_{R_1} \\ \boldsymbol{x}_2 - \boldsymbol{X}_{R_2} \end{pmatrix} \\
&\qquad + \int_0^1 dt\, {}^t\begin{pmatrix} \boldsymbol{x}_1 - \boldsymbol{X}_{R_1} \\ \boldsymbol{x}_2 - \boldsymbol{X}_{R_2} \end{pmatrix} \nabla^2_{\boldsymbol{X}_{R_1},\boldsymbol{X}_{R_2}} \tilde{I}^{\mathrm{CC}}(\boldsymbol{Y},\boldsymbol{V},(1-t)\boldsymbol{X}_{R_1} \\
&\qquad\qquad + t\boldsymbol{x}_1, (1-t)\boldsymbol{X}_{R_2} + t\boldsymbol{x}_2) \begin{pmatrix} \boldsymbol{x}_1 - \boldsymbol{X}_{R_1} \\ \boldsymbol{x}_2 - \boldsymbol{X}_{R_2} \end{pmatrix}.
\end{aligned}
$$

Denote $\delta\boldsymbol{x} = \begin{pmatrix} \delta\boldsymbol{x}_1 \\ \delta\boldsymbol{x}_2 \end{pmatrix} \in \mathbb{R}^6$, $\delta\boldsymbol{x}_1, \delta\boldsymbol{x}_2 \in \mathbb{R}^3$ an arbitrary vector. Essentially, $\delta\boldsymbol{x}_m$ would stand for $\boldsymbol{x}_m - \boldsymbol{X}_{R_m}$ $(m = 1, 2)$. We thus have

$$
\begin{aligned}
&\nabla_{\boldsymbol{X}_{R_1},\boldsymbol{X}_{R_2}} \tilde{I}^{\mathrm{CC}}(\boldsymbol{Y},\boldsymbol{V},\boldsymbol{X}_{R_1},\boldsymbol{X}_{R_2}) \cdot \delta\boldsymbol{x} \\
&\quad= C\int_{-T_{\mathrm{tot}}/2}^{T_{\mathrm{tot}}/2} ds \int_{\mathbb{R}} d\tilde{\omega} |\hat{F}(\tilde{\omega})|^2 \exp\Big(i\big(\psi(\boldsymbol{Y},\boldsymbol{V},\boldsymbol{X}_{R_1}) - \psi(\boldsymbol{Y},\boldsymbol{V},\boldsymbol{X}_{R_2})\big)\Big) \\
&\qquad\times i\frac{\omega_o + B\tilde{\omega}}{c_o}(\nabla_{\boldsymbol{X}_R}\psi(\boldsymbol{Y},\boldsymbol{V},\boldsymbol{X}_{R_1}) \cdot \delta\boldsymbol{x}_1 - \nabla_{\boldsymbol{X}_R}\psi(\boldsymbol{Y},\boldsymbol{V},\boldsymbol{X}_{R_2}) \cdot \delta\boldsymbol{x}_2)
\end{aligned}
$$

and

$$
\begin{aligned}
&{}^t\delta\boldsymbol{x}\nabla^2_{\boldsymbol{X}_{R_1},\boldsymbol{X}_{R_2}} \tilde{I}^{\mathrm{CC}}(\boldsymbol{Y},\boldsymbol{V},\boldsymbol{X}_{R_1},\boldsymbol{X}_{R_2})\delta\boldsymbol{x} \\
&\quad= C\int_{-T_{\mathrm{tot}}/2}^{T_{\mathrm{tot}}/2} ds \int_{\mathbb{R}} d\tilde{\omega} |\hat{F}(\tilde{\omega})|^2 \exp\Big(i\big(\psi(\boldsymbol{Y},\boldsymbol{V},\boldsymbol{X}_{R_1}) - \psi(\boldsymbol{Y},\boldsymbol{V},\boldsymbol{X}_{R_2})\big)\Big) \\
&\qquad\Big(i\big({}^t\delta\boldsymbol{x}_1\nabla^2_{\boldsymbol{X}_R}\psi(\boldsymbol{Y},\boldsymbol{V},\boldsymbol{X}_{R_1})\delta\boldsymbol{x}_1 - {}^t\delta\boldsymbol{x}_2\nabla^2_{\boldsymbol{X}_R}\psi(\boldsymbol{Y},\boldsymbol{V},\boldsymbol{X}_{R_2})\delta\boldsymbol{x}_2\big) \\
&\qquad\quad - \big(\nabla_{\boldsymbol{X}_R}\psi(\boldsymbol{Y},\boldsymbol{V},\boldsymbol{X}_{R_1}) \cdot \delta\boldsymbol{x}_1 - \nabla_{\boldsymbol{X}_R}\psi(\boldsymbol{Y},\boldsymbol{V},\boldsymbol{X}_{R_2}) \cdot \delta\boldsymbol{x}_2\big)^2 \Big).
\end{aligned}
$$

Let $(\boldsymbol{Y},\boldsymbol{V}) \in \mathcal{R}^{k,l}_{\boldsymbol{Y}_T,\boldsymbol{V}_T,q,\boldsymbol{r}}$, then only the curly bracket terms in (4.4) will matter for the first order derivative (the other terms being negligible). Thus,

$$
\begin{aligned}
&\nabla_{\boldsymbol{X}_R}\psi(\boldsymbol{Y},\boldsymbol{V},\boldsymbol{X}_{R_m}) \cdot \delta\boldsymbol{x}_m \\
&\quad= \frac{\omega_o + B\tilde{\omega}}{c_o}\Big(-\frac{1}{H_T}(\boldsymbol{Y} - \boldsymbol{Y}_T)_\perp - \frac{1}{H_T^2}\boldsymbol{X}_{R_m}(\boldsymbol{Y} - \boldsymbol{Y}_T)_3 - \frac{s}{H_T}(\boldsymbol{V} - \boldsymbol{V}_T)_\perp \\
&\qquad + \frac{s}{2H_T^2}(\boldsymbol{V}_T)_\perp(\boldsymbol{Y} - \boldsymbol{Y}_T)_3 + \frac{s^2}{2H_T^2}(\boldsymbol{V}_T)_\perp(\boldsymbol{V} - \boldsymbol{V}_T)_3 + \frac{s}{H_T^2}(\boldsymbol{X}_{R_m})_\perp(\boldsymbol{V} - \boldsymbol{V}_T)_3\Big) \\
&\quad\cdot \delta\boldsymbol{x}_m
\end{aligned}
$$

Copyright © by SIAM. Unauthorized reproduction of this article is prohibited.

Downloaded 11/28/17 to 171.67.216.21. Redistribution subject to SIAM license or copyright; see http://www.siam.org/journals/ojsa.php

and

$$
\begin{aligned}
&|\nabla_{\boldsymbol{X}_R}\psi(\boldsymbol{Y},\boldsymbol{V},\boldsymbol{X}_{R_m})\cdot\delta\boldsymbol{x}_m| \\
&\quad\le\left(\frac{1}{H_T\lambda_o a}\|(\boldsymbol{Y}-\boldsymbol{Y}_T)_\perp\|_p\|\delta\boldsymbol{x}_m\|_{p^*}+2\frac{\|\delta\boldsymbol{x}_m\|_{p^*}}{a}2^p\left(\left|\frac{(\boldsymbol{V}-\boldsymbol{V}_T)_3}{r_6}\right|+\left|\frac{(\boldsymbol{Y}-\boldsymbol{Y}_T)_3}{r_3}\right|\right)\right. \\
&\qquad\left.+\frac{s}{H_T\lambda_o}\|(\boldsymbol{V}-\boldsymbol{V}_T)_\perp\|_p\|\delta\boldsymbol{x}_m\|_{p^*}\right)(1+o(1)).
\end{aligned}
$$

As we have $(\boldsymbol{x}-\boldsymbol{X}_R)_3=0$ (but all the results can be also proven under the weaker condition $(\boldsymbol{x}-\boldsymbol{X}_R)_3=o(\|\boldsymbol{x}-\boldsymbol{X}_R\|)$) and that $\delta\boldsymbol{x}_1$ and $\delta\boldsymbol{x}_2$ are located in a square of radius $\frac{a}{\sqrt{N}}$, then

$$
\left|{}^t\delta\boldsymbol{x}_m\nabla^2_{\boldsymbol{X}_R}\psi(\boldsymbol{Y},\boldsymbol{V},\boldsymbol{X}_{R_m})\delta\boldsymbol{x}_m\right|\le\frac{2}{N}\left(\frac{|(\boldsymbol{V}-\boldsymbol{V}_T)_3|}{r_6}+\frac{|(\boldsymbol{Y}-\boldsymbol{Y}_T)_3|}{r_3}\right)
$$

and

$$
\left|\nabla_{\boldsymbol{X}_R}\psi(\boldsymbol{Y},\boldsymbol{V},\boldsymbol{X}_{R_m})\cdot\delta\boldsymbol{x}_m\right|\le\frac{1}{\sqrt{N}}\frac{G_p^1(\boldsymbol{Y},\boldsymbol{V})}{2}.
$$

Hence

$$
\begin{aligned}
&\Big|\, i\big({}^t\delta\boldsymbol{x}_1\nabla^2_{\boldsymbol{X}_R}\psi(\boldsymbol{Y},\boldsymbol{V},\boldsymbol{X}_{R_1})\delta\boldsymbol{x}_1-{}^t\delta\boldsymbol{x}_2\nabla^2_{\boldsymbol{X}_R}\psi(\boldsymbol{Y},\boldsymbol{V},\boldsymbol{X}_{R_2})\delta\boldsymbol{x}_2\big) \\
&\qquad-\big(\nabla_{\boldsymbol{X}_R}\psi(\boldsymbol{Y},\boldsymbol{V},\boldsymbol{X}_{R_1})\cdot\delta\boldsymbol{x}_1-\nabla_{\boldsymbol{X}_R}\psi(\boldsymbol{Y},\boldsymbol{V},\boldsymbol{X}_{R_2})\cdot\delta\boldsymbol{x}_2\big)^2\,\Big| \\
&\le\frac{1}{N}G_p^2(\boldsymbol{Y},\boldsymbol{V})
\end{aligned}
$$

with

$$
\begin{aligned}
G_p^1(\boldsymbol{Y},\boldsymbol{V})\overset{(def)}{=}2\Bigg(&4\frac{|(\boldsymbol{Y}-\boldsymbol{Y}_T)_3|}{r_3}+2^{\frac{1}{p^*}}\sqrt[p]{\frac{|(\boldsymbol{Y}-\boldsymbol{Y}_T)_1|^p}{r_1^p}+\frac{|(\boldsymbol{Y}-\boldsymbol{Y}_T)_2|^p}{r_2^p}} \\
&+4\frac{|(\boldsymbol{V}-\boldsymbol{V}_T)_3|}{r_6}+2^{\frac{1}{p^*}}\sqrt[p]{\frac{|(\boldsymbol{V}-\boldsymbol{V}_T)_1|^p}{r_4^p}+\frac{|(\boldsymbol{V}-\boldsymbol{V}_T)_2|^p}{r_5^p}}\Bigg),
\end{aligned}
$$

and

$$
G_p^2(\boldsymbol{Y},\boldsymbol{V})\overset{(def)}{=}4\frac{|(\boldsymbol{V}-\boldsymbol{V}_T)_3|}{r_6}+4\frac{|(\boldsymbol{Y}-\boldsymbol{Y}_T)_3|}{r_3}+G_p^1(\boldsymbol{Y},\boldsymbol{V})^2
$$

for $p<\infty$ and

$$
\begin{aligned}
G_\infty^1(\boldsymbol{Y},\boldsymbol{V})\overset{(def)}{=}2\Bigg(&4\frac{|(\boldsymbol{Y}-\boldsymbol{Y}_T)_3|}{r_3}+2\left(\frac{|(\boldsymbol{Y}-\boldsymbol{Y}_T)_1|}{r_1}\wedge\frac{|(\boldsymbol{Y}-\boldsymbol{Y}_T)_2|}{r_2}\right) \\
&4\frac{|(\boldsymbol{V}-\boldsymbol{V}_T)_3|}{r_6}+2\left(\frac{|(\boldsymbol{V}-\boldsymbol{V}_T)_1|^p}{r_4}\wedge\frac{|(\boldsymbol{V}-\boldsymbol{V}_T)_2|}{r_5}\right)\Bigg)
\end{aligned}
$$

Copyright © by SIAM. Unauthorized reproduction of this article is prohibited.

for $p = \infty$. Consequently, all things put together, we get

$$\left|\mathcal{I}^{\mathrm{CC}}(\boldsymbol{Y},\boldsymbol{V}) - \tilde{I}_N^{\mathrm{CC}}(\boldsymbol{Y},\boldsymbol{V})\right| \leq 2\|\mathcal{I}^{\mathrm{MF}}\|_\infty \left(\frac{G_p^1(\boldsymbol{Y},\boldsymbol{V})}{\sqrt{N}} \wedge \frac{G_p^2(\boldsymbol{Y},\boldsymbol{V})}{2N} + \frac{1}{2N} o(1) \left(G_p^2(\boldsymbol{Y},\boldsymbol{V})\right) \right).$$

Indeed the reader could show by the same calculus that a first order expansion for approximation would have led to the bound $\|\mathcal{I}^{\mathrm{MF}}\|_\infty \frac{G_p^1(\boldsymbol{Y},\boldsymbol{V})}{\sqrt{N}}$. Here also $o(1)$ means a small quantity with respect to 1 according to Hypothesis 2 (section 4.2), $(\boldsymbol{Y},\boldsymbol{V}) \in \mathcal{R}^{k,l}_{\boldsymbol{Y}_T,\boldsymbol{V}_T,q,\boldsymbol{r}}$, and $q = O(1)$.

Acknowledgment. Work carried out while the first and fourth authors were visiting the Mathematics Department at Stanford University.

REFERENCES

[1] *Special Issue on Passive Radar* (*Part* I), IEEE Aerospace and Electronic Systems Magazine, 27 (October, 2012).

[2] L. Borcea, J. Garnier, G. Papanicolaou, K. Solna, and C. Tsogka, *Resolution analysis of passive synthetic aperture imaging of fast moving objects*, SIAM J. Imaging Sci., 28 (2017), pp. 665–710.

[3] H. Brézis, *Analyse Fonctionnelle - Théorie et Applications*, Dunod, Paris, 1983.

[4] C. H. Casteel, L. R. A. Gorham, M. J. Minardi, S. M. Scarborough, K. D. Naidu, and U. K. Majumder, *A challenge problem for 2d/3d imaging of targets from a volumetric data set in an urban environment*, in Algorithms for Synthetic Aperture Radar Imagery XIV, Proc. SPIE 6568, SPIE, Bellingham, WA, 2007, 65680D.

[5] M. Cheney and B. Borden, *Imaging moving targets from scattered waves*, Inverse Problems, 24 (2008), 035005.

[6] M. Cheney and B. Borden, *Fundamentals of Radar Imaging*, CBMS-NSF Regional Conf. Ser. in Appl. Math. 79, SIAM, Philadelphia, 2009.

[7] J. C. Curlander and R. N. McDonough, *Synthetic Aperture Radar*, Wiley, New York, 1991.

[8] G. Franschetti and R. Lanari, *Synthetic Aperture Radar Processing*, CRC Press, Boca Raton, FL, 1999.

[9] J. Garnier and G. Papanicolaou, *Correlation based virtual source imaging in strongly scattering media*, Inverse Problems, 28 (2012), 075002.

[10] J. Garnier and G. Papanicolaou, *Passive Imaging with Ambient Noise*, Cambridge University Press, Cambridge, 2016.

[11] J. Garnier, G. Papanicolaou, A. Semin, and C. Tsogka, *Signal-to-noise ratio analysis in virtual source array imaging*, SIAM J. Imaging Sci., 8 (2015), pp. 248–279.

[12] J. A. Haimerl and G. P. Fonder, *Space fence system overview*, in Proceedings of the Advanced Maui Optical and Space Surveillance Technology Conference, Curran, Red Hook, NY, 2015, 45.

[13] M. E. Lawrence, C. T. Hansen, S. P. Deshmukh, and B. C. Flickinger, *Characterization of the effects of atmospheric lensing in SAR images*, in Radar Sensor Technology XIII, SPIE Proc. 7308, SPIE, Bellingham, WA, 2009, 73080C.

[14] M.S. Mahmud, S. U. Qaisar, and C. Benson, *Tracking low earth orbit small debris with GPS satellites as bistatic radar*, in Proceedings of the Advanced Maui Optical and Space Surveillance Technology Conference, Curran, Red Hook, NY, 2016, 18.

[15] R. W. McMillan, *Atmospheric turbulence effects on radar systems*, in Proceedings of the IEEE 2010 National Aerospace & Electronics Conference, IEEE, Piscataway, NJ, 2010, pp. 181–196.

[16] D. Mehrholz, L. Leushacke, W. Flury, R. Jehn, H. Klinkrad, and M. Landgraf, *Detecting, tracking and imaging space debris*, ESA Bulletin, 109 (2002), pp. 128–134.

[17] S. V. Tsynkov, *On the use of start-stop approximation for spaceborne SAR imaging*, SIAM J. Imaging Sci., 2 (2009), pp. 646–669.

[18] M. T. Valley, S. P. Kearney, and M. Ackermann, *Small Space Object Imaging: LDRD Final Report*, Technical report, SAND 2009-0692, Sandia National Laboratories, Albuquerque, NM, 2009.

Downloaded 11/28/17 to 171.67.216.21. Redistribution subject to SIAM license or copyright; see http://www.siam.org/journals/ojsa.php

Copyright © by SIAM. Unauthorized reproduction of this article is prohibited.

[19] L. Wang, M. Cheney, and B. Borden, *Multistatic radar imaging of moving targets*, IEEE Trans. Aerosp. Electron. Systems, 48 (2012), pp. 230–242.

[20] L. Wang, C. E. Yarman, and B. Yazici, *Doppler-hitchhiker: A novel passive synthetic aperture radar using ultranarrowband sources of opportunity*, IEEE Trans. Geosci. Remote Sensing, 49 (2011), pp. 3521–3537.

[21] L. Wang, C. E. Yarman, and B. Yazici, *Theory of passive synthetic aperture imaging, in excursions in harmonic analysis*, Appl. Numer. Harmon. Anal., 1 (2013), pp. 211–236.

[22] K. Wormnes, R. Le Letty, L. Summerer, R. Schonenborg, O. Dubois-Matra, E. Luraschi, A. Cropp, H. Kragg, and J. Delaval, *ESA technologies for space debris remediation*, in Proceedings of 6th European Conference on Space Debris, Darmstadt, Germany, ESA Communications, Nourdwigk, The Netherlands, 2013, 65.

Downloaded 11/28/17 to 171.67.216.21. Redistribution subject to SIAM license or copyright; see http://www.siam.org/journals/ojsa.php

Copyright © by SIAM. Unauthorized reproduction of this article is prohibited.